Universidade do Estado do Rio de Janeiro
Centro de Tecnologia e Ciências
Faculdade de Geologia

Carla Cristine Aguiar Neto

Desenvolvimento de técnicas de análise isotópica de Nd e Sr por espectrometria de massas por termo-ionização (TIMS): aplicação a materiais de referência de rochas e à análise de apatita

Rio de Janeiro
2025

Carla Cristine Aguiar Neto

Desenvolvimento de técnicas de análise isotópica de Nd e Sr por espectrometria de massas por termo-ionização (TIMS): aplicação a materiais de referência de rochas e à análise de apatita

Tese apresentada, como requisito parcial para obtenção do título de Doutor, ao Programa de Pós-Graduação em Geociências, da Universidade do Estado do Rio de Janeiro. Área de concentração: Geociências

Orientador: Prof. Dr. Cláudio de Morisson Valeriano

Rio de Janeiro

2025

CATALOGAÇÃO NA FONTE
UERJ/REDE SIRIUS/CTCC

A282 Aguiar Neto, Carla Cristine.
Desenvolvimento de métodos de análise isotópica de Nd e Sr por espectrometria de massas por termo-ionização (TIMS): aplicação a materiais de referência de rochas e à análise de apatita / Carla Cristine Aguiar Neto.– 2025.
131 f. : il.

Orientador: Claudio de Morisson Valeriano.
Tese (Doutorado) – Universidade do Estado do Rio de Janeiro, Faculdade de Geologia**.**

1. Geologia isotópica - Teses. 2. Rochas ígneas - Teses. 3. Magmatismo – Teses. 4. Orogenia - Teses. 5. Ionização – Teses. I. Valeriano, Claudio de Morisson. II. Universidade do Estado do Rio de Janeiro. Faculdade de Geologia. III. Título.

CDU: 550.42

Bibliotecária Responsável: Priscila Freitas Araujo/ CRB-7: 7322

_____ _____

Assinatura Data

Carla Cristine Aguiar Neto

Desenvolvimento de métodos de análise isotópica de Nd e Sr por espectrometria de massas por termo-ionização (tims): aplicação a materiais de referência de rochas e à análise de apatita

Tese apresentada, como requisito parcial para obtenção do título de Doutor, ao Programa de Pós-Graduação em Geociências, da Universidade do Estado do Rio de Janeiro. Área de concentração: Geociências

Aprovada em 25 de março de 2025.

Banca Examinadora:

_____

Prof. Dr. Claudio de Morisson Valeriano (Orientador)

Faculdade de Geologia – UERJ

_____

Prof. Dr. Júlio Mendes
Instituto de Geociências – UFRJ

_____

Prof. Dr. Guilherme Gonçalves
Instituto de Geociências – UnB

_____

Prof. Dr. Elton Dantas
Instituto de Geociências – UnB

_____

Prof. Dr. Henrique Bruno
Faculdade de Geologia – UERJ

_____

Prof. Dr. Samuel Bersan
Faculdade de Geologia – UERJ

Rio de Janeiro

2025

AGRADECIMENTOS

Ao orientador Dr. Claudio de Morisson Valeriano, pelos ensinamentos e suporte financeiro que viabilizou esta pesquisa: CNPq-PQ (46817/2000-0), (479932/2013-1) (310585/2021-0), FAPERJ (E-26/170-684/00), (E-26/170-523/00) e FAPERJ- Cientistas do Nosso Estado (E-26/151.915/2000), (202.974/2016) e (E-26/200-420/2023). FAPERJ Manutenção de Equipamento Multiusuários (E-26-210-065/2021).

À Dra. Monica Heilbron e ao Dr. Henrique Bruno, pela participação nas etapas de amostragem e suporte financeiro: FAPERJ TEMÁTICO (E-28/2021) e Instituto CNPq-INCT GeoAtlântico (405653/2022-0).

À equipe do Laboratório de Geocronologia e Isótopos Radiogênicos (LAGIR-UERJ), Gilberto Vaz e Janis Schutte, assim como João Ricardo Coutinho (Petrobras) e Juliana Pereira (Petrobras), pela indispensável ajuda nas preparações químicas para as análises isotópicas.

Ao Dr. Gabriel Paravidini (UERJ) e Dra. Manuela Carvalho (Pós-doc/FAPERJ) pela assistência na interpretação de dados.

Às Dras. Caroline Peixoto e Mariana Carvalho (UERJ), pelo auxílio na confecção dos mapas geológicos.

Ao Dr. Rasec Almeida (UERJ), pela colaboração e discussões sobre matemática e análises estatísticas aplicadas às pesquisas.

À Dra. Jacinta Enzweiler (Unicamp), pela doação do material de referência BRP-1 e pelos ensinamentos compartilhados.

Ao Serviço Geológico do Brasil (CPRM), pelo incentivo e suporte na preparação do material de referência BRP-1.

Aos dedicados colaboradores do Laboratório Geológico de Processamento de Amostras **(**LGPA-UERJ), Gabriela, Ms. Felipe Martins e Thiago, Núbia e Luis por todo o auxílio no processamento das amostras.

Ao Dr. Guilherme Gonçalves e Ms. Jeane Grasyelle do Laboratório de Estudos Geodinâmicos, Geocronológicos e Ambientais (LEGGA) da Universidade de Brasília (UnB), pelo suporte do laboratório e pela doação do material de referência NIST SRM 987.

Ao Laboratório de Geologia Isotópica (LAGIS-Unicamp) e Dra. Margareth Navarro, pelas análises químicas dos grãos de apatita.

Ao Dr. Cristiano Lana e à equipe técnica do Laboratório de Geocronologia da UFOP pelo suporte nas análises de U-Pb.

Ao Dr. W.R. Van Schmus (*Kansas University*, USA), pela doação do duplo spike de Sm-Nd e por compartilhar parte de sua profunda expertise.

Ao Dr. Craig Storey (*University of Portsmouth*, UK), pela doação do material de referência Apatita Durango.

À Dra. Diana Ragakty (*in memoriam*; FGEL-UERJ), por seu legado de ensinamentos e pela aquisição do material de referência EN-1 (USGS).

Ao Dr. Nuno Machado (*in memoriam*; GEOTOP, *Université du Québec à Montréal*/ UQAM), que, no ano 2000, plantou as sementes do LAGIR.

DEDICATÓRIA

Ao meu querido e amado pai, Mário Paulo da Costa Neto (*in memoriam*).

RESUMO

AGUIAR NETO, Carla Cristine. **Desenvolvimento de técnicas de análise isotópica de Nd e Sr por espectrometria de massas por termo-ionização (TIMS**): aplicação a materiais de referência de rochas e à análise de apatita. 2025. 131 f. Tese (Doutorado em Geociências) – Faculdade de Geologia, Universidade do Estado do Rio de Janeiro, Rio de Janeiro, 2025.

Este estudo teve como objetivo desenvolver e otimizar procedimentos analíticos para a medição das razões isotópicas Sm-Nd e Sr-Sr em rocha total e no mineral apatita. A pesquisa envolveu a implementação de métodos avançados para garantir medições precisas e reprodutíveis, contribuindo para a compreensão e refinamento de dados utilizados no estudo da gênese e evolução de rochas. Dois artigos foram produzidos, enfatizando a importância dos materiais de referência para a obtenção de dados confiáveis e a eficiência da análise de Sr em apatita por TIMS, uma técnica de alta precisão e custo relativamente baixo. O primeiro artigo apresenta as razões isotópicas de Sm-Nd e Sr-Sr do material de referência BRP-1 ("Basalto Ribeirão Preto"), com base em medições repetidas ao longo de doze anos realizadas no LAGIR. As razões isotópicas medidas para Nd e Sr no BRP-1 são: $^{143}Nd/^{144}Nd = 0.512408 \pm 0.000010$ (2s) e $^{87}Sr/^{86}Sr = 0.706011 \pm 0.000017$ (2s). A precisão desses resultados foi validada por meio da medição de materiais de referência bem caracterizados do USGS, como AGV-1, BCR-1, BHVO-1, G-2 e GSP-1. O segundo artigo investiga o uso da composição isotópica de Sr em grãos de apatita de rochas magmáticas como proxy para as razões iniciais de $^{87}Sr/^{86}Sr$. A análise de Sr em apatita é fundamental para entender a origem do magma, a contaminação crustal e a diferenciação magmática. O estudo se concentra em rochas granitóides da Orogenia Ribeira, Brasil, e propõe uma abordagem de menor custo e maior eficiência em comparação com as análises tradicionais de rocha total. O método, validado com incerteza de 0,5%, representa uma alternativa confiável e eficiente. Ambos os artigos convergem no aprimoramento dos métodos analíticos que resultou em procedimentos mais eficientes e validados para as análises isotópicas. O refinamento metodológico desenvolvido ao longo deste trabalho proporciona uma abordagem mais confiável e precisa, essencial para os estudos petrogenéticos.

Palavras-chave: material de referência; isótopos radiogênicos; digestão química; diluição isotópica; apatita; cromatografia de troca iônica; ionização térmica espectrometria de massa.

ABSTRACT

AGUIAR NETO, Carla Cristine. **Development of Nd and Sr isotopic analysis techniques by thermal ionization mass spectrometry (TIMS)**: application to rock reference materials and apatite analysis. 2025. 131f. PhD Thesis (Geosciences) – Faculty of Geology, Rio de Janeiro State University, Rio de Janeiro, 2025.

This study aimed to develop and optimize analytical procedures for measuring the Sm-Nd and Sr-Sr isotopic ratios in whole rock and in the mineral apatite. The research involved the implementation of advanced methods to ensure precise and reproducible measurements, contributing to the understanding and refinement of data used in the study of the genesis and evolution of rocks. Two papers were produced, highlighting the importance of reference materials for obtaining reliable data and the efficiency of Sr analysis in apatite by TIMS, a relatively low-cost, and high-precision technique. The first paper presents Sm-Nd and Sr isotopic ratios of the BRP-1 ("Basalto Ribeirão Preto") reference material based on repeated TIMS measurements over twelve years carried out by the LAGIR laboratory. The measured Nd and Sr isotopic ratios of BRP-1 are: $^{143}Nd/^{144}Nd = 0.512408 \pm 0.000010$ (2s) and $^{87}Sr/^{86}Sr = 0.706011 \pm 0.000017$ (2s). The accuracy of these results was evaluated through the measurement of well-characterized reference materials, such as AGV-1, BCR-1, BHVO-1, G-2, and GSP-1 by USGS. The second paper investigates the use of Sr isotopic composition in apatite grains from magmatic rocks as a proxy for the initial $^{87}Sr/^{86}Sr$ ratios. Sr analysis in apatite is essential for understanding magma origin, crustal contamination, and magmatic differentiation. The study focuses on granitoid rocks from the Ribeira Orogeny, Brazil, and proposes a lower-cost, more efficient approach compared to traditional whole-rock analyses. The method, validated with 0.5% uncertainty, represents a reliable and efficient alternative. Both papers converge in enhancing analytical methods, resulting in more efficient and validated procedures for isotopic analyses. The methodological refinement developed throughout this work provides a more reliable and precise approach, essential for petrogenetic studies.

Keywords: reference material; radiogenic isotopes; chemical digestion; isotope dilution; apatite; ion exchange chromatography; thermal ionization mass spectrometry.

LISTA DE FIGURAS

Figura 1 – Fluxograma de materiais e métodos indicando os processos (cor da fonte azul), materiais (cor da fonte vermelha) e produtos (cor da fonte verde). DI - diluição isotópica..... 24

Figura 2 – Overview of the analytical procedure. X_n represents one isotopic ratio analysed in the mass spectrometer referring to the sample loaded in the chromatographic column. 38

Figura 3 – LAGIR and literature data mean values and horizontal bars are the measurement reproducibility (2s) with a confidence interval of 95 %. The grey bands indicate the LAGIR uncertainties range. The abscissa axis is represented by $^{143}Nd/^{144}Nd$. 45

Figura 4 – LAGIR and literature data mean values and horizontal bars are the measurement reproducibility (2s) with a confidence interval of 95 %. Gray bands indicate the LAGIR standard deviation of the mean [2s] range. Abscissa axis represented by $^{87}Sr/^{86}Sr$. 46

Figura 5 – Individual values and mean of the BRP-1 from LAGIR. Categories and group comparison of the digestion types. A) Flow chart summarizing the sample digestions of the BRP-1 reference material. Square symbols indicate bomb digestion and circle symbol, PFA vials digestion. B) Individual values and mean for Nd isotope ratios. Blue symbols are measured ratio normalised to JNdi-1. The vertical bars on each blue symbol represent the measurement repeatability (2s) associated with of the individual sample analysis. Orange line is the normalised mean and light grey band corresponded to measurement reproducibility (2s) at the 95 % CI. C) Individual values and mean for Sr isotope ratios. Blue symbols are ratios to NIST SRM 987. The vertical bars of each blue symbol represent the measurement repeatability (2s) associated with the individual sample analysis. The orange line is the normalised mean, and the light grey band corresponds to measurement reproducibility (2s) at 95 % CI. To the right of each diagram are KDEs with histograms and a set of vertical lines that mark the individual measurements. ……. 48

Figura 6 – Categories and group comparison of the digestion types – range bars represent the standard deviation of the mean [2s] and (*) represents that there is no significant statistical difference with 95 % confidence intervals..... 49

Figura 7 – Diagram of signal intensity (cps) versus volume of the solution of the aliquot loaded in the column (µl), used in the chromatographic separation of Sr with 20 ng of Durango Apatite. The red line represents Sr signals, and the blue line represents Rb*1000 signals. The blue band represents elution with HNO_3 3M, and the yellow band of HNO_3 0.05M..... 57

Figura 8 – (A) Subdivision of the Mantiqueira Orogenic System (modified from Heilbron et al., 2004a,b) and a cut out of Ribeira Orogen tectonic organization (modified from Peixoto et al., 2022); (B) Geological map showing the Oriental Terrane..... 60

Figura 9 – Zoom of the Oriental Terrain with emphasis on pre-, syn- and post-collisional granitogenesis of Figure 2B showing sample locations..... 61

Figura 10 – Individual and average values of Sr isotopic ratios for apatite reference material. (A) EN-1 and (B) Durango Apatite. The blue circles are the values of Sr ratios normalized to NIST SRM 987. The vertical bars of each blue circle represent the repeatability measurements (2s) with a 95 % confidence interval associated with the analysis of the individual sample. The solid black line represents the average values measured in LAGIR-UERJ. The gray band corresponds to the intermediate precision (2s) of the average with 95 % CI. The dashed red line and the red square represent the average of the reference materials..... 64

Figura 11 – U-Pb analysis of sample BG-14B: A) All zircon grains; B) Upper intercept age; C) zoom in detail on the Concordia Age of crystallization; D) selected zircon crystals showing spot locations with measured $^{206}Pb/^{238}U$ ages (Ma), and discordance..... 65

Figura 12 – U-Pb analysis of sample BG-200: A) All zircon grains; B) zoom in detail on the Concordia Age of crystallization; C) Zoom in detail on the Concordia Age of metamorphism; D) Selected zircon crystals showing spot locations for rim and core with measured $^{206}Pb/^{238}U$ ages (Ma)……. 66

Figura 13 – Thin-section photographs under cross-polarized light of major mineral assemblages of the (A) SMM-CMM-172, (B) BG-200, (C) BG-14B. Thin-section photographs under plane-polarized light showing (D) euhedral prismatic apatite of the SMM-CMM-172 with apatite inclusions in the phenocrysts, (E) BG-200 and (F) BG-14B. Kfs = K-feldspar; Pl = plagioclase; Qtz = quartz; Bi = biotite; Ap = apatite..... 69

Figura 14 – Comparison of groups separated by Sr mass according to their order of magnitude, the average of all values measured in LAGIR and literature data average. (A) EN-1 and (B) Durango Apatite..... 70

Figura 15 – The blue circle represents the individual values of the "All values" group (complete set of isotopic measurements). The red and green circles correspond to the values of the "Single-grain" and "Multi-grain" subgroups (derived from the complete set), respectively. The squares indicate the average or central values of each group..... 72

Figura 16 – The variability of the individual values of the apatite grains of the samples SMM-CMM-172, BG-200, and BG-14B with their respective uncertainties under repeatability conditions (2s) and the average of all the values and their uncertainties (2s) under intermediate precision conditions..... 73

Figura 17 – Comparison of the RSDs of the $^{87}Sr/^{86}Sr$ ratios of the apatite grains in this work with the literature..... 74

Figura 18 – εNd vs. $^{87}Sr/^{86}Sr$ diagram, considering that εNd values of whole-rock and apatite grains are equivalent. Data in plotted fields for pre-, syn- and post-collisional granitoid rocks are from Medeiros et al. (2000); Silva (2011); Machado et al. (2016); Peixoto et al. (2017); Heilbron et al. (2020); Coelho et al. (2023), Potratz et al. (2025) 75

LISTA DE TABELAS

Tabela 1 –	Valores de concentração certificados dos MRs do USGS.....	27
Tabela 2 –	Isotopic composition of the KU ^{149}Sm-^{150}Nd mixed tracer solution.....	37
Tabela 3 –	Chemical procedures for elution Sr, Nd, and Sm.....	40
Tabela 4 –	Multi-collector cup configuration.....	41
Tabela 5 –	Operating parameters for TIMS Sr, Nd and Sm isotopic measurement.....	42
Tabela 6 –	Means and uncertainties for categories and group comparison of the digestion types.	49
Tabela 7 –	Chemical procedures for Sr elution with modifications from Charlie et al. (2006)	56
Tabela 8 –	Operating parameters for TIMS Sr isotopic measurement.....	59
Tabela 9 –	Summary of isotopic data from granitoid samples.....	75

LISTA DE ABREVIATURAS E SIGLAS

ACT Labs	*Activation Laboratories Ltd*
Ca	Cálcio
CHUR	*CHondritic Uniform Reservoir*
ETR	Elemento terra rara
FGEL	Faculdade de Geologia
GCDkit	*GeoChemical Data Toolkit*
H_3PO_4	Ácido fosfórico
HCl	Ácido clorídrico
HF	Ácido fluorídrico
HNO_3	Ácido nítrico
ICP-MS	*Inductively Coupled Plasma Mass Spectrometry*
LAGIR	Laboratório de Geocronologia e Isótopos Radiogênicos
LGPA	Laboratório geológico de processamento de amostras
MORB	*Middle Ocean Ridge Basalt*
Nd	Neodímio
P	Fósforo
QAP	Quartzo, Álcali-feldspato e Plagiocásio
Rb	Rubídio
Re	Rênio
RT	Rocha total
Sm	Samário
Sr	Estrôncio
Ta	Tântalo
TD-ICP	*Total Digestion - Inductively Coupled Plasma Mass Spectrometry*
TIMS	*Thermal Ionization Mass Spectrometry*
UERJ	Universidade do Estado do Rio de Janeiro
USGS	*United States Geological Survey*

LISTA DE SÍMBOLOS

%	porcentagem
±	mais ou menos
µg	micrograma
µl	microlitro
µm	micrômetro
cm	centímetro
km	quilômetros
mA	miliampere
min	minuto
ml	mililitro
ºC	graus Celsius
pg	picograma
ppm	parte por milhão
ε	épsilon

SUMÁRIO

	INTRODUÇÃO	18
1	**OBJETIVOS**	22
1.1	**Objetivo geral**	22
1.2	**Objetivos específicos**	22
2	**MATERIAIS E MÉTODOS**	23
2.1	**Revisão bibliográfica**	25
2.2	**Materiais de estudo**	25
2.2.1	Material de Referência: Basalto de Ribeirão Preto	25
2.2.2	Materiais de Referência do USGS	26
2.2.3	Material de Referência mineral: Apatita Durango	27
2.2.4	Amostras de rochas granitóides	28
2.2.4.1	Amostras BG-200 e BG-14B	28
2.2.4.2	Amostra SMM-CMM-172	29
2.3	**Preparação de amostras de rocha total**	29
2.4	**Separação de minerais pesados: apatita e zircão**	30
2.5	**Análise química elementar em rocha total.**	31
2.6	**Análise isotópica de Estrôncio, Samário e Neodímio**	31
2.7	**Análise química elementar em apatita**	32
2.8	**Geocronologia Urânio-Chumbo em zircão**	32
3	**RESULTADOS**	33
3.1	**1º Artigo científico: ID-TIMS Sm-Nd and Sr Isotopic Composition of Reference Material Basalt Ribeirão Preto (BRP-1)**	34
3.1.1	Introduction	34
3.1.2	The BRP-1 Reference Material	35
3.1.3	Materials and Methods	36
3.1.3.1	Chemicals reagents and vessels	36
3.1.3.2	Chemical digestion	37
3.1.3.3	Chromatographic procedures	39
3.1.3.4	Thermal Ionisation Mass Spectrometry	41
3.1.3.5	Data reduction	42
3.1.3.6	Statistical analysis by comparison of means	43

3.1.4 Results and Discussion..... 43
3.1.4.1 USGS RMs isotopic results from LAGIR..... 43
3.1.4.1.1 Nd isotopic composition..... 44
3.1.4.1.2 Sr isotopic composition..... 45
3.1.4.2 Nd and Sr isotope compositions of the BRP-1 reference material..... 47
3.1.4.3 Nd and Sm mass fraction values..... 50
3.1.5 Conclusions..... 50
3.2 **2º Artigo científico: TIMS techniques for measuring strontium isotope ratios in apatite grains and application to igneous rock petrology**..... 51
3.2.1 Introduction..... 52
3.2.2 Materials and methods..... 53
3.2.2.1 Samples and Reference Materials..... 53
3.2.2.2 Analytical procedures..... 54
3.2.2.2.1 Chemical procedures..... 54
3.2.2.2.2 Surface leaching of apatite grains..... 55
3.2.2.2.3 Chemical digestion, chromatographic columns and resins..... 55
3.2.2.2.4 Ion exchange column calibration and chemical separation of Sr..... 55
3.2.2.3 U-Pb zircon LA-ICP-MS geochronology 57
3.2.2.4 Whole rock geochemistry..... 58
3.2.2.5 Whole rock TIMS Nd-Sr isotopes..... 58
3.2.2.6 ICP-MS analysis of Sr in apatites..... 59
3.2.3 Geological setting of studied apatite from granitoid rocks..... 60
3.2.4 Results..... 63
3.2.4.1 Measured isotope compositions of EN-1 and Durango Apatite..... 63
3.2.4.2 Zircons U-Pb ages..... 64
3.2.4.3 Initial $^{87}Sr/^{86}Sr$ ratio in whole rock..... 66
3.2.4.4 Statistical analysis by comparison of avareges..... 67
3.2.4.5 $^{87}Sr/^{86}Sr$ ratios of apatites from granitoid rocks of the Brasiliano orogen..... 67
3.2.4.5.1 Sample SMM-CMM-172..... 67
3.2.4.5.2 Sample BG-200..... 68
3.2.4.5.3 Sample BG-14B..... 69
3.2.5 Discussion..... 70

3.2.5.1 Relationship between $^{87}Sr/^{86}Sr$ isotopic fractionation and the Sr mass fraction in the reference materials and samples 70
3.2.5.2 Variability of $^{87}Sr/^{86}Sr$ ratios between apatite grains and whole rock analysis..... 73
3.2.5.3 Advantages and limitations of the technique..... 75
3.2.6 Conclusions..... 76
CONSIDERAÇÕES FINAIS..... 77
REFERÊNCIAS..... 79
APÊNDICE A – Material suplementar do 1º artigo científico..... 105
APÊNDICE B – Material suplementar do 2º artigo científico..... 124

INTRODUÇÃO

Os isótopos radiogênicos são produto do decaimento de isótopos radioativos a partir da emissão de radiação alfa, beta ou gama (OKUNO e YOSHIMURA, 2010). Esses isótopos têm sido amplamente utilizados como traçadores de fontes e processos dos mais variados ramos de pesquisa, abrangendo geociências, biologia, arqueologia, saúde humana, meio-ambiente, aplicações forenses, entre outros (BÜRGER et al. 2015). Nas geociências, sua aplicação é proeminente na geocronologia, utilizada para a obtenção de idades de rochas e minerais, e na geoquímica, como traçadores de fontes e processos geológicos de natureza endógena e exógena, assim como análise de proveniência petrogenética e sedimentar (FAURE, 1986, ROLLINSON, 1993; TESSALINA et al. 2014, AWADH, 2021).

Nesse sentido, os traçadores isotópicos fornecem informações petrogenéticas essenciais, que possibilitam, a identificação da participação relativa de fontes crustais e mantélicas em uma rocha. Assim, torna-se possível solucionar questões relacionadas à ocorrência e duração de eventos magmáticos, sedimentares e metamórficos (ALLÈGRE, 2008; FAURE, 1986). Tais interpretações permitem a construção de modelos a partir das reconstituições de eventos geológicos significativos (JAGER E HUNZIKER, 1977; DE PAOLO, 1988, ROLLINSON, 1993). De acordo com WU (2010), as composições isotópicas das amostras de rochas e minerais podem ser consideradas como uma assinatura análoga ao “DNA” dos seres vivos, sendo elementos fundamentais para compreender a história evolutiva dos materiais e processos geológicos.

A espectrometria de massas por termo-ionização (TIMS) é uma técnica analítica que mede razões isotópicas e destaca-se por sua mais alta sensibilidade e precisão dentre os demais métodos analíticos por espectrometria de massas, proporcionando a eliminação de interferências moleculares, resultante da eficiência na evaporação e ionização do analito (ALLÈGRE, 2008; CARLSON, 2014).

Contudo, é importante salientar que a TIMS apresenta desafios, especialmente relacionados à necessidade de separação química de elementos e digestão ácida das amostras visando a eliminação de interferências isobáricas e moleculares. Além disso, a técnica TIMS exige a implementação de procedimentos de microquímica, que por sua vez demandam condições rigorosas de filtragem e pureza do ar com uma sala tipo classe 100 com pressão positiva. Isso também implica na necessidade de cuidados específicos de limpeza e descontaminação de todos os recipientes utilizados, além da alta pureza dos reagentes.

Laboratórios que contribuem com dados para interpretações geológicas, necessitam de materiais de referências homogêneos e bem caracterizados (WEIS et al. 2022). É fundamental contar com instrumentos calibrados e submetidos a um rigoroso controle de qualidade nos procedimentos analíticos. Dessa forma, as amostras de composição isotópica desconhecidas são validadas por meio da medição de análises precisas, realizadas em condições de repetibilidade e reprodutibilidade de materiais de referência que acompanham todas as etapas analíticas das amostras. Esse processo assegura a confiabilidade dos dados, garantindo interpretações seguras e evidenciando a credibilidade dos dados analíticos (FAURE E POWELL 1972, FLANAGAN 1986, RACZEK et al. 2003, WRITE, 2005, WEIS et al. 2006, JOCHUM e ENZWEILER 2014, JWEDA et al. 2016).

A demanda por análises isotópicas precisas para estudos petrogenéticos, impulsionada pela crescente exigência do desenvolvimento de novas técnicas analíticas nos laboratórios, é a principal motivação para a elaboração desta Tese. Considerando a qualidade de infraestrutura e do avançado parque analítico disponível na Faculdade de Geologia da Universidade do Estado do Rio de Janeiro, optou-se por concentrar os esforços em análises isotópicas de estrôncio (Sr) e neodímio (Nd) em rocha total e no mineral apatita utilizando a espectrometria de massas por termo-ionização.

A aplicação dos procedimentos analíticos descritos em detalhe nesta pesquisa, juntamente com a implementação e/ou otimização de procedimentos analíticos, possibilita a caracterização das composições isotópicas de Sr-Sm-Nd em estudos de rocha total. Tais estudos possibilitam a classificação das rochas no que diz respeito à sua fonte, seja crustal ou mantélica, contribuindo para a compreensão de sua gênese e evolução. Além disso, permitem identificar processos relacionados a contaminação de fontes, mistura de magmas e os processos envolvidos na formação das rochas (McCULLOCH e WASSERBURG, 1978; FAURE, 1986).

A apatita, o fosfato mais abundante da Terra, encontra-se amplamente distribuída na litosfera e está presente em diversos tipos de rochas, ambientes e processos geológicos (RAKOVAN e HUGHES, 2013, RAKOVAN e SCOVIL, 2021), e tem se tornado um mineral importante para abordagem de questões fundamentais na história terrestre, como destacado por PICCOLI e CANDELA (2002) e KENNEDY et al. (2023). Deste modo, a pesquisa científica sobre esse mineral tem se expandido com a implementação de uma variedade de métodos isotópicos para abordar questões cosmoquímicas em meteoritos, assim como explorar a evolução e história lunar e marciana, conforme evidenciado por estudos como os de BELLUCCI et al. (2015), SANTOS et al. (2015) e GRANGE et al. (2013). A pesquisa dos

isótopos de Sr em apatita também oferece uma ampla gama de aplicações significativas, como o rastreamento de sistemas hidrotermais em depósitos minerais (ZHAO et al. 2015, TROLL, et al. 2019; DANESHVAR, et al. 2020; SUO, et al. 2023). Além disso, esses isótopos constituem excelentes marcadores para acompanhar a evolução isotópica da curva da água do mar (AHMAD et al, 2000, BURKE et al. 1982, CAPO E DEPAOLO, 1992; KANI e ISOZAKI, 2021). Nos estudos de cristais de apatita detrítica, sua importância abrange desde a geocronologia até a compreensão de processos tectônicos e erosivos. Comumente encontrados em sedimentos e rochas sedimentares, os isótopos atuam como indicadores das condições de deposição, e oferecem informações detalhadas sobre a origem dos sedimentos e as condições geológicas do ambiente deposicional (MORTON, et al. 2007, GLEASON et al. 2011; GILLESPIE et al. 2018). Adicionalmente, os isótopos de Sr em apatita desempenham um papel interessante em estudos arqueológicos, fornecendo dados essenciais para a reconstrução de padrões de mobilidade de populações antigas, refletindo as características geoquímicas das regiões e permitindo a identificação de migrações e deslocamentos populacionais ao longo do tempo (BENTLEY, 2002; SLOVAK, 2012; LAHTINEN et al. 2021).

Nos estudos dos isótopos de Sr em grãos de apatita, destaca-se sua aplicação como *proxy* para as razões iniciais de $^{87}Sr/^{86}Sr$ em investigações geológicas detalhadas de rochas ígneas, evidenciando a importância dessa metodologia. Para alcançar uma maior eficiência em relação à produção de análises isotópicas de Sr, é essencial desenvolver um procedimento que inclua a digestão da amostra e a separação dos elementos de interesse da matriz, utilizando métodos espectrométricos que envolvem digestão e separação química de maneira rápida e eficaz. Essa nova abordagem resulta em um aumento geral no rendimento químico/analítico em sala limpa, redução do branco laboratorial, uso otimizado de reagentes, menor custo e a manutenção da precisão alcançáveis por meio da espectrometria de massa de termo-ionização (TIMS).

A importância deste trabalho reside na crescente relevância e expansão das aplicações dos sistemas isotópicos Sm-Nd e Sr na geoquímica, particularmente em estudos envolvendo rocha total, sedimentos, aerossol e minerais específicos, representando um avanço significativo ao oferecer o desenvolvimento de procedimentos analíticos detalhados para a composição isotópica de Sm-Nd e Sr, garantindo dados analíticos confiáveis e precisos (GIOIA et al. 2017; VALERIANO et al. 2019; SANTOS et al. 2020, BRUNO et al. 2020; EVANGELISTA et al. 2021; NOGUEIRA, et al. 2021; ALMEIDA et al. 2022; CARVALHO et al. 2023).

Nesta tese foram exploradas duas vertentes analíticas: (i) análises Sm-Nd-Sr de alta precisão em rocha total e (ii) razões isotópicas de Sr em apatita de amostras de rochas granitoides. A estrutura dessa pesquisa é composta por três capítulos: no capítulo 1 são delineados os objetivos gerais e específicos propostos; no capítulo 2 são descritos os materiais e métodos utilizados nesse trabalho; e no capítulo 3 são reportados os resultados obtidos sob forma de dois artigos científicos. O trabalho se encerra com as considerações finais, referências bibliográficas e apêndices.

1 **OBJETIVOS**

1.1 **Objetivo geral**

O objetivo geral dessa pesquisa é desenvolver e otimizar procedimentos analíticos em amostras de rocha total e em apatita, visando a aplicação em estudos petrogenético regionais, utilizando os sistemas isotópicos Sm-Nd e Sr-Sr em espectrometria de massas por termo-ionização.

1.2 **Objetivos específicos**

Os objetivos específicos do trabalho são:

a) Estabelecer os procedimentos precisos para análise de rocha total, considerando diferentes combinações de digestão e separação química. Para isso, utilizou-se o material de referência BRP-1 (Basalto Ribeirão Preto) produzido pela Unicamp, com a colaboração de várias instituições, entre elas o Serviço Geológico do Brasil.

b) Determinar/otimizar um procedimento analítico preciso, mais rápido e de menor custo para determinação da composição isotópica inicial de uma amostra a partir da análise de isótopos de Sr em grãos de apatita por TIMS, utilizando amostras de rochas graníticas do magmatismo pré, sin e pós-colisional da Orogenia Ribeira.

2 **MATERIAIS E MÉTODOS**

Neste capítulo, são apresentados os materiais de estudo utilizado nos dois artigos resultantes desta pesquisa, oferecendo informações adicionais sobre as preparações e processamento de amostras que precedem esses procedimentos, os quais não foram incluídos nos artigos. Os métodos e os parâmetros analíticos empregados são brevemente descritos. O fluxograma apresentado na Figura 1 sintetiza as informações deste capítulo, abordando os materiais empregados e os processos realizados, resultando na obtenção dos produtos, que compreendem o artigo 1 e o artigo 2. Ambos serão apresentados na íntegra no Capítulo 3. Para oferecer uma visão mais completa, os apêndices A e B apresentam os materiais suplementares que foram utilizados como suporte aos capítulos de resultados dos artigos 1 e 2, incluindo figuras, tabelas e diagramas.

Figura 1 – Fluxograma de materiais e métodos indicando os processos (cor da fonte azul), materiais (cor da fonte vermelha) e produtos (cor da fonte verde). DI - diluição isotópica.

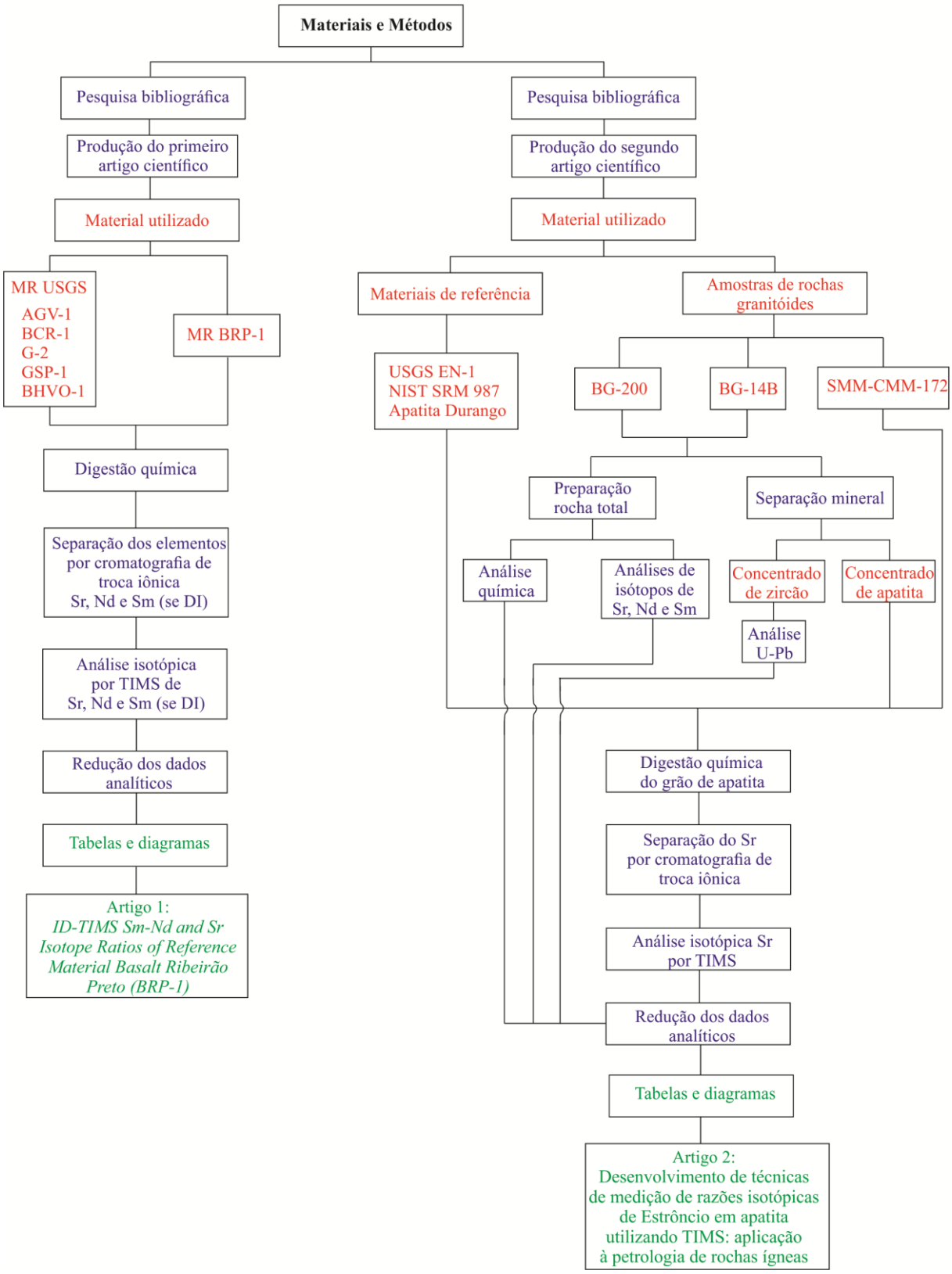

Fonte: A autora, 2025.

2.1 **Revisão bibliográfica**

A pesquisa bibliográfica realizada teve como base a revisão da literatura especializada disponível em livros, artigos e sites disponibilizados na internet, com base nos trabalhos anteriores relacionados à geologia isotópica dos métodos Sm-Nd e Sr e utilizando a técnica analítica TIMS.

Na primeira etapa, conduziu-se um levantamento bibliográfico abrangente dos métodos isotópicos, além das ferramentas analíticas empregadas para compreensão dos fundamentos conceituais da geoquímica dos sistemas isotópicos. Isso inclui análises de técnicas de microquímica e o estudo estatístico para comparação de dados.

Em seguida, foi organizada uma compilação das razões isotópicas Sr e Nd publicadas em periódicos dos materiais de referência do USGS, realizadas por TIMS, para compor a base de dados de comparação com os dados do LAGIR.

Por fim, foram consultados estudos sobre o desenvolvimento de procedimentos de separação química do Sr, Nd e Sm, de espectrometria de massas por termo ionização e tratamento dos dados analíticos em rocha total e em grãos de apatita, a fim se obter informações sobre quais métodos utilizar para tais fins, e o aprimoramento e refinamento dessas técnicas.

2.2 **Materiais de estudo**

2.2.1 Material de Referência: Basalto de Ribeirão Preto

Para desenvolver procedimentos analíticos visando a determinação das composições isotópicas Nd e Sr em amostras de rocha total, utilizou-se o material de referência (MR) BRP-1 de rocha total, produzido pela Universidade de Campinas (Unicamp), com a colaboração de várias instituições, entre elas o Serviço Geológico do Brasil (CPRM) e com o *United States Geological Survey* (USGS), seguindo os protocolos estabelecidos pela *International Association of Geoanalysts*, (IAG) (KANE et al. 2003, 2007, COTTA et al. 2007).

O MR BRP-1 foi produzido a partir de um basalto toleitico relacionado ao evento magmático Serra Geral do Cretáceo Inferior, que cobriu grandes porções da Bacia do Paraná, no sudeste do Brasil, há cerca de 130 Ma. Esse evento precedeu o processo de rifteamento continental que resultou na abertura do Oceano Atlântico Sul. A coleta de aproximadamente 180 kg de basalto ocorreu em uma pedreira da Formação Serra Geral, localizada nas proximidades da cidade de Ribeirão Preto, estado de São Paulo, nas coordenadas 21°15' S e 47°47' W (COTTA e ENZWEILER 2008).

Posteriormente, 150 kg desse material foram reduzidos a fragmentos de 3 a 5 cm por meio de uma prensa hidráulica de aço. Esses fragmentos foram enviados para o USGS em Denver, EUA, onde foram pulverizados com um britador de mandíbulas, seguido de um moinho de bolas, até atingirem um tamanho de partícula inferior a que 75 μm. O material resultante foi homogeneizado e dividido em 1920 frascos, cada um contendo 55 g (Cotta et al. 2007). Os valores de referência certificados do BRP-1 para os elementos terras raras seguem as diretrizes ISO (*International Organization for Standardization*), para materiais de referência, conforme citado em JOCHUM et al. (2016). Esse material foi submetido a rigorosos testes de homogeneidade (COTTA et al. 2007) e caracterização química, resultando na produção de um material geoquímico brasileiro com Certificado de Análise, publicado em COTTA e ENZWEILER (2008).

Desde 2009, quando uma alíquota do BRP-1 (frasco #18) foi disponibilizada no LAGIR, foram realizadas repetidas análises TIMS para fins de calibração interna. Essas análises seguiram os procedimentos químicos e espectrométricos estabelecidos para a determinação das razões isotópicas Sm-Nd e Sr.

2.2.2 Materiais de Referência do USGS

Adicionalmente, para verificar validar o método de medição das razões isotópicas de BRP-1, os RMs de rocha total do USGS, amplamente estudados em vários laboratórios ao redor do mundo como BCR-1 (*Basalt Columbia River*), BHVO-1 (*Basalt Hawaiian Volcanic Observatory*), AGV-1 (*Andesite Guano Valley*), G-2 (*Granite*), GSP-1 (*Granodiorite Silver Plume*) e EN-1 (*bilvalve shells; Enewatek lagoon, Marshall Islands*) foram analisados repetidamente no LAGIR. Os resultados dessas análises foram comparados com valores publicados no banco de dados GeoReM (http://georem.mpch-mainz.gwdg.de) sendo

utilizados para obter resultados precisos das razões isotópicas de Nd e Sr do MR BRP-1 (Tabela 1).

Tabela 1 – Valores de concentração certificados dos MRs do USGS

			Valores certificados (ppm) *					
MR USGS	Tipo	Nome/local	Sr	U	Nd	U	Sm	U
AGV-1	andesito	*Guano Valley, Lake County, Oregon, USA*	661	3,7	32,1	0,3	5,8	0,1
BCR-1	basalto Intraplaca continental	*Columbia River Group basalt, Bridal Veil Flow Quarry, Washington, USA*	335	3,5	28,7	0,1	6,6	0,0
G-2	granito	*Westerly granite, from Sullivan quarry, Bradford, Rhode Island, USA*	475	6,1	53,8	0,7	7,2	0,1
GSP-1	granodiorito	*Silver Plume, Colorado, USA*	234	5,4	196	3,3	26,3	5,5
BHVO-1	basalto Intraplaca oceânico	*Kilauea caldera, Kilauea volcano, Hawaii, USA*	399	5,0	24,3	0,3	6,2	0,1
EN-1	conchas bivalves	*Enewatek lagoon, Marshall Islands*	1400					

Legenda: U- incerteza; *Referência: JOCHUM et al. (2016).

2.2.3 Material de Referência mineral: Apatita Durango

A apatita Durango é uma fluorapatita encontrada na mina de ferro a céu aberto em Cerro de Mercado, ao norte da cidade de Durango, no México. Se manifesta como grãos de granulometria grossa, apresentando uma coloração amarelo-esverdeada, livres de inclusões fluidas e sólidas, e tem a sua origem associada a processos hidrotermais relacionados a rochas vulcânicas alcalinas do Oligoceno (LYONS, 1988). Com uma idade U-Pb ID-TIMS de 32,7 ± 0,1 Ma (PAUL et al. 2021) e uma concentração de Sr de 486 ppm, a apatita Durango é utilizada como material de referência em diversos tipos de análises, incluindo a de elementos traço (BRUAND et al., 2014), U-Th/He e datação por traço de fissão (HASEBE et al. 2004; al., 2005; FLOWERS et al. 2009) análise de microssonda em halogênios (HAMMOUDA et al. 2010) e isótopos de U-Pb, Nd e Sr (FISHER 2011; YANG et al. 2014).

2.2.4 Amostras de rochas granitóides

2.2.4.1 Amostras BG-200 e BG-14B

A campanha de campo para coleta de amostras foi realizada em junho de 2020 pelos Professores Dr. Claudio Valeriano, Dr. Henrique Bruno e Dra. Monica Heilbron. Foram selecionadas amostras de rochas graníticas do magmatismo sin- e pós-colisional da Orogenia Ribeira (BG-200 e BG-14B) para determinação da composição isotópica de Sr em grãos de apatita, aplicando os procedimentos analíticos descritos neste trabalho.

O ortognaisse de composição granítica e idade Ediacarana, intrusivo no Complexo Rio Negro (TUPINAMBÁ et al., 2000; 2012), representa o exemplar sin-colisional desta pesquisa na região de Petrópolis, Rio de Janeiro, correspondente à unidade Bingen, conforme descrito em PENHA et al. (1980). A amostra BG-200, coletada nas coordenadas -22,55499, -43,22531 (WGS-84), é caracterizada como um biotita gnaisse sienogranítico homogêneo, conforme o diagrama QAP (STRECKEISEN, 1976), apresentando quartzo, K-feldspato, plagioclásio, biotita e minerais acessórios, como zircão e apatita. Possui granulação média a grossa e textura inequigranular, devido à presença de megacristais de plagioclásio. Com base no teor de SiO_2 e álcalis ($Na_2O + K_2O$), a amostra é classificada como granito, segundo COX et al. (1979) caracterizada por um alto teor de SiO_2 de 69,7% em peso e $Na_2O + K_2O$ de 6,9% em peso, com uma afinidade cálcio-alcalina fracamente peraluminosa e de alto K. A amostra exibe fracionamento pronunciado entre LREE e HREE, posicionando-a dentro do campo de granitóides de arco vulcânico (PEARCE et al. 1984).

A amostra BG-14B, localizada nas coordenadas -22.603.914 e -43.28459 (WGS84), intrusiva do Complexo Rio Negro (TUPINAMBÁ et al. 2000; 2012) e é classificada como um granitóide pós-colisional cambriano. A rocha exibe granulação fina a média com uma textura inequigranular e os conjuntos minerais desta amostra incluem quartzo, plagioclásio, biotita e minerais acessórios como hornblenda, zircão e apatita. É caracterizado por uma composição química diorítica, segundo COX et al. (1979), com baixo teor de SiO_2 56,2% em peso e $Na_2O + K_2O$ totalizando 5,5% em peso, e exibe uma afinidade metaluminosa, cálcio-alcalina. A amostra mostra fracionamento fraco entre LREE e HREE e plota dentro do campo de granitóides de arco vulcânico (PEARCE et al. 1984).

Para calcular a razão inicial $^{87}Sr/^{86}Sr$ da rocha, de acordo com a equação fundamental da geocronologia (FAURE, 1986), necessária para comparação com as razões $^{87}Sr/^{86}Sr$ medidas em grãos de apatita, foram utilizados dados de análise isotópica da razão $^{87}Sr/^{86}Sr_{(0)}$, as concentrações de Rb e Sr (em ppm) obtidas na análise química de rocha total e a idade U-Pb em zircão das amostras BG-200 e BG-14B, realizadas nesse trabalho.

2.2.4.2 Amostra SMM-CMM-172

A amostra SMM-CMM-172 (PEIXOTO et al. 2017), coletada na região noroeste do Estado do Rio de Janeiro, está localizada nas coordenadas -21,75413, -42,99508 (WGS-84) e representa os ortognaisses do Complexo Rio Negro, no Domínio Costeiro da Orogenia Ribeira. Este exemplar, classificado como pré-colisional e datado em 629 ± 10 Ma (U-Pb em zircão; PEIXOTO et al. 2017), corresponde a um ortognaisse, cuja composição química granodiorítica é classificada segundo COX et al. (1979). Apresenta granulação grossa e pode exibir uma estrutura variando de magmática a fracamente foliada, com mineralogia predominante de ortoclásio, quartzo e plagioclásio, sendo a biotita o principal componente máfico identificado (PEIXOTO et al. 2017).

2.3 **Preparação de amostras de rocha total**

A preparação das amostras BG-200 e BG-14B foi realizada no Laboratório Geológico de Processamento de Amostras (LGPA) da Faculdade de Geologia (FGEL) da Universidade do Estado do Rio de Janeiro (UERJ). A preparação envolveu processos de pulverização para análise química e isotópica e concentração de minerais pesados para seleção de grãos de apatita (isótopos de Sr) e zircão (análises U-Pb).

Inicialmente, uma amostra representativa, livre de alterações do intemperismo, foi submetida à britagem manual, utilizando uma bigorna e um martelo, para redução da amostra até a fração de aproximadamente de 1 cm.

Posteriormente, as amostras foram quarteadas até obter-se uma quantidade de aproximadamente 100 g. Em seguida, foram processadas no moinho de bolas de carbeto de

tungstênio por 10 minutos, resultando em um material pulverizado na fração granulométrica < 75 µm, representando assim, a fração rocha total.

2.4 **Separação de minerais pesados (apatita e zircão)**

Na campanha de campo, foram coletados aproximadamente 15 kg das amostras BG-200 e BG-14B isentas de intemperismo, representativas de sua unidade geológica, destinada à concentração de minerais pesados. O objetivo era separar os grãos de apatita para o estudo das razões isotópicas de Sr e o grãos de zircão para determinação da idade de cristalização U-Pb. O processo de desfragmentação foi conduzido por meio de um britador de mandíbulas e moinho de discos. Em seguida, a amostra foi submetida à mesa hidrodinâmica para a separação dos grãos pela diferença de densidade.

Após a secagem do material concentrado na mesa, realizou-se uma segunda separação densimétrica com bromofórmio, isolando os minerais de densidade > 2,65 g/cm^3. Em seguida, efetuou-se a separação dos minerais magnéticos com o auxílio de um imã de mão e, por fim, a separação eletromagnética no Frantz®. A fração eletromagnética, que concentra os cristais de zircão e apatita livres de inclusões, foi obtida na etapa final do Frantz (FF), com a régua inclinada a -1/2º, caracterizando-se como a fração não-atraível.

Os grãos de zircão das amostras BG-200 e BG-14B foram selecionados em uma lupa binocular e montados com resina epóxi de alta dureza e polidos para exposição dos centros dos grãos. Para o imageamento em um microscópio eletrônico de varredura (MEV), aplicou-se uma fina camada de ouro para metalização da superfície. Foram realizados mapas EDS (*Energy Dispersive X-ray Spectroscopy*) sobrepostos em imagens SEM-BSE (*Backscattered electron*) e SEM-CL (catodoluminescência) para identificação de diferenças químicas, estruturas internas e seleção dos alvos para análises isotópicas *in situ*. As imagens SEM-CL dos grãos de zircão foram obtidas no Laboratório de Geocronologia Isotópica da Escola de Minas da Universidade Federal de Ouro Preto (UFOP).

2.5 **Análise química elementar em rocha total**

As análises químicas de duas amostras de rocha total (BG-200 e BG-14B) foram realizadas no laboratório ACTLABS (*Activation Laboratories Ltda*) em Ontário, no Canadá. O pacote analítico 4Litho compreende combinações de pacotes de códigos preparados e analisados em um sistema em lote, incluindo um branco de reagente do método e um material de referência certificado. O *Code* 4B refere-se à técnica de fusão de metaborato/tetraborato de lítio TD-ICP-OES (*Total Digestion - Inductively Coupled Plasma)*, utilizada para a análise de elementos maiores e dos elementos Ba, Sc, Sr, V, Y e Zr. A análise dos elementos terras raras é realizada com o *Code* 4B2 por ICP-MS (*Inductively Coupled Plasma - Mass Spectrometry*) utilizando um PerkinElmer Sciex ELAN ICPMS. A recalibração de rotina do instrumento é executada a cada 40 amostras. Detalhes específicos sobre a metodologia analítica podem ser encontrados em http://www.actlabs.com - *Geochemistry/Assay - Methods - Code 4E-Research*.

2.6 **Análise dos isotópicos de Estrôncio, Samário e Neodímio**

As amostras pulverizadas foram encaminhadas ao Laboratório de Geocronologia e Isótopos Radiogênicos (LAGIR; VALERIANO et al. 2003), localizado na Faculdade de Geologia (FGEL) da Universidade do Estado do Rio de Janeiro (UERJ), para análise isotópica a partir da separação química dos elementos Sr, Sm e Nd e espectrometria de massa. O LAGIR conta com um moderno sistema de climatização e filtragem de ar, onde os procedimentos químicos e espectrométricos são realizados em salas limpas, sob pressão positiva e filtros HEPA, incluindo as capelas de fluxo laminar. As análises espectrométricas são executadas em um espectrômetro de massas por termo-ionização (TIMS), modelo TRITON multicoletor da ThermoScientific®.

Os reagentes e recipientes utilizados, bem como a descrição dos procedimentos químicos e espectrométricos das análises isotópicas de Sr, Sm e Nd em rocha total e Sr em grãos de apatita, constituem o objeto de estudo desta tese e estão detalhados no artigo apresentado nos resultados do capítulo 4.

2.7 **Análise química de Sr em grãos de apatita**

As análises químicas de Sr em grãos de apatita das amostras SMM-CMM-172, BG-200 e BG-14B foram realizadas em ICP-MS Element XR (Thermo) no Laboratório de Geologia Isotópica (LAGIS) do Instituto de Geociências da Universidade Estadual de Campinas (Unicamp). A digestão química das amostras foi realizada no LAGIR. Foram selecionados 10 grãos de apatita de cada amostra utilizando uma lupa binocular e transferidos para recipientes Savillex® e adicionados 200 µl de HNO_3 65% supra puro. Após, os recipientes fechados foram colocados em chapa aquecedora a 140 ^oC por 24 horas e em seguida foram abertos e mantidos em uma chapa aquecedora a 90 ^oC até a evaporação completa, em capela de exaustão.

No LAGIS, as amostras secas foram retomadas em 10 ml de HNO_3 1%. Todas as soluções foram preparadas com água ultrapura (18,2 MΩ.cm), obtida por sistema Milli-Q® e os ácidos foram purificados por sub-ebulição. Os frascos utilizados para as diluições foram previamente limpos com HNO_3 10% e enxaguados com água ultrapura. O limite de detecção (LD) foi determinado como sendo a média (x) mais 3 desvios-padrão (s) de dez medidas do branco do laboratório (LD= x +3s). O controle de qualidade das medidas foi efetuado pela análise de material de referência BRP-1 (COTTA et al. 2008).

2.8 **Geocronologia Urânio-Chumbo em zircão**

As datações U-Pb em zircão (LA-ICP-MS) foram realizadas no Laboratório de Geocronologia Isotópica da Escola de Minas da Universidade Federal de Ouro Preto (UFOP), utilizando equipamento *Element 2* da ThermoScientific®, com SF-ICP-MS acoplado e sistema de laser CETAC LSX-213 G2+ (λ = 213 nm) Nd: YAG. Duas amostras, BG-200 e BG-14B, foram analisadas por ablação a laser para obtenção das razões isotópicas pelo método U-Pb, empregando um *spot* de 20 µm, frequência de laser de 10 Hz e fluência de ~3 J/cm^{-2}. O MR primário GJ-1, utilizado para calibração, com idade de 602 ± 0,4 Ma (2s) e razões $^{207}Pb/^{206}Pb$ de 0,06014 e $^{206}Pb/^{238}U$ de 0,09891 (JACKSON *et al* 2004), e o MR secundário BB9, com idade de 565,1 ± 1,8 Ma (2s; SANTOS et al. 2017), foram utilizados para avaliar a acurácia e precisão.

3 **RESULTADOS**

Os resultados obtidos foram consolidados em dois artigos científicos para a publicação em periódicos internacionais especializados:

a) O primeiro artigo, intitulado "*ID-TIMS Sm-Nd and Sr Isotope Ratios of Reference Material Basalt Ribeirão Preto (BRP-1)"*, aborda procedimentos químicos e espectrométricos detalhados em rocha total em materiais de referência do USGS e do BRP-1 e está publicado na revista *Geostandards and Geoanalytical Research*, (NETO et al. 2023).

b) O segundo artigo intitulado *"TIMS techniques for measuring strontium isotope ratios in apatite grains and application to igneous rock petrology"*, trata da implantação, desenvolvimento/otimização da técnica analítica em isótopos de Sr em apatita em TIMS, explorando o potencial da composição isotópica de Sr em grãos de apatita de rochas magmáticas como um *proxy* para razões iniciais de $^{87}Sr/^{86}Sr$.contendo sua aplicação em três estudos de casos em rochas granitoides do magmatismo pré, sin e pós-colisional da Orogenia Ribeira, Este manuscrito, foi submetido para avaliação no periódico *Chemical Geology* em 24 de fevereiro de 2025.

3.1 **ID-TIMS Sm-Nd and Sr isotopic composition of reference material Basalt Ribeirão Preto (BRP-1)**

Vol. 47 — N° 4 12 23 p. 841 – 854

GEOSTANDARDS and GEOANALYTICAL RESEARCH

ID-TIMS Sm-Nd and Sr Isotope Ratios of Reference Material Basalt Ribeirão Preto (BRP-1)

Carla **Neto** (1, 2, 3)*, Claudio de **Morisson Valeriano** (1, 2), Jacinta **Enzweiler** (4), Gabriel **Paravidini** (2, 3), Manuela **Carvalho** (2, 3, 5), Monica **Heilbron** (1, 2), Cristiano **Lana** (6) and João Henrique **Larizzatti** (7)

(1) Laboratório de Geocronologia e Isótopos Radiogênicos, LAGIR, Universidade do Estado do Rio de Janeiro, Rua São Francisco Xavier 524, 20550-013 Rio de Janeiro, RJ, Brazil
(2) Grupo de Pesquisa em Geotectônica, Tektos/UERJ, Universidade do Estado do Rio de Janeiro, Rua São Francisco Xavier 524, 20550-013 Rio de Janeiro, RJ, Brazil
(3) Programa de Pós-graduação em Geociências, PPGG/UERJ, Universidade do Estado do Rio de Janeiro, Rua São Francisco Xavier 524, 20550-013 Rio de Janeiro, RJ, Brazil
(4) Universidade de Campinas, Unicamp, Rua Carlos Gomes 250, Cidade Universitária, 13083-855 Campinas, SP, Brazil
(5) Fundação de Amparo à Pesquisa do Estado do Rio de Janeiro, FAPERJ, Avenida Erasmo Braga 118, 20020-000 Rio de Janeiro, RJ, Brazil
(6) Departamento de Geologia, Escola de Minas, Universidade Federal de Ouro Preto, Campus Universitário Morro do Cruzeiro s/n, 35400-000, Ouro Preto, MG, Brazil
(7) Serviço Geológico do Brasil, CPRM, Avenida Pasteur 404, 22290-240 Rio de Janeiro, RJ, Brazil
* Corresponding author. e-mail: neto.carla@hotmail.com

This work presents Sm-Nd and Sr isotopic ratios of the BRP-1 ("Basalt Ribeirão Preto") reference material (RM) based on repeated TIMS measurements over twelve years carried out by the LAGIR laboratory, Brazil. The BRP-1 RM was produced by the Brazilian Geological Survey from a *ca.* 130 Ma within-plate basalt, collected from a quarry near Ribeirão Preto city in the Paraná basin. Isotope ratios were measured using a TRITON mass spectrometer. Instrumental bias and fractionation corrections were performed based on repeated measurements of the certified RMs JNdi-1 and NIST SRM 987. The measured Nd and Sr isotopic ratios of BRP-1 are: $^{143}Nd/^{144}Nd = 0.512408 \pm 0.000010$ (2*s*), and $^{87}Sr/^{86}Sr = 0.706011 \pm 0.000017$ (2*s*). The mass fractions of Sm and Nd are 11.0 ± 0.2 and 51.9 ± 0.6 µg g^{-1}, respectively, showing no significant differences compared with the accepted values from the literature. No significant difference between measurements was observed, whether digesting samples in single or batch mode, using metal-jacketed PTFE bombs or PFA vials, or with or without the addition of a spike. The accuracy of these results was evaluated through the measurement of well-characterised USGS RMs, such as AGV-1, BCR-1, BHVO-1, G-2 and GSP-1.

Keywords: reference material, radiogenic isotopes, chemical digestion, isotope dilution, ion exchange chromatography.

Received 20 Jul 22 – Accepted 14 Mar 23

3.1.1 Introduction

Well-characterized rock and mineral RMs are necessary for isotope geochemistry and geochronology laboratories (WEIS et al. 2022), used for calibration of instruments, and routine quality control of analytical data (FLANAGAN 1986, RACZEK et al. 2003, WEIS et al. 2006, JOCHUM and ENZWEILER 2014, Jweda et al. 2015). Therefore, RMs with

accurately (precise and unbiased) measured isotopic ratios are widely used in geochemical, geochronological, petrogenetic, and sedimentary provenance studies, as well as in biological, and human health, environmental and forensic applications (BÜRGER et al. 2005). This requires repeated analyses of the RMs, that accompany all analytical steps of the samples (FAURE and POWELL 1972, WHITE 2005).

This research reports the first detailed Sm-Nd and Sr isotope compositional data for the Basalt Ribeirão Preto BRP-1 RM (COTTA et al. 2007, COTTA et al. 2008, COTTA and ENZWEILER 2008; BABINSKI et al. 2014). The isotope data reported results from 53 and 63 analyses of $^{143}Nd/^{144}Nd$ and $^{87}Sr/^{86}Sr$ ratios, respectively. Using certified Nd and Sr solution RMs, respectively JNdi-1 and NIST SRM 987, the measured isotope ratios were corrected for mass fractionation and instrumental bias. This work also evaluated different combinations of chemical digestion procedures to check whether there are differences in resulting isotope ratios.

In order to access the accuracy of the BRP-1 results, analyses of the BCR-1 (Columbia River Basalt), BHVO-1 (Basalt Hawaiian Volcanic Observatory), AGV-1 (Andesite Guano Valley), G-2 (Granite) and GSP-1 (Granodiorite Silver Plume) rock RMs from the United States Geological Survey, USGS were performed and the results subjected to classic statistical tests for comparison between groups of results and comparison with literature reference data.

3.1.2 The BRP-1 Reference Material

The BRP-1 basalt is a whole-rock RM prepared by researchers from the State University of Campinas (Unicamp) and by the Brazilian Geological Survey (CPRM), in collaboration with the USGS and following IAG protocols (COTTA et al. 2007, COTTA et al. 2008, KANE et al. 2003, 2007). BRP-1 RM certified reference values for trace elements follow ISO guidelines for frequently requested rock reference materials, as cited in JOCHUM et al. (2016). It is the only continental within-plate Cretaceous basalt among the main RMs, e.g. BHVO-1, BCR-1, BIR-1, BEM, BE-N, JB-1 and JB-2 (Supplementary Material 1 Table S1.1).

The BRP-1 RM was produced from a tholeiitic basalt belonging to the Early Cretaceous Serra Geral magmatic event, which flooded large portions of the Paraná Basin, southeast Brazil, at *ca.* 130 Ma, preceding continental rifting that led to the opening of the South Atlantic Ocean. Approximately 180 kg of basalt were collected from a quarry located

near Ribeirão Preto city, São Paulo State, at coordinates 21º15 'S and 47º47' W (COTTA and ENZWEILER, 2008). Approximately 150 kg of the material was reduced to 3 to 5 cm size fragments using a steel hydraulic press and sent to the USGS in Denver, USA, where it was pulverized with a jaw-crusher, followed by a ball mill, to a particle size smaller than 75 μm. The material was then homogenized and split into 1920 vials, each one containing 55 g (COTTA et al. 2007).

The BRP-1 RM was rigorously submitted to homogeneity tests (COTTA et al. 2007) and chemical characterization to represent a Brazilian geochemical material with a Certificate of Analysis published in COTTA and ENZWEILER, (2008). The BRP-1 is available for distribution and may be ordered directly from the Geological Survey of Brazil (CPRM), which encourages widespread laboratory use.

3.1.3 Materials and Methods

This section briefly describes the chemical and the TIMS mass spectrometric procedures carried out at the Laboratory of Geochronology and Radiogenic Isotopes (LAGIR, VALERIANO et al. 2003) of the Rio de Janeiro State University (UERJ), including the statistical treatment of the analytical data.

Since 2009, when a BRP-1 aliquot (bottle #18) was made available at the LAGIR, repeated TIMS analyses have been performed for internal calibration purposes, following established chemical and spectrometric procedures for the determination of the Sm-Nd and Sr isotopic compositions, which are not available in the literature for this RM.

Additionally, in order to check the accuracy of the measurement of BRP-1 isotopic ratios, USGS whole-rock RMs were also repeatedly analyzed, and the results were compared with published values in the GeoReM (http://georem.mpch-mainz.gwdg.de).

3.1.3.1 Chemicals reagents and vessels

The chemical and spectrometric procedures were performed in clean rooms under positive air pressure and HEPA filters. All chemical procedures were performed within HEPA-filtered laminar flow hoods.

High purity acids, HF (48 % *m/v*)**,** HCl (37 % *m/v*) and HNO_3 (65 % *m/v*)**,** (all p.a. grade, Merck KGaA, Darmstadt, Germany) were produced by double distillation using a sub-boiling unit DST-1000, Savillex (Eden Prairie, MN, USA) except for H_3PO_4 (85 % *m/v*)**,**

which is bought in supra-pure quality (p.a. grade, Merck KGaA, Darmstadt, Germany). Ultrapure water (18.2 $\Omega \bullet cm^{-1}$) was obtained by 1 µm, 3 µm and 5 µm particle filtration, followed by deionization using Rios5 (Millipore, SP, Brazil) device and further purification with a NanoPure® unit (Milli Q-Millipore, SP, Brazil).

For measurements using the isotope dilution (ID) technique, a ^{150}Nd-^{149}Sm double spike solution was used, kindly donated by Dr William Randall Van Schmus, from Kansas University (KU). The compositional and isotopic characteristics of the KU spike are described in Table 2.

Table 2 - Isotopic composition of the KU ^{149}Sm-^{150}Nd mixed tracer solution.

Ratio	Value	Ratio	Value
$^{144}Sm/^{149}Sm$	0.000286405	$^{142}Nd/^{150}Nd$	0.004211417
$^{147}Sm/^{149}Sm$	0.003765752	$^{143}Nd/^{150}Nd$	0.002507536
$^{148}Sm/^{149}Sm$	0.007901039	$^{144}Nd/^{150}Nd$	0.005069650
$^{150}Sm/^{149}Sm$	0.005723202	$^{145}Nd/^{150}Nd$	0.002213552
$^{152}Sm/^{149}Sm$	0.003975750	$^{146}Nd/^{150}Nd$	0.004477888
$^{154}Sm/^{149}Sm$	0.001731610	$^{148}Nd/^{150}Nd$	0.003742278

Note.: [149Sm] = 3.4000 ug g-1 and [150Nd] = 3.0354 ug g-1

Prior to use, all containers, i.e. Parr®-type steel-jacketed PTFE bomb (20 ml) and PFA Savillex® vials (10 ml, 15 ml and 22 ml) were cleaned on hot plates following three alternate cycles of 6 mol l^{-1} HCl and H_2O at 90 °C for 1 day each, during a total of six purifying procedure days.

3.1.3.2 Chemical digestion

Several combinations of digestion procedures were tested over time, regarding vessel type (PTFE bomb or PFA vial), and single or batch sample digestion.

In the single digestion procedure, between 16 mg and 58 mg are digested and the resulting solution was loaded entirely in one single chromatographic column. The sample mass of single digestion was repeatedly changed aiming for optimal conditions of chromatographic separation and resulting beam intensity in the mass spectrometer (Figure 4).

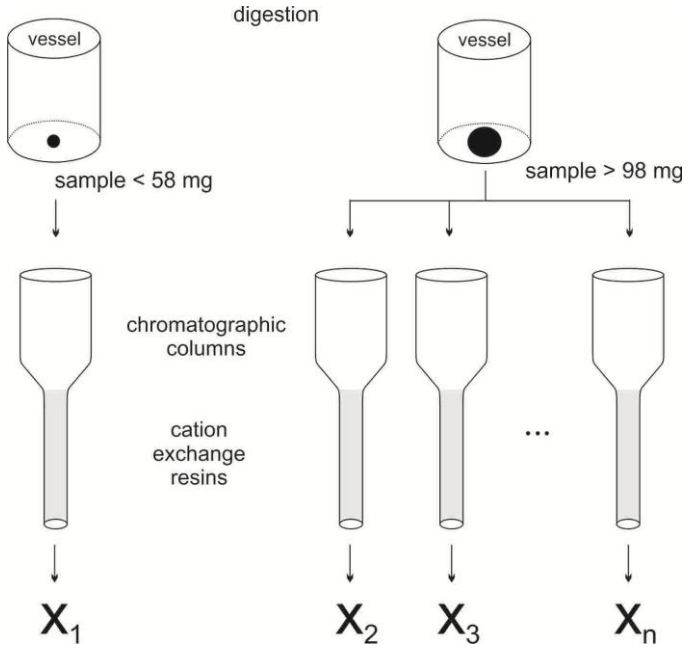

Figure 2 - Overview of the analytical procedure. X_n represents one isotopic ratio analysed in the mass spectrometer referring to the sample loaded in the chromatographic column.

In the batch digestion, larger sample masses are digested and prior to the chromatographic separation the resulting solution was divided into smaller aliquots with equivalent sample mass to single digestion. After each aliquot is separated, the solution was stored in 2.5 mol l^{-1} HCl and then used in different series and periods of analysis. Each of these aliquots was reported as a single spectrometric measurement in the analytical data of Supplementary Material 2 Figures S2.1, S2.2 and S2.3 and Supplementary Material 3 Tables S3.1, S3.2 and S3.3.

The samples were analysed with or without the addition of the isotopic spike solution and are referred to as respectively Isotope Dilution (ID) or "natural" analyses. When measured by ID, a mixed ^{150}Nd-^{149}Sm isotopic spike solution was added to the sample prior to digestion in order to ensure thorough homogenisation. The amount of spike added was that calculated to achieve equivalent signals of ^{150}Nd (the most abundant isotope in the spike) and ^{144}Nd (one of the most abundant isotopes in the sample) during spectrometric measurements (DICKIN, 2005).

The digestion was performed in a 5-day cycle: the first 3 days using a mixture of HF (3 ml) and **7** mol l^{-1} HNO_3 (0.5 ml), followed by 2 days using 3 ml of 6 mol l^{-1} HCl. For high-pressure digestion of PTFE bombs, 3 days within stove with steel-jacketed in temperature 180 ºC and PFA vials, 3 days on a hotplate at 130 ºC. After digestion, the containers were cooled and opened for evaporation in a hotplate at 90 ºC.

The digestion method used at LAGIR has evolved over time, during which several combinations between vessel types, spike addition or absence, and of single or batch digestion were tested. Since January 2018, however, the specific configuration of single isotopic digestion in PFA vials, with the addition of a double (Sm-Nd) isotopic spike has been followed as a standard procedure.

3.1.3.3 Chromatographic procedures

Elements of interest (Sr, Sm, Nd) were separated using cation exchange column chromatography procedures after adding 1 ml of 2.5 mol l^{-1} HCl to the previously dried sample. The columns used in LAGIR for the elution Sr and REE, referred to as the primary column, have an internal diameter of 6 mm and height of 150 mm, filled with 136 mm of the Bio-Rad® AG-50W-X-8 (200-100 mesh) resin (Bio-Rad Laboratories, Inc, USA) stocked in 2.5 mol l^{-1} HCl. The resin conditioning was carried out with 10 ml of 2.5 mol l^{-1} HCl and then, 1 ml of the sample dissolved in 2.5 mol l^{-1} HCl was loaded into the column. The column cup was washed afterwards three times with 1 ml 2.5 mol l^{-1} HCl, rinsing its sides with the help of a pipette to ensure that the entire sample passed through the resin. Subsequently, 21 ml of 2.5 mol l^{-1} HCl was added to the resin and discarded to eliminate the matrix elements of the sample. Next, in a new clean vial, 8 ml of 2.5 mol l^{-1} HCl was used for elution of the Sr, followed by the discarding of 3 ml of solution. The REE elution was also performed in a clean vial with the addition of 15 ml 6 mol l^{-1} HCl. The REE solution was then left to evaporate on a hot plate at ~ 90-100 °C to dryness. After the REE solution was dry, it was added 0.2 ml of 0.18 mol l^{-1} HCl for the re-dissolution (conditioning) of the sample.

The separation of Nd and Sm was then performed in PFA secondary columns, which have an internal diameter of 4 mm and height of 120 mm, filled with 78 mm Eichrom® LN-Spec (50-100 μm) resin (Eichrom Technologies, Lisle, IL, USA). The resin was previously conditioned with 3 ml of 0.18 mol l^{-1} HCl. The sample was transferred to the secondary column and then the cup and its sides were washed and rinsed three times with 0.2 ml of 0.18 mol l^{-1} HCl. Afterwards 9 ml of 0.18 mol l^{-1} HCl were discarded, and, in a clean vial, the Nd fraction was collected with 3 ml of 0.18 mol l^{-1} HCl. The next 2 ml of 0.18 mol l^{-1} HCl were discarded, and the elution of Sm was carried out with 2 ml 0.5 mol l^{-1} HCl in a new clean vial. A matrix-free Nd cut is important to minimise isobaric interference given by Sm that can compromise the resulting isotopic ratios, since this element ionizes at the same temperature during TIMS analyses.

Before storage, the primary and secondary columns were both cleaned with 6 mol l^{-1} HCl and respectively conditioned in 2.5 mol l^{-1} HCl and in 6 mol l^{-1} HCl. The total chemical procedure is detailed in Table 3.

Table 3 - Chemical procedures for elution Sr, Nd, and Sm

Task	HCl concentration (mol l^{-1})	Capacity (ml)
Elution Sr and REE (primary column)		
Sample conditioning	2.5	1
Resin conditioning	2.5	10
Sample transfer		
Column cup washing (rinsing)	2.5	1
	2.5	1
	2.5	1
Discard	2.5	21
Change to a clean vial		
Elution of Sr	2.5	8
Discard	2.5	3
Change to a clean vial		
Elution of REE	6	15
Cleaning of resin	6	Fill columns and cup
Resin conditioning and storage	2.5	Fill columns
Elution Nd and Sm (secondary column)		
Sample conditioning	0.18	0.2
Resin conditioning	0.18	3
Sample transfer		
Column cup washing (rinsing)	0.18	0.2
	0.18	0.2
	0.18	0.2
Discard	0.18	9
Change to a clean vial		
Elution of Nd	0.18	3
Discard	0.18	2
Change to a clean vial		
Elution of Sm	0.5	2
Cleaning of resin	6	Fill columns and cup
Resin conditioning and storage	0.18	Fill columns

The solutions are taken to a hotplate at ~ 90 ºC for complete evaporation and then loaded onto previously degassed double Re filaments (H-Cross, USA), with 2 µl of 0.33 mol

l^{-1} H_3PO_4 as ionization activator and dried under a 2.5 A current. For some Sr analyses, Ta single filaments were used. The "sandwich" technique for activation of ionization, described in the TRITON HARDWARE MANUAL (2002), was adopted, with 1 µl of 0.33 mol l^{-1} H_3PO_4 between (1+1) µl of Ta_2O_5, and dried under a current of up to 2.0 A.

3.1.3.4 Thermal Ionization Mass Spectrometry

The measurements of Sr, Nd and Sm isotope composition samples were accomplished with the TRITON Thermo-Scientific thermal-ionization multi-collector mass spectrometer, in operation since 2006. For the Sr analyses in Re double filaments, an array of 5 Faraday cups (Table 4) was used for the 100 measurement cycles. Electric currents of the ionization and evaporation filaments were respectively, 3200 mA and ranged from 1800 mA to 2200 mA or ionization temperatures close to 1300 ºC, in Ta single filaments analyses (n = 9). All isotopic ratios were corrected for isobaric interference of Rb ($^{87}Rb/^{85}Rb$ = 0.386, MEIJA et al. 2015, BÜRGER et al. 2005) and for mass fractionation assuming the stable $^{88}Sr/^{86}Sr$ ratio of 8.375209 (NIER, 1938).

For the Sm and Nd analyses, electric currents of the ionisation and evaporation filaments were 4500 mA and ranged from 2000 mA to 2200 mA, respectively. For each run, 160 cycles were analysed for Nd and 80 cycles for Sm, using an array of eight Faraday cups (Table 4). The isotopic ratios were corrected for mass fractionation using the constant $^{146}Nd/^{144}Nd$ ratio of 0.7219 (PATCHETT, 1989) and $^{152}Sm/^{149}Sm$ = 0.56083 (DE PAOLO, 1981). Beam intensities average were approximately 8000 mV for ^{88}Sr, 500 mV for ^{146}Nd and 300 mV for ^{147}Sm. In data acquisition, the $^{85}Rb/^{86}Sr$ and $^{147}Sm/^{144}Nd$ ratios were used to monitor the quality of chemical separation and assessment of isobaric interference. If these ratios are below 10^{-5}, they are considered as indicating negligible interference. The total blanks yielded amounts below 200 pg for Nd and 70 pg for Sm and were considered negligible for the isotopic ratio correction. All the measurements were performed with TIMS operating parameters listed in Table 5.

Table 4 - Multi-collector cup configuration.

Faraday cups	L4	L3	L2	L1	Central	H1	H2	H3
Nd	^{142}Nd	^{143}Nd	^{144}Nd	^{145}Nd	^{146}Nd	^{147}Sm	^{148}Nd	^{150}Nd
Sm	^{146}Nd	^{147}Sm	^{148}Sm	^{149}Sm	^{150}Sm	^{151}Eu	^{152}Sm	^{154}Sm
Sr		^{84}Sr	^{85}Rb	^{86}Sr	^{87}Sr	^{88}Sr		

Table 5 - Operating parameters for TIMS Sr, Nd and Sm isotopic measurement.

Operating conditions parameters	**Method**		
	Sr	**Nd**	**Sm**
Gain calibration	before wheel analysis		
Baseline	start each analysis		
High voltage	10 kV		
Rates consume N_2 liq in the ionization source	~2 mL/min		
Detection system (resistors)	8 Faraday collectors (10^{-11} Ω)		
Multi-collector mode	static		
Instrument resolution	400 (low)		
Integration time (s)	4,194		
Idle time (s)	3		
Acquisition number (blocks/cycles)	10/ 100	10/ 160	80/ 100
Measurement repeatability	2s		
Source vacuum conditions	10^{-7} mBar		
Ionic vacuum conditions	10^{-9} mBar		
Rate current (ION/EVA) mA/min	380/200	500/200	500/200
Zoom optic (Focus/dispersion) (V)			0/-10

Analyses of each new batch of rock samples, blanks, RMs and reference solutions were made under the same operating conditions. About 150 ng of JNdi-1 (TANAKA et al. 2000) and ~ 120 ng of NIST SRM 987 solutions were repeatedly measured in all analytical runs for evaluation of the intermediate measurement precision (laboratory reproducibility) and to correct for the instrumental bias according to equation 1 (LANA et al. 2017). The obtained average result for the JNdi-1 was $^{143}Nd/^{144}Nd = 0.512100 \pm 0.000012$ (2s, $n = 323$), which was compared to the recommended value of $^{143}Nd/^{144}Nd = 0.512115 \pm 0.000007$ (TANAKA et al. 2000). The NIST SRM 987 LAGIR measurement was $^{87}Sr/^{86}Sr = 0.710236 \pm 0.000020$ (2s, $n = 147$), and compared to the recommended value $^{87}Sr/^{86}Sr = 0.710248 \pm 0.000008$.

$$R(sample)_{true} = R(sample)_{measured} \; x \; [R(reference)_{true} / R(reference)_{measured}] \quad (1)$$

3.1.3.5 Data reduction

Sm-Nd data from the mass spectrometer were reduced using an Excel spreadsheet written by faculty and former students from the Isotope Geochemistry Laboratory at the University of Kansas and passed on to LAGIR during a visit in 2006 (VAN SCHMUS, PERSONAL COMMUNICATION, 2006). Instrumental fractionation was corrected for by linear normalization of measured isotope ratios based on the constant ratios of $^{146}Nd/^{144}Nd =$

0.7219 (PATCHETT, 1989) and of $^{152}Sm/^{149}Sm$ = 0.56083 (DE PAOLO, 1981). The measured isotope ratios are then corrected for laboratory blank (which render negligible results), and for the double ^{149}Sm-^{150}Nd spike using the equations presented by BOELRIJK, (1968), prior to the calculation Sm and Nd mass fractions and the $^{147}Sm/^{144}Nd$ isotope ratio.

3.1.3.6 Statistical analysis by comparison of means

Statistical analyses were performed in order to compare the LAGIR average with literature data, using the IsoplotR® Online London version (VERMEESCH, 2018), JamoviR 1.2.27 (THE JAMOVI PROJECT 2020, R CORE TEAM 2019), and Microsoft Excel® software. The independent Student's test and one-way ANOVA were used to assess significant differences within two or more groups from the mean. Data were submitted to normality (SHAPIRO and WILK, 1960) and homogeneity of variances test (LEVENE, 1960), as pre-requisite for these statistical tests.

The estimate of precision measurement was evaluated according to the conditions of repeatability and reproducibility (VIM, 2008). Repeatability conditions (2s) were associated with individual sample analyses and the intermediate precision (2s) was given using two standard deviations to show the precision data variability, both within a 95% confidence level (VIM, 2008). Between different data, however, the uncertainties related to the arithmetic mean ($\overline{x}$) must be compared based on the experimental standard deviation of the mean [2s], which is calculated by $s*t_{0.05(n-1)}/(n)^{1/2}$, where "s" is the standard deviation, "t" is the Student distribution at the 95% confidence level and "*n*" is the number of datasets, being n-1 degrees of freedom.

To calculate the confidence interval (CI) by equation 2, the two-tailed Student's t-distribution at the 95% confidence level was used, based on the critical values (t) from the table by LANGE et al. (1989).

$$CI\ [\mu, 0.95] = [\overline{x} + [2s]; \overline{x} - [2s]] \quad (2)$$

The Grubbs test outliers were used to detect spurious values based on a table of critical values for T (GRUBBS and BECK 1972).

3.1.4 Results and Discussion

3.1.4.1 USGS RMs isotopic results from LAGIR

The reliability of the BPR-1 measurements was achieved through the RMs USGS analyses from LAGIR, compared to data reported by the GeoReM database (http://georem.mpch-mainz.gwdg.de). Details such as rock type, sample site and mass fractions from the USGS RMs and the LAGIR data are presented in the Supplementary Material 1 Table S1.2.

The average comparison in this work only used data from published works with analyses obtained using TIMS that provided mean, standard deviation (s) and/or standard deviation of the mean (formerly known as the standard error of the mean), with a sample size greater than 2, and with correction for measurement laboratory reproducibility using solution/RMs. All standard deviations of the mean were calculated in this work, except for the data from BEARD et al. (1995). Calculations assumed that the data had a symmetrical distribution, considering the parameters provided by the studies such as mean, standard deviation and sample size (*n*).

Statistical analysis was used to compare the data presented in this work with published ones from the literature that report individual values in their works. For the comparison of two groups (one reference value and LAGIR value) is applied the Student's t-test, while for three or more groups the ANOVA statistical test is performed (Supplementary Material 1 Table S1.3).

3.1.4.1.1 Nd isotopic composition

The obtained $^{143}Nd/^{144}Nd$ ratios for AGV-1, BCR-1, G-2 and GSP-1 were 0.512799 ± 0.000010 (2s, *n* = 51), 0.512644 ± 0.000014 (2s, *n* = 08), 0.512227 ± 0.000006 (2s, *n* = 03) and 0.511373 ± 0.000006 (2s, *n* = 03), respectively (Supplementary material 1 Table S1.4). The low uncertainties of the total 65 analyses of the USGS RMs had repeatability measurement within-run better than 0.000021.

Published data of USGS RMs, with mean, uncertainties (provided and/or calculated) as standard deviation (2s) and standard deviation of the mean [2s] with a confidence interval at 95 %, as well LAGIR data, are provided in Supplementary material 1 Table S1.5.

Comparisons between LAGIR data and reference data (Figure 5), and considering the $^{143}Nd/^{144}Nd$ LAGIR confidence interval of 95 % shows that the LAGIR mean and/or range bars overlaps the two of three AGV-1 references, seven of twelve BCR-1 references and both

G-2 references. Data for Nd GSP-1 was not plotted in figure 5 as there was only one reference for statistical comparison (RACZEK et al. 2003) which agreed entirely with the LAGIR mean.

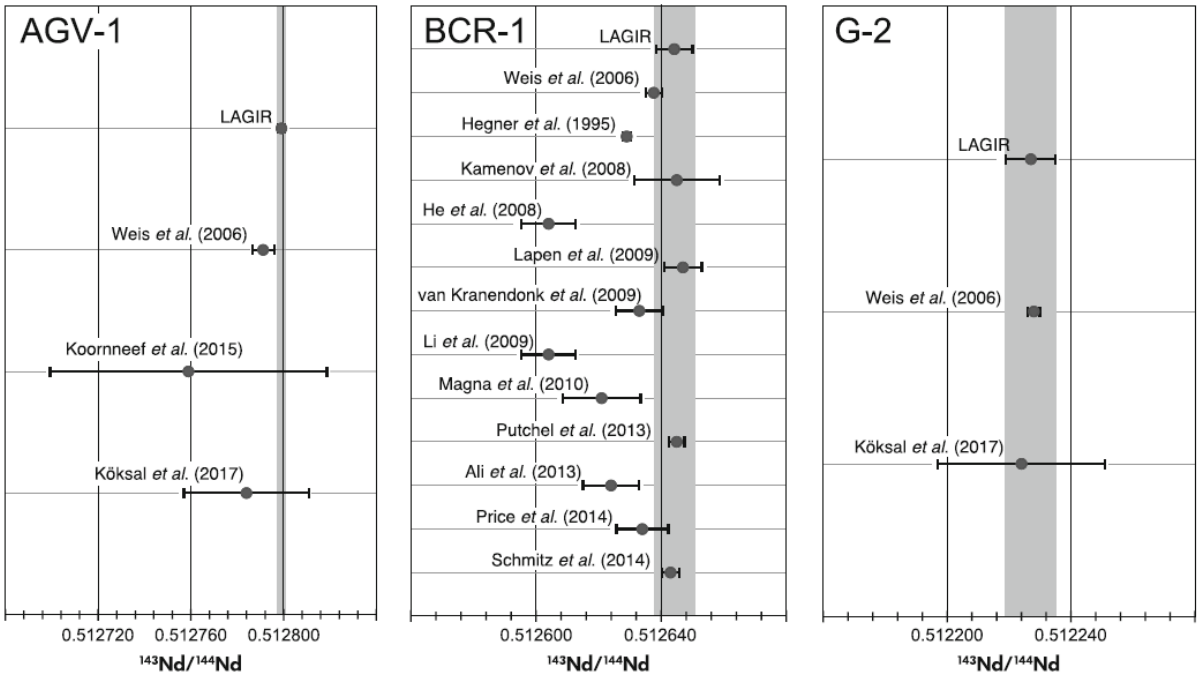

Figure 3 - LAGIR and literature data mean values and horizontal bars are the measurement reproducibility (2s) with a confidence interval of 95 %. The grey bands indicate the LAGIR uncertainties range. The abscissa axis is represented by $^{143}Nd/^{144}Nd$.

There was a significant difference for values of $^{143}Nd/^{144}Nd$ in AGV-1, for the groups LAGIR and WEIS et al. (2006) ($t(59) = 4.204$; $p = 9.03e\text{-}5$). However values of $^{143}Nd/^{144}Nd$ in G-2 between these same two groups were not significantly different ($t(10) = -0.703$; $p = 0.498$). For BCR-1, LAGIR, WEIS et al. (2006), PUCHTEL et al. (2013) and ALI et al. (2014) showed a statistical difference between the groups (ANOVA: $F(3,5) = 59.716$, $p = 1.560e^{-4}$) and Tukey Post-Hoc test confirmed the statistical difference between LAGIR and ALI et al. (2014), with $p = <0.01$ (Supplementary material 1 Table S1.3).

3.1.4.1.2 Sr isotopic composition

The $^{87}Sr/^{86}Sr$ ratios obtained in LAGIR for USGS RMs AGV-1, BCR-1, G-2, GSP-1 and BHVO-1 are 0.703978 ± 0.000015 (2s, *n* = 52), 0.705016 ± 0.000017 (2s, *n* = 08), 0.709759 ± 0.000012 (2s, *n* = 04), 0.768895 ± 0.000106 (2s, *n* = 06) and 0.703475 ± 0.000019 (2s, *n* = 09) respectively (Supplementary material 1 Table S1.6). The repeatability

measurement of 72 analyses of the USGS RMs yielded precision better than 0.000026. Figure 6 shows the graphical comparison of the LAGIR mean with the standard deviation of the mean [2s] to reference data. The $^{87}Sr/^{86}Sr$ ratios of the LAGIR (CI 95%) compared to reference data show that the LAGIR mean and/or range bars overlaps the two of five AGV-1 references, five of nine BCR-1 references, all five G-2 references, six of eight BHVO-1 references and both GSP-1 references (Supplementary material 1 Table S1.7).

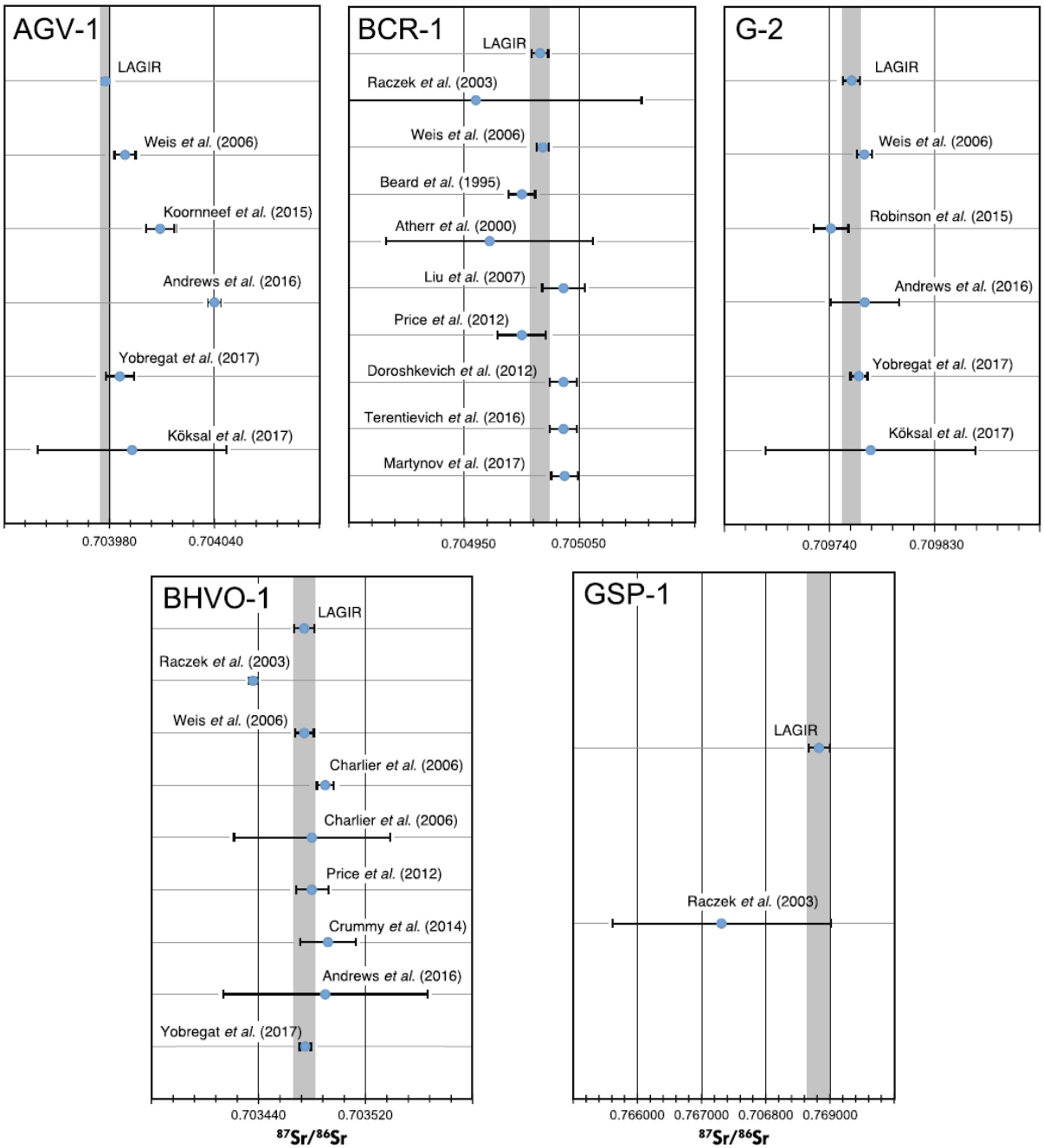

Figure 4 - LAGIR and literature data mean values and horizontal bars are the measurement reproducibility (2s) with a confidence interval of 95 %. Gray bands indicate the LAGIR standard deviation of the mean [2s] range. Abscissa axis represented by $^{87}Sr/^{86}Sr$.

Statistical analysis for values of $^{87}Sr/^{86}Sr$ in AGV-1 for the group of samples from LAGIR, WEIS et al. (2006) and YOBREGAT et al. (2017) showed statistical differences (ANOVA: F (2,67) = 11.445, p = $5.30e^{-5}$). Tukey Post-Hoc test checked statistical differences between data from LAGIR and WEIS et al. (2006), with p = $1.57e^{-4}$. For the G-2 and BHVO-1 RMs, there is no statistical difference between data from LAGIR, WEIS et al. (2006) and YOBREGAT et al. (2017), with ANOVA Welch's: W (2,14) = 3.764, p = 0.059 and ANOVA: F (2,21) = 0.037, p = 0.964, respectively. For the BCR-1 RM, LAGIR and Weis *et al.* (2006) show t(14) = -0.584; p = 0.569, with no significant statistical difference (Supplementary Material 1 Table S1.3).

3.1.4.2 Nd and Sr isotope compositions of the BRP-1 reference material

The isotopic composition of BRP-1 RM is 0.512408 ± 0.000010 (2s, *n* = 53) for $^{143}Nd/^{144}Nd$ ratio and 0.706011 ± 0.000017 (2s, *n* = 63) for $^{87}Sr/^{86}Sr$ ratio. The results are illustrated in Figure 7. The Grubbs test outliers excluded 4 out of 57 measurements for Nd and 5 out of 68 measurements for Sr, below 7.5 % of all measurements. The flowchart (Figure 7A) shows the number of analyses in each digestion set, as well as their value plots (Figures 7B and 7C). Diagrams show the graphical distributions over time of each category and group. Kernel density estimates KDE's (Vermeersch 2012) were drawn along with the histogram representing the data sets (IsoplotR®) also shown in Figure 7. A detailed description is given in Supplementary Material 3 Table S3.4.

The average isotopic composition of BRP-1, considering the sample size and the standard deviation of the mean, is $^{143}Nd/^{144}Nd$ = 0.512408 ± 0.000001 [2s], CI [μ, 0.95] = [0.512407; 0.512409], and $^{87}Sr/^{86}Sr$ = 0.706011 ± 0.000002 [2s], CI [μ, 0.95] = [0.706009; 0.706013]. In other words, with 95 % confidence, this range contains the true population average. The repeatability measurements (in run) in the isotopic analyses of BRP-1 are better than 0.000020 and 0.000031 for Nd and Sr, respectively. The isotopic composition of $^{143}Nd/^{144}Nd$ and $^{87}Sr/^{86}Sr$ of the BRP-1 RM, under repeatability conditions, is given by six and nine means, respectively. Each mean was calculated from individual values analysed under the same conditions (the same date of digestion, chemistry procedures and spectrometry). The tables and figures in Supplementary Material 3 Table S3.5 and Table S3.6 (Figures S3.61 and S3.6.2) show that mean values under repeatability conditions with their respective precisions (2s) overlap the mean value under intermediate precision conditions (n=53 for Nd and n=63 for Sr).

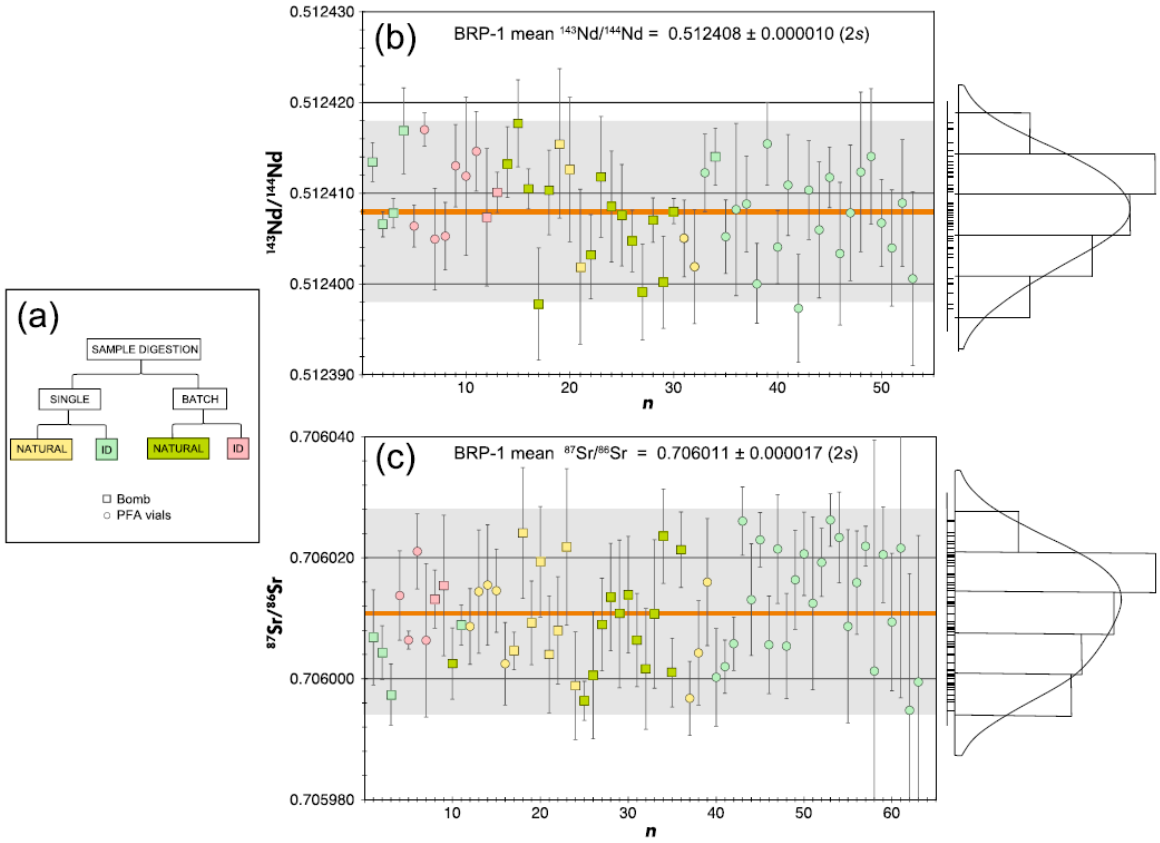

Figure 5. Individual values and mean of the BRP-1 from LAGIR. Categories and group comparison of the digestion types. A) Flow chart summarizing the sample digestions of the BRP-1 reference material. Square symbols indicate bomb digestion and circle symbol, PFA vials digestion. B) Individual values and mean for Nd isotope ratios. Blue symbols are measured ratio normalised to JNdi-1. The vertical bars on each blue symbol represent the measurement repeatability (2s) associated with of the individual sample analysis. Orange line is the normalised mean and light grey band corresponded to measurement reproducibility (2s) at the 95 % CI. C) Individual values and mean for Sr isotope ratios. Blue symbols are ratios normalised to NIST SRM 987. The vertical bars of each blue symbol represent the measurement repeatability (2s) associated with the individual sample analysis. The orange line is the normalised mean, and the light grey band corresponds to measurement reproducibility (2s) at 95 % CI. To the right of each diagram are KDEs with histograms and a set of vertical lines that mark the individual measurements.

Of the 53 Nd measurements of the BRP-1, 32 were performed in single digestion and 21 in batch digestion. These samples had their digestions done either in a PTFE bomb or PFA vials and either with Isotope Dilution (ID) or natural, i.e., without isotopic spike solution added. For 56 BRP-1 Sr measurements, 44 were performed in single and 19 in batch digestion. In order to compare each group, the results were grouped by the digestion mode (single and batch digestion), digestion vessel (PTFE bomb and PFA vials) and ID or natural analysis (see Table 5 and Figure 8).

Table 6 - Means and uncertainties for categories and group comparison of the digestion types.

Parameters	Number of Digestion		Vessel Type		Spike Solution	
	Single	Batch	Bomb	PFA vials	Natural	ID
n (Nd)	32	21	24	29	19	34
$^{143}Nd/^{144}Nd$ (mean)	0.512408	0.512408	0.512409	0.512408	0.512407	0.512409
2s	0.000010	0.000011	0.000011	0.000010	0.000011	0.000010
[2s]	0.000002	0.000002	0.000002	0.000002	0.000003	0.000002
n (Sr)	46	17	27	36	29	34
$^{87}Sr/^{86}Sr$ (mean)	0.706012	0.706010	0.706010	0.706013	0.706010	0.706012
2s	0.000018	0.000015	0.000016	0.000018	0.000016	0.000018
[2s]	0.000003	0.000004	0.000003	0.000003	0.000003	0.000003

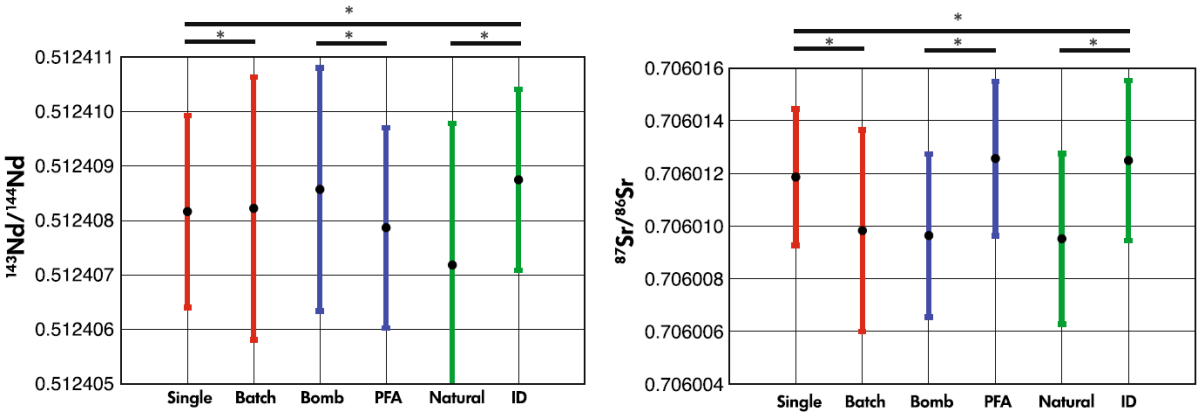

Figure 6. Categories and group comparison of the digestion types – range bars represent the standard deviation of the mean [2s] and (*) represents that there is no significant statistical difference with 95 % confidence intervals.

Comparative statistics analysis of these groups shows that the distribution of data does not differ significantly from a normal distribution. The Shapiro-Wilk normality test and Levene's test show that there is homogeneity in variability between each group assessed by p-values > 0.05 (Supplementary Material 3 Table S3.7). The independent Student's t-test is used to compare the $^{143}Nd/^{144}Nd$ means and checks that the within the groups single vs batch digestion ($t(51) = -0.040$; $p=0.969$), bomb vs PFA vials digestion ($t(51) = 0.491$; $p = 0.625$) and ID vs natural digestion ($t(51) = -1.061$; $p=0.294$), there is no significant statistical difference, considered by p-values >0.05 with a confidence level of 95%. The Student's t-test performed for $^{87}Sr/^{86}Sr$ analyses yields values for single groups single vs batch digestion ($t(61) = 0.838$; $p = 0.405$), bomb vs PFA vials digestion ($t(61) = -1.353$; $p = 0.181$) and ID vs natural digestion ($t(61) = -1.339$; $p = 0.186$) (Supplementary Material 3 Table S3.7). For these comparisons, confidence intervals were calculated by the standard deviation of the mean.

3.1.4.3 Nd and Sm mass fraction values

The mass fractions of Sm and Nd of the BRP-1 measured at LAGIR, presented by their means, are 11.0 ± 0.2 ug g^{-1} (2s, *n* = 36) for Sm and 51.9 ± 0.6 ug g^{-1} (2s, *n* = 36) for Nd, following a normal distribution verified by Shapiro-Wilk (W(36) = 0.983; p = 0.834) for Sm and (W(36) = 0.974; p = 0.529) for Nd. The values are within the analytical uncertainties of published data from certified values by COTTA and ENZWEILER, (2008): 51.9 ± 0.6 ug g^{-1} for Nd and 11.2 ± 0.2 ug g^{-1} for Sm (Supplementary Material 3 Table S3.8). The Sm values from LAGIR are slightly lower than those from COTTA and ENZWEILER, (2008) but are acceptable because the range of the reference value was reported at a 95 % confidence level.

Among the USGS RMs, the AGV-1 data from LAGIR and WEIS et al. (2006) showed significant differences: a) overlapping of the standard deviation of the mean and b) in the statistical tests. The absolute difference between the averages is 0.000008 for Nd and 0.000011 for Sr. This is probably due to the large sample size of LAGIR, which greatly reduces the standard deviation of the mean.

The averages $^{143}Nd/^{144}Nd$ in LAGIR for AGV-1 and BCR-1 are more radiogenic than most of the earlier reported values. For AGV-1, the LAGIR value may be close to the true value, and this is based on the exhaustive number of repetitions performed (*n*=51), while the LAGIR BCR-1 value corresponds to the highest number of values reported in the literature (*N*=4).

3.1.5 Conclusions

This work provides the first detailed Sm-Nd and Sr isotopic composition of the Brazilian basalt RM BRP-1, available from the Geological Survey of Brazil.

The averages for the BRP-1 are $^{143}Nd/^{144}Nd$ = 0.512408 ± 10 (2s) and $^{87}Sr/^{86}Sr$ = 0.706011 ± 17 (2s) are recommended for use by the scientific community for interlaboratory comparison and quality control.

Statistical tests show insignificant differences in the BRP-1 results, regardless of different combinations of digestion conditions (single or batch, using PFTE bomb or PFA vials), and with isotopic spike addition or not.

The reliability of the obtained data for BRP-1 is demonstrated by the parallel analysis of USGS RMs AGV-1, BCR-1, BHVO-1, G-2 and GSP-1, which show good reproducibility in comparison with literature reference values.

3.2 **TIMS techniques for measuring strontium isotope ratios in apatite grains and application to igneous rock petrology**

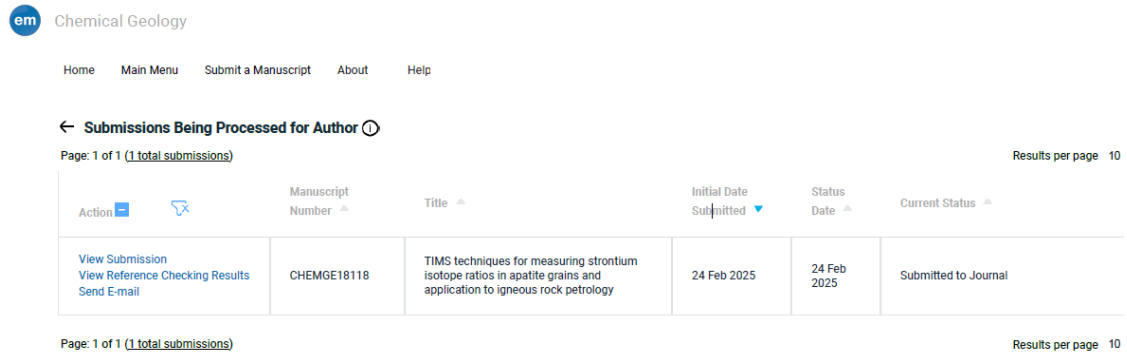

Chemical Geology

Home Main Menu Submit a Manuscript About Help

← Submissions Being Processed for Author ⓘ

Page: 1 of 1 (1 total submissions) Results per page 10

Action	Manuscript Number	Title	Initial Date Submitted	Status Date	Current Status
View Submission View Reference Checking Results Send E-mail	CHEMGE18118	TIMS techniques for measuring strontium isotope ratios in apatite grains and application to igneous rock petrology	24 Feb 2025	24 Feb 2025	Submitted to Journal

Page: 1 of 1 (1 total submissions) Results per page 10

Carla Neto (1,2,4)*, Claudio de Morisson Valeriano (1,2,3), Henrique Bruno (1,2,3), Manuela Carvalho (1,2,5), Gabriel Paravidini (1,4), Rasec Almeida (6), Caroline Peixoto (1,3), Mariana Carvalho (1,3), Monica Heilbron (1,2,3)

1 – Faculdade de Geologia (FGEL), Universidade do Estado do Rio de Janeiro (UERJ)
2 – LAGIR - Laboratório de Geocronologia e Isótopos Radiogênicos (FGEL-UERJ)
3 – TEKTOS - Grupo de Pesquisa em Geotectônica (FGEL-UERJ)
4 – PPGG - Programa de Pós-graduação em Geociências (FGEL-UERJ)
5 – FAPERJ - Fundação de Amparo à Pesquisa do Estado do Rio de Janeiro
6 – CAp-UERJ - Departamento de Matemática e Desenho, Universidade do Estado do Rio de Janeiro (UERJ)

Abstract

Whole-rock analyses of Sr composition by thermal ionization mass spectrometry (TIMS) require age calculations and Rb-Sr ratio determinations, which are expensive, high-time consuming, and susceptible to compositional heterogeneity. A significant knowledge gap exists in the development of alternative TIMS methods that provide accurate and representative Sr isotope data while addressing these challenges. This study explores the potential of Sr isotopic composition in apatite grains from magmatic rocks as a proxy for initial $^{87}Sr/^{86}Sr$ ratios. Understanding the isotopic composition of magmatic systems through apatite is crucial for deciphering magma origin, crustal contamination, and magmatic differentiation, especially in tectonically complex regions. Therefore, this research focuses on

granitoid rocks from the Ribeira Orogeny, Brazil, which is shaped by pre-, syn-, and post-collisional magmatic events. The proposed TIMS-based method for analyzing Sr isotopes in apatite grains offers a reliable, cost-effective, and time-efficient alternative to traditional whole-rock analyses, with validation showing consistent results within an uncertainty of 0.5 %.

Keywords: Strontium isotopes; Apatite; Radiogenic isotopes; Ion exchange chromatography; Petrogenesis; Thermal ionization. Mass spectrometry.

Highlights

- Apatite grains are used as an effective proxy for Sr initial isotope ratios.
- TIMS measurements of $^{87}Sr/^{86}Sr$ in apatite are easily obtained by an accessible technique.
- Reduced cost and time in petrogenetic studies.
- Results accuracy remains even with a small sample quantity (e.g. 0.3 ng of Sr).
- Apatite analysis can be applicable in large-scale magmatic studies, such as crustal differentiation and mantle source discrimination.

3.2.1 Introduction

The use of apatite to solve several complex geological problems has experienced remarkable growth in recent years, and this mineral has become a promising tool for addressing fundamental questions in Earth's history (PICCOLI and CANDELA, 2002; KENNEDY et al. 2023). Apatite is a calcium phosphate [$Ca_5(PO_4)_3$ (F, Cl, OH)] widely distributed in the lithosphere and is present in several rock types, environments, and throughout geological processes (BELOUSOVA et al. 2002; HARLOV, 2015; BRUAND et al., 2020; RAKOVAN and SCOVIL, 2021). Particularly, in studies of orogenies, which are tectonically complex regions, the application of Sr initial ratios in petrogenesis studies with regional scope offers a valuable tool to differentiate mantellic and crustal sources, offering opportunities for the interpretation of processes such as partial melting, crustal contamination, and mantle-crust interaction (JAHN et al. 1999; LAN et al. 2011; LI et al. 2021; DU et al. 2022).

Sr isotope composition can be of great utility in the geochemical understanding of apatite, which has very low Rb/Sr ratios formation making it suitable for retaining initial

$^{87}Sr/^{86}Sr$ ratios, and has been widely used to investigate the origin of rocks, providing important petrogenetic data about their source rock and the conditions during apatite crystallization (RAMOS et al. 2005; TSUBOI, 2005; YANG et al. 2014; ZHAO et al. 2015; SUN et al. 2019; GILLESPIE et al. 2021; SUO et al. 2023). Measuring initial $^{87}Sr/^{86}Sr$ ratio of an igneous rock traditionally requires the determination of the crystallization age, the Rb-Sr ratio and $^{87}Sr/^{86}Sr$ ratio in whole rock samples (FAURE. 1986). Although widely consolidated, this process presents significant challenges, including high costs and long execution time. Nevertheless, it faces problems of representativity, since the small portions of rock, also used in isotopic analyses, may not accurately reflect the initial isotopic composition of the rock, compared to using a mineral concentrate obtained from larger volumes of collected material.

Given the relevance of Sr isotopic ratios in apatite for petrogenetic applications, it is essential to develop accessible and viable techniques for obtaining isotopic data. Therefore, the goal of this work is to validate the use of Sr isotopic composition in apatite as a proxy for initial $^{87}Sr/^{86}Sr$ ratios in granitoid rocks. To this end, an analytical technique was applied to analyzing apatite single- and multi-grains, which stands out for its efficiency in reducing costs and analysis time, while preserving the analytical precision already achieved by thermal ionization mass spectrometry (TIMS).

The $^{87}Sr/^{86}Sr$ isotopic ratios obtained from apatites of representative samples of pre-, syn- and post-collisional magmatism of the Ribeira Orogeny were compared to the initial ratios calculated in the whole-rock of the same samples. Validation of this methodology has the potential to offer an efficient and affordable alternative for obtaining initial ratios applied for regional studies.

3.2.2 Materials and Methods

3.2.2.1 Samples and Reference Materials

The studied apatite grains were extracted from three granitoid rocks associated with the pre-, syn- and post-collisional magmatism of the Neoproterozoic Ribeira Orogen in southeastern Brazil. Sample SMM-CMM-172 is from PEIXOTO et al. (2017). In this study, BG-200 and BG-14B samples were analyzed for whole-rock major and trace element composition, and for U-Pb geochronology.

Three well-characterized reference materials (RMs) are used to measure Sr isotope ratios in apatite grains. The NIST SRM 987 Sr solution is employed for instrumental calibration and isotopic bias corrections. The accuracy of the proposed technique was assessed through Sr isotopic analyses of RMs, such as EN-1 (Enewatek lagoon; bilvalve shells; FICHTNER et al. 2017) and Durango Apatite (LYONS, 1988; YANG et al. 2014). The latter has a matrix compatible with the studied samples. These RMs were used to check external reproducibility and empirically validate blank conditions.

3.2.2.2 Analytical procedures

In this section, all the chemical and spectrometric procedures performed at the Laboratory of Geochronology and Radiogenic Isotopes (LAGIR) of the Rio de Janeiro State University (UERJ) for the determination of Sr isotopic composition in apatite grains will be detailed.

3.2.2.2.1 Chemical procedures

Chemical procedures were performed in clean rooms, under positive pressure and HEPA filters, including laminar flow and exhaust hoods. Savillex® PFA vials were previously cleaned on hot plates following four cycles of HCl 6 M and ultrapure H_2O cleaning at 90 °C for 1 day each. Ultrapure H_2O (18.2 MΩ cm^{-1} at 25ºC) was used, and obtained by filtration of 1 μm, 3 μm and 5 μm particles, followed by deionization using Rios5 (Millipore) and subsequent purification in a NanoPure® unit (Milli Q-Millipore). Hydrofluoric (48 % m/v) and hydrochloric (37 % m/v) acids were distilled in sub-boil mode three times using a DST-1000 unit (Savillex®). Nitric (65 % m/v) and phosphoric (85 % m/v) acids are ultrapure (PA grade) from Merck KGaA.

The approach for separating apatite grains for TIMS analysis follows principles that include factors such as: ensuring efficient separation of Sr employing ion exchange chromatography, avoiding interferences from elemental (Rb and Ca) and molecular compounds, and ensuring that the recovery of Sr in the chemical procedures is as high as possible to obtain significant Sr signals even in small samples, with less than 100 ng, and obtaining low contamination of the total laboratory blank since the volumes of reagents used in the procedures are small.

3.2.2.2.2 Surface leaching of apatite grains

Cleaning procedures were carried out to ensure the determination of the Sr isotopic composition in apatite, free from potential contaminant interferences originating from the mineral concentrate (MACHADO et al. 1986). These contaminants range from anthropogenic "dust" to fine particles of other minerals that may have adhered to the surface of the grains. For surface leaching of apatite grains, acetic acid 0.5 M was used in PFA vials on a hot plate at 90 ºC for 1 hour and 30 minutes (OLIVEIRA, 2015). Afterward, centrifugation was performed to decant the acetic acid, followed by three consecutive washes with ultrapure H_2O for 15 minutes. Drying was done cold in the exhaust hood for 1 day.

3.2.2.2.3 Chemical digestion, chromatographic columns and resins

Chemical digestion of single-grain or multiple-grain post-leaching procedures was performed in previously decontaminated PFA vials with 3 ml capacity. In chemical digestion, 200 µl of 65 % HNO_3 (ultrapure) was used for 1 day on a hot plate at 140 ºC (BUZENCHI et al. 2023). The digestion of EN-1 was in HCl 1M for 1 day on a hot plate at 90 ºC.

The Sr separation from matrix elements was performed using cation exchange chromatography microcolumns handcrafted from a PTFE tube by hot air shrinkage at the GEOTOP-UQAM laboratory (Montréal, Canada), resulting in an internal diameter of 3.1 mm and a height of 10 mm, with a small reservoir cup above the tube (NETO et al. 2014). The resin used for Sr separation was Sr-Spec resin (50-100 µm, Eichrom® Technologies LLC, Darien, IL, USA) filling a column with a volume of 70 mm^3 (CHARLIER et al. 2006).

3.2.2.2.4 Ion exchange column calibration and chemical separation of Sr

Ion exchange microcolumn calibration consists of establishing the volumes of solution that pass through the resin to collect Sr and separate it from other matrix elements, free of interferents. The separation follows the method of CHARLIE et al. (2006), using Sr-Spec resin and HNO_3 for Sr elution. After digestion, the sample is completely evaporated and re-dissolved with 200 µl of HNO_3 3M before being transferred to the column. The procedure begins with washing the column alternately with HCl 6M and ultrapure H_2O_3 three times before filling with 70 µl of Sr-Spec resin. The resin is also washed alternately with HCl 6M and ultrapure H_2O three times and then is conditioned with 200 µl of HNO_3 3M three times in

a row. The sample is transferred, and four washing stages (50, 100, 150, 200 µl) of HNO_3 3M are performed to remove matrix elements, including Rb and Ca. An ultra-clean PFA collection vessel is placed under the column and Sr is eluted in 300 µl of HNO_3 0.05 M in three 100 µl stages (Table 7). The volume fractions of the seven Sr aliquots are evaporated on a hot plate at 90 °C, ready for deposition on Re filament and TIMS analysis. After each use, the resin is discarded to avoid possible memory effects and maintain low blank levels, according to CHARLIE et al. (2006). The column efficiency for Sr is approximately 70 %, with a loss of ~ 4 % of total Sr in the washing steps with HNO_3 3M and approximately 26 % remaining firmly bound to the Sr-Spec resin (CHARLIE et al. 2006).

Table 7 - Chemical procedures for Sr elution with modifications from CHARLIE et al. (2006)

Task	Reagent type	Molarity (M)	Capacity (µl)
Sample conditioning	HNO_3	3	200
Column cup washing (rinsing)	HCl	6	Fill columns
	H_2O ultrapure	-	
	HCl	6	Fill columns
	H_2O ultrapure	-	
	HCl	6	Fill columns
	H_2O ultrapure	-	
Fill the column with 70 ul of resin			
Resin washing	HCl	6	Fill columns
	H_2O ultrapure	-	
	HCl	6	Fill columns
	H_2O ultrapure	-	
	HCl	6	Fill columns
	H_2O ultrapure	-	
Resin washing and conditioning	HNO_3	3	200
	HNO_3	3	200
	HNO_3	3	200
Sample transfer			
Sample washing (elution of matrix elements)	HNO_3	3	50
	HNO_3	3	100
	HNO_3	3	150
	HNO_3	3	200
Change to a clean vial			
Elution of Sr	HNO_3	0.05	100
	HNO_3	0.05	100
	HNO_3	0.05	100
Resin discard			

The calibration solution was prepared from a grain of Durango Apatite, with a 20 ng of Sr loading quantity in the column. To determine the best aliquots for Sr extraction, free of

Rb, a calibration curve was constructed with the intensity of the analytical signal in TIMS (cps) versus aliquot volume following the procedure shown in Figure 7. After checking the efficiency of the calibration performance, the separation of Sr from the sample was established according to Charlie et al. (2006), in the aliquot 300 ul (100+100+100) of HNO_3 0.05M.

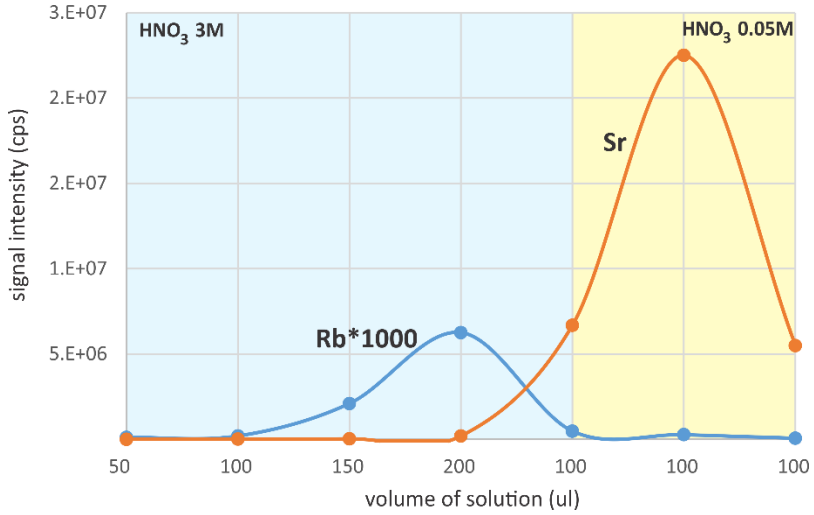

Figure 7 - Diagram of signal intensity (cps) versus volume of the solution of the aliquot loaded in the column (µl), used in the chromatographic separation of Sr with 20 ng of Durango Apatite. The red line represents Sr signals, and the blue line represents Rb*1000 signals. The blue band represents elution with HNO_3 3M, and the yellow band of HNO_3 0.05M.

3.2.2.3 U-Pb zircon LA-ICP-MS geochronology

U-Pb zircon geochronology was carried out in a Thermo Scientific® Element 2 sector field ICP-MS coupled with CETAC LSX-213 G2+ (λ = 213 nm) Nd: YAG laser system at the Isotopic Geochronology Laboratory of the Ouro Preto Federal University (UFOP). U-Pb laser ablation analysis was performed with a 20 µm spot size, laser frequency of 10 Hz, and fluency of ~3 J/cm^{-2}.

To test the accuracy and quality control, primary (GJ-1, JACKSON et al. 2004) and secondary (BB-9, SANTOS et al., 2017) reference materials were used, respectively. Raw data were corrected offline using the GLITTER® software package (VAN ACHTERBERGH et al. 2001).

3.2.2.4 Whole-rock geochemistry

Chemical analyses of two whole-rock samples were performed at the Activation Laboratories Ltda. (ACTLABS), Canada, by Inductively Coupled Plasma Mass Spectrometry (ICP-MS). Majors and trace elements, including rare earth elements, were obtained by fusion, total digestion, and INAA analysis. Detailed analytical methodology can be found at http://www.actlabs.com - Geochemistry/Assay - Methods - Code 4E-Research. Data interpretations and diagrams generations were made using the Geochemical Data Toolkit (GCDkit 6.0, JANOUŠEK et al. 2006), Microsoft Excel®, and CorelDraw® programs.

3.2.2.5 Whole-rock TIMS Nd-Sr isotopes

Whole-rock Nd-Sr isotopic analyses were performed at LAGIR-UERJ. Isotopic ratios were measured in a multi-collector TIMS Thermo Scientific® TRITON mass spectrometer (Table 8). For Sm-Nd isotopes, the isotopic dilution technique was applied, while for Sr isotope analysis was used natural technique (no spiked). Chemical and analytical procedures were executed according to NETO et al. (2023). The reference materials used were AGV-1 and BRP-1, and the total blanks for Nd and Sm were, respectively, below 200 pg and 70 pg.

The ionic activator is an ultrapure solution that, when used in small quantities on the metal filament together with the sample, ensures the ionization efficiency of elements with high ionization potential (GUO et al. 2023). The TaF_5 solution is an ionic activator used to increase the efficiency of analyses with small amounts of Sr by TIMS, and its use is exclusively for samples with Sr amounts below 100 ng (CHARLIE et al. 2006). To obtain TaF_5, $TaCl_5$ was initially acquired, followed by the production of Ta_2O_5 as described in the TRITON HARDWARE MANUAL (2002). Subsequently, Ta_2O_5 was converted to $Ta(OH)_5$ (Charlie et al., 2006), thus allowing the production of TaF_5. The Re filament used in this work for Sr analysis is produced with 99.99 % purity (H-Cross Company, USA), with dimensions of 0.025 mm thick and 1 mm wide mounted on a single-arrangement bead. The Sr samples were dissolved 1 µl of HNO_3 (65 % m/v) with 1 µl of the ionic activator TaF_5 for deposition in degassed Re filament in a simple mount.

Table 8 - Operating parameters for TIMS Sr isotopic measurement.

Running conditions parameter	**Sr method**
Gain calibration	before wheel analysis
Baseline	start each analysis
High voltage	10 kV
Rates consume N liq in the ionization source	~2 mL/min

Detection system (resistors)	5 Faraday collectors (10^{-11} Ω)
Multi-collector mode	static
Instrument resolution	400 (low)
Integration time (s)	4.194
Idle time (s)	3
Acquisition number (blocks/cycles)	10/100
Measurement repeatability	2s
Source vacuum conditions	10^{-7} mBar
Ionic vacuum conditions	10^{-9} mBar
Rate current (ION/EVA) mA/min	300
Zoom optic (Focus/dispersion) (V)	1.5/0

The best ionization temperature for Sr analyses in Re filaments varies from 1350 to 1600 °C. The acquisition of Sr isotopic ratios was performed within 100 cycles, with an integration time of 4.194 seconds, and an idle time of 3 seconds. In addition to the 4 masses of the Sr isotopes, the ^{85}Rb mass was monitored and measured to correct for any possible interference in the ^{87}Sr mass. Exponential law fractionation correction of the $^{87}Sr/^{86}Sr$ isotope ratio was based on the $^{88}Sr/^{86}Sr$ ratio equal to 8.375209 (NIER, 1938). Correction of possible isobaric interference was based on the $^{87}Rb/^{85}Rb$ ratio equal to 0.386 (MEIJA et al. 2016; BÜRGER et al. 2015). The NIST SRM 987 LAGIR measurement was: $^{87}Sr/^{86}Sr = 0.710238 \pm 0.000045$ (2s, n = 32), compared with the recommended value $^{87}Sr/^{86}Sr = 0.710248 \pm 0.000008$.

3.2.2.6 ICP-MS analysis of Sr in apatite

Mass determination of Rb and Sr fractions in apatite grains was performed using the ICP-MS Element XR (ThermoScientific®) at the Isotopic Geology Laboratory (LAGIS) of the Institute of Geosciences of the State University of Campinas (Unicamp). To ensure the quality of the measurements, the certified reference material BRP-1 was analyzed, obtaining results consistent with the uncertainties associated with the certified material, as described by COTTA and ENZWEILER, (2008). The accuracy was evidenced by an average variation coefficient of -1.4 % in duplicate samples. Furthermore, the blank samples presented concentrations below the detection limit for all the elements analyzed.

3.2.3 Geological setting of studied apatite from granitoid rocks

The Mantiqueira Province is a 1400 km-long orogenic system along the Brazilian Atlantic coast, subdivided into three sectors, including the Central Sector, which hosts the Ribeira Orogen (Figure 8A). This orogenic system comprises a complex array of Neoproterozoic terranes that were diachronically amalgamated between ca. 840-520 Ma during the assembly of the West Gondwana supercontinent (ALMEIDA et al. 1977, 1981; HEILBRON et al. 2004; MEERT and LIEBERMAN, 2008; GRAY et al. 2009; BRITO NEVES & Fuck, 2013).

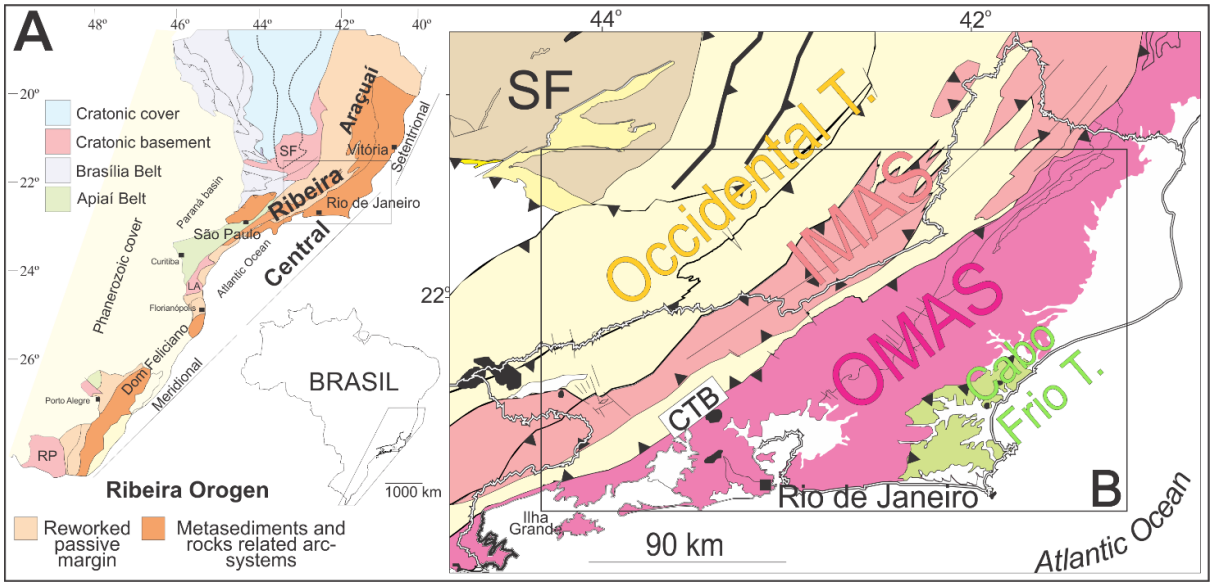

Figure 8 – (A) Subdivision of the Mantiqueira Orogenic System (modified from HEILBRON et al. 2004a,b) and a cut out of Ribeira Orogen tectonic organization (modified from PEIXOTO et al. 2022); (B) Geological map showing the Oriental Terrane.

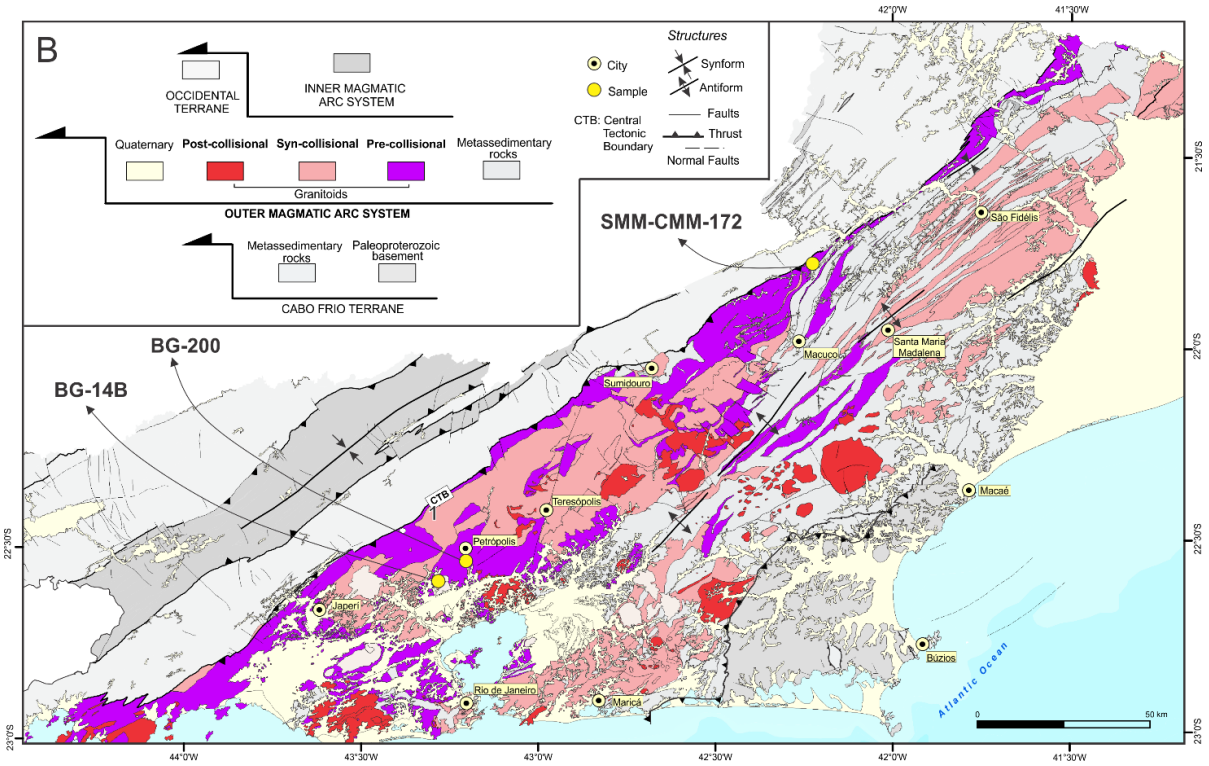

Figure 9 – Zoom of the Oriental Terrain with emphasis on pre-, syn- and post-collisional granitogenesis of Figure 8B showing sample locations.

The structure of the Ribeira Orogen is characterized by the imbrication of magmatic arc systems in a WNW direction against the São Francisco paleocontinent (Figure 8B) (MACHADO et al. 1996; TROUW et al. 2000; HEILBRON and MACHADO, 2003; HEILBRON et al. 2020). The Occidental Terrane represents a reworked segment of the São Francisco Craton's passive margin. At the same time, the southern portion of the orogen contains the Inner and Outer Magmatic Arc Systems (IMAS and OMAS), which comprise Neoproterozoic magmatic arcs (CORDANI et al. 2002; HEILBRON and MACHADO, 2003; PASSARELLI et al. 2004; TUPINAMBÁ et al. 2012; PEIXOTO et al. 2017; HEILBRON et al., 2020, 2025). The IMAS represents an internal continental arc that developed between 650 and 595 Ma (JANASI and ULBRICH, 1991; CAMPOS NETO, 2000; JANASI et al. 2001), whereas the OMAS corresponds to a juvenile intra-oceanic to immature continental arc system that formed between 860 and 605 Ma (PEIXOTO et al. 2017, 2022; CORRALES et al. 2020; HEILBRON et al. 2020). Finally, the Cabo Frio Terrane was incorporated later during the Cambrian (SCHMITT et al. 2004, 2016).

The evolution of the Ribeira Orogen encompasses intense subduction-related arc magmatism between approximately 850 and 620 Ma. Moreover, diachronic collisional processes led to significant deformation and multiple phases of high-grade metamorphism,

accompanied by associated granitogenesis (MACHADO and GAUTHIER, 1996; TROUW et al. 2000; CAMPOS NETO and CABY, 2000; HEILBRON et al. 2008, 2013).

Notably, the development of the OMAS was discontinuous, with volcanic and plutonic rock generation occurring in two distinct arc stages. The OMAS evolution began in the Tonian (860–838 Ma) with the formation of the juvenile intra-oceanic Serra da Prata arc (εNd = -3.7 to +5.2; TDM =1.09-0.92 Ga; $^{87}Sr/^{86}Sr$ =0.7062 e 0.7113 - HEILBRON and MACHADO 2003; PEIXOTO et al. 2017; DECOL et al. 2021), which later evolved into the immature continental Rio Negro arc (εNd = -14 a +5; TDM = 2.47-0.99; $^{87}Sr/^{86}Sr$ = <0.705 – 0.730 - TUPINAMBÁ et al., 2000, 2012; HEILBRON and MACHADO 2003; PEIXOTO et al. 2017, and references therein) during the Cryogenian–Ediacaran (650–620 Ma).

The collisional episode resulted in the docking of the OMAS against both the IMAS and the São Francisco paleocontinent, marking the onset of the earliest metamorphic event, M1 (602–580 Ma). This event led to intense Ediacaran syn-collisional granitic magmatism (PEIXOTO et al. 2022, and references therein), forming several granitoid bodies, including the Desengano gneiss and the Bela Joana charnockite (580–560 Ma), the augen gneiss (560 ± 7 Ma), and the Serra dos Órgãos batholith (569 ± 6 Ma) (SILVA et al. 2002; TUPINAMBÁ et al. 2007). These granitoid formations exhibit similar ages and characteristics to those described by HEILBRON AND MACHADO (2003), such as the 578 ± 19 Ma augen gneiss and intrusive leucogneisses dated at 576 ± 2 Ma intruding the orthogneisses of the Rio Negro magmatic arc (PEIXOTO et al. 2022).

The second metamorphic event, M2 (ca. 545–533 Ma), persisted until the Cambrian and marked the final closure of the back-arc basin between the OMAS and the restricted oceanic domain represented by the Búzios ophiolites (HEILBRON and MACHADO, 2003; CAPISTRANO et al. 2017; PEIXOTO et al. 2022; FREITAS et al. 2024).

Finally, a significant Cambro-Ordovician tectonic-magmatic event (ca. 520–475 Ma) marked the collapse of the orogenic building and the transition to a stable Gondwana supercontinental configuration. This regional collapse facilitated post-collisional granitogenesis (HEILBRON et al. 2004), which resulted in the formation of several granitoid suites, including the Sana (495-480 Ma; POTRATZ et al. 2021; VALERIANO et al. 2011), Itaoca (476 Ma; NETO et al. 2014) e Parati (520-505 Ma; COELHO et al. 2023) granites.

3.2.4 Results

Three Neoproterozoic Brasiliano granitoid rocks from the Oriental Terrane of the Ribeira Belt (Figure 9) were selected for study to determine the Sr isotopic composition in apatite grains and compare it with the initial ratio calculated using the $^{87}Sr/^{86}Sr$ ratio measured, the Rb and Sr contents, and the crystallization age.

3.2.4.1 Measured isotope compositions of EN-1 and Durango Apatite

EN-1 and Durango Apatite reference materials were applied to evaluate the reproducibility of the measured $^{87}Sr/^{86}Sr$ ratio values in the RMs with masses in different orders of magnitude. The EN-1 was used before the acquisition of the Durango Apatite, which has a similar matrix to the studied apatite grains.

The analytical results tables and their uncertainties are given in Tables S1 and S2 of the Supplementary Material. The results of EN-1 analyses are presented in Figure 10A. Tables with individual measurements, statistical parameters, and references of the values searched in GeoReM are available in Table S.3 of the Supplementary Material. The average of $^{87}Sr/^{86}Sr$ measured in EN-1 is 0.709174 ± 0.000032 (2s, n = 15), with a relative standard deviation (RSD) of 0.002 %. The amounts of Sr loaded in the column ranged from 1 to 30 ng. Repeated analyses of the $^{87}Sr/^{86}Sr$ ratio from EN-1 performed at LAGIR-UERJ are compared with values published in the GeoReM database (http://georem.mpch-mainz.gwdg.de) that provide an average of 0.709172 ± 0.000027 (2s, n = 24). The reproducibility of the value measured at LAGIR-UERJ, which is less than 0.001 %, is comparable to values reported in GeoReM.

Sr isotopic analyses of the Durango Apatite (486 ppm; YANG et al. 2014) were performed on grain fragments, with approximate Sr masses of 1-70 μg (0.5-35 ng Sr) with average $^{87}Sr/^{86}Sr$ of 0.706334 ± 0.000023 (2s, n = 16), with a RSD of 0.002 %. The difference between the value obtained by YANG et al. (2014) of the $^{87}Sr/^{86}Sr$ ratio equal to 0.706328 ± 0.000023, and the measured value in this study is less than 0.001 %, demonstrating consistency between the data. The Durango Apatite results are presented in Figure 10B.

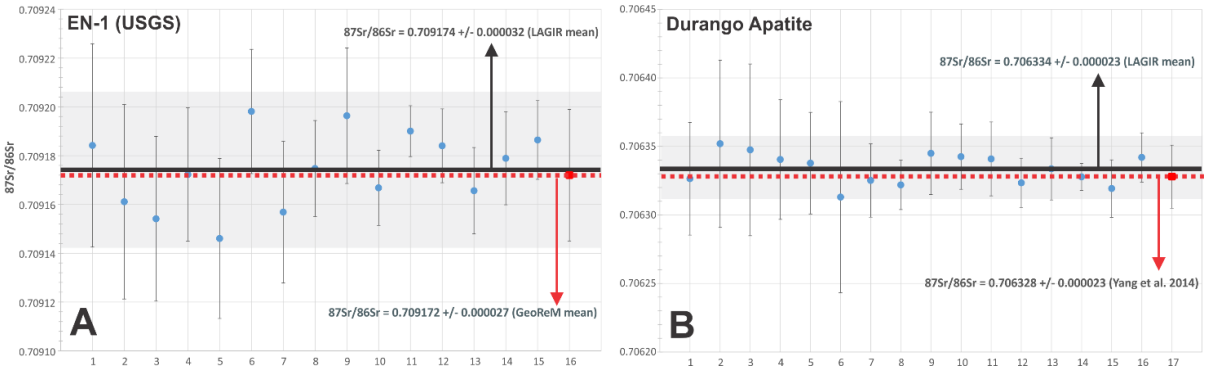

Figure 10 -Individual and average values of Sr isotopic ratios for apatite reference material. (A) EN-1 and (B) Durango Apatite. The blue circles are the values of Sr ratios normalized to NIST SRM 987. The vertical bars of each blue circle represent the repeatability measurements (2s) with a 95 % confidence interval associated with the analysis of the individual sample. The solid black line represents the average values measured in LAGIR-UERJ. The gray band corresponds to the intermediate precision (2s) of the average with 95 % CI. The dashed red line and the red square represent the average of the reference materials.

3.2.4.2 Zircons U-Pb ages

U-Pb zircon dating was carried out in the BG-14B and BG-200 samples. Concordia diagrams were constructed with analytical data considering individual uncertainties of $^{206}Pb/^{238}U$ and $^{207}Pb/^{235}U$ ratios with 2s less than 4 %, error correlation more than 0.6 %, discordance less than 1.1 %, and low common Pb values.

Zircon grains from sample BG-14B have c-axis dimensions of ~ 250 μm, generally with a 4:1 to 2:1 ratio, and are prismatic, sub-euhedral, and colorless/transparent. Zircon grains from sample BG-200 have c-axis dimensions of ~ 200 μm with a 3:1 ratio, and are prismatic, colorless/transparent, and sub-euhedral. Internal zoning domains of the zircon grains and spot location were determined based on cathodoluminescence images. The grains mostly show concentric compositional zoning parallel to the c-axis.

The concordant ages are interpreted as crystallization or metamorphic age for sample BG-200. For sample BG-14B, a Concordia Age calculated based on six concordant zircon grains indicates crystallization in 518.3 ± 21.9 Ma (Figure 11), while in sample BG-200, a Concordia Age calculated for six concordant zircon grains gives crystallization in 602.2 ± 4.9 Ma (Figure 12). Metamorphic ages are dated in 574.5 ± 2.4 Ma, based on eleven concordant zircon grains, for sample BG-200.

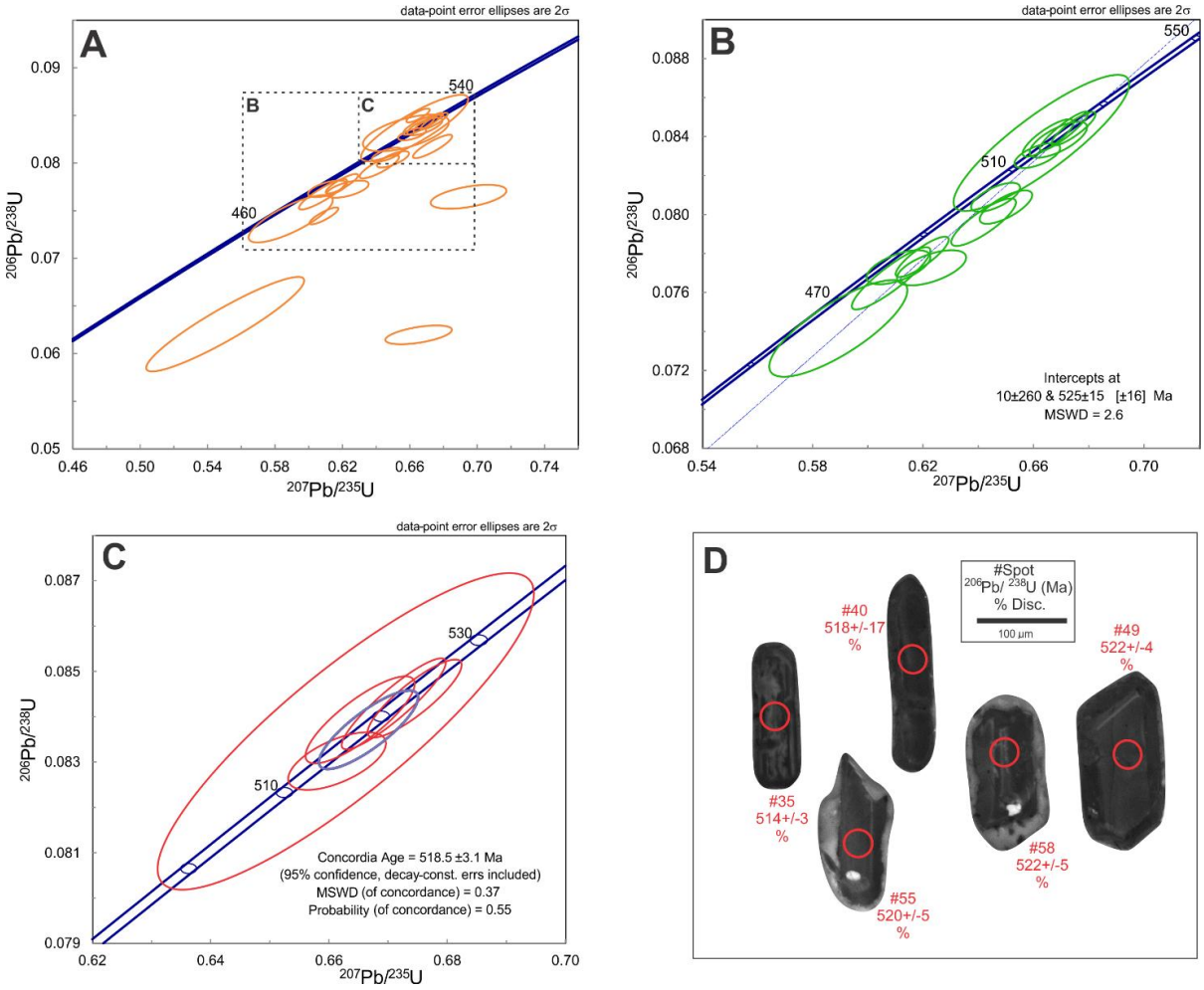

Figure 11 - U-Pb analysis of sample BG-14B: A) All zircon grains; B) Upper intercept age; C) zoom in detail on the Concordia Age of crystallization; D) selected zircon crystals showing spot locations with measured $^{206}Pb/^{238}U$ ages (Ma), and discordance.

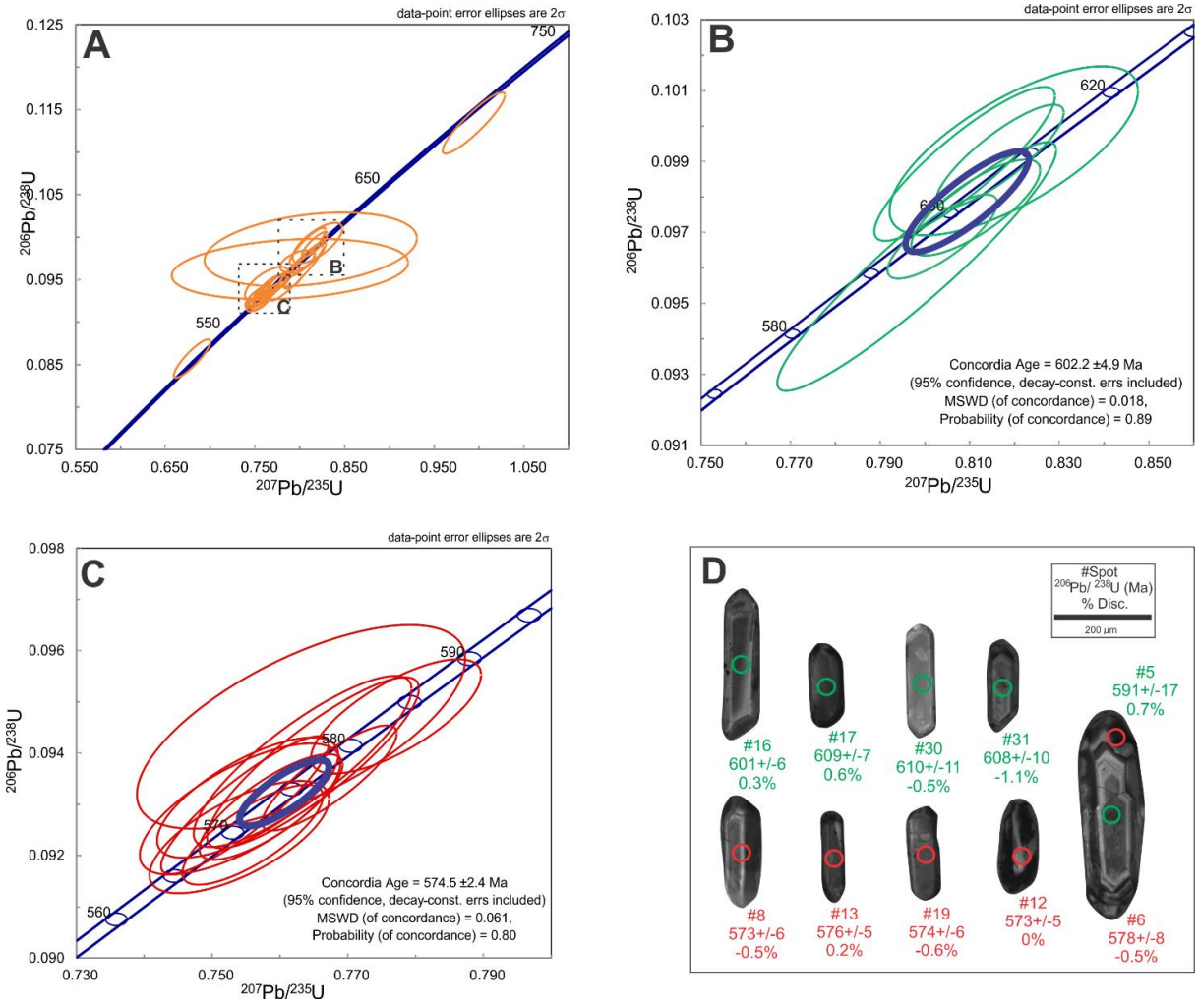

Figure 12 - U-Pb analysis of sample BG-200: A) All zircon grains; B) zoom in detail on the Concordia Age of crystallization; C) Zoom in detail on the Concordia Age of metamorphism; D) Selected zircon crystals showing spot locations for rim and core with measured $^{206}Pb/^{238}U$ ages (Ma), and discordance.

The reference materials used for quality control were Plesovice, with an age of 337 ± 0.37 Ma (SLÁMA et al., 2008); and BB9, with an age of 565.1 ± 1.8 Ma (SANTOS et al., 2017). All data are given in Table S.4 of the Supplementary Material.

3.2.4.3 Initial $^{87}Sr/^{86}Sr$ ratio in whole-rock

To calculate the initial $^{87}Sr/^{86}Sr$ ratio, using the geochronology equation (FAURE, 1986), the following parameters were considered: Rb and Sr concentrations of the whole-rock (in ppm), measured $^{87}Sr/^{86}Sr$ isotope ratio, crystallization age and their respective measurement uncertainties. The uncertainties of the Rb and Sr concentrations were estimated based on the analysis of the reference material BIR-1a, resulting in an uncertainty of 2 % for Rb, using the FUS-MS method, and of 1 % for Sr, using the FUS-ICP method. The

propagation of the uncertainties of the calculated initial ratio was represented by the expanded uncertainty (U), obtained from the combined uncertainty (u_c) with coverage factor (k = 2), corresponding to a 95 % confidence interval. The calculations followed the guidelines established by VIM (2008).

3.2.4.4. Statistical analysis by comparison of averages

The statistical analysis for comparing the averages of $^{87}Sr/^{86}Sr$ values in the EN-1 and Durango Apatite was performed with the aim of comparing the groups separated based on the Sr mass loaded in the chromatographic column to verify whether there is a significant difference between the averages. The independent Student's test and one-way ANOVA were used to assess significant differences between two or more groups from the average. To verify the reliability assumptions of the tests, the normality test of data distribution (SHAPIRO and WILK, 1960) and the homogeneity of variances test (LEVENE, 1960) were used, both evaluated by p-values > 0.05, showing groups with normal distribution and homogeneous variances. All statistical parameters were obtained using Jamovi 1.2.27 (THE JAMOVI PROJECT, 2020; R CORE TEAM, 2019).

3.2.4.5. $^{87}Sr/^{86}Sr$ ratios of apatites from granitoid rocks of the Brasiliano orogen

The apatite samples consist of grains with relatively uniform sizes, determined based on their dimensions and density. The hand-picked apatite grains are carefully selected to ensure they belong to the same population, based on their morphology, color, and size, using a magnifying glass. Typically, these grains exhibit proportions of 2:1 (c-axis ~150 µm) to 3:1 (c-axis ~ 200 µm), corresponding to masses of approximately 3 µg.

In this work, the Sr content obtained for each sample through chemical analysis and the estimated masses were used to determine the masses of Sr loaded onto the column for isotopic analyses. The Sr concentrations in apatites range from approximately 80 to 950 ppm, yielding Sr masses of 0.3–3 ng for single-grains and up to 30 ng for multi-grains, covering mass variations of up to three orders of magnitude.

3.2.4.5.1 Sample SMM-CMM-172

Sample SMM-CMM-172 is a weakly foliated granodioritic gneiss from the Rio Negro Complex, studied by PEIXOTO et al. (2017), with a pre-collisional U-Pb zircon crystallization age of 629 ± 10 Ma (2s). The dominant mineralogy consists of K-feldspar, quartz, and plagioclase, with biotite as the main mafic component, along with accessory minerals such as zircon and apatite (Figure 13A). Apatite crystals occur in euhedral to subhedral shapes, often displaying faces with a hexagonal form, and are easily identified by their relief. They are typically found as interstitial phases between quartz and feldspars (Figure 13D). The sample is characterized by moderate SiO_2 content of 64.8 wt % and Na_2O + K_2O of 6.1 wt %, classifying it as granodiorite. It exhibits an affinity with the high-K calc-alkaline series and is weakly peraluminous. The sample shows strong fractionation between light rare earth elements (LREE) and heavy rare earth elements (HREE) and plots within the field of volcanic arc granitoids (PEARCE et al., 1984). The whole-rock isotopic analysis provides an initial εNd of -8.4 and an initial $^{87}Sr/^{86}Sr$ ratio of 0.710833 ± 0.000628 (U, k = 2). The apatite $^{87}Sr/^{86}Sr$ ratios range from 0.713948 to 0.714727, with an average isotopic composition of 0.714313 ± 0.000442 (2s, n = 17), a RSD of 0.03 %, and a Sr content of 945 ppm.

3.2.4.5.2 Sample BG-200

The BG-200 sample is located at coordinates -22,55499 and -43,22531 (WGS84) and corresponds to an orthogneiss from the Bingen Unit, that is intrusive in Rio Negro Complex (TUPINAMBÁ et al. 2000; 2012). The sample exhibits medium- to coarse-grained with a hypidiomorphic inequigranular texture due to the presence of megacrysts of plagioclase. Its mineralogical composition consists of quartz, K-feldspar, plagioclase, biotite, and accessory minerals such as zircon and apatite (Figure 13B). The apatite grains occur enclosed within biotite plagioclase and also occur as interstitial phases between quartz and feldspar (Figure 13E). BG-200 represents a syn-collisional granite with a U-Pb zircon crystallization age of 602.2 ± 4.9 Ma. It exhibits a granitic chemical composition, characterized by a high SiO_2 content of 69.7 wt % and Na_2O + K_2O of 6.9 wt %, with a weakly peraluminous, high-K calc-alkaline affinity. The sample exhibits pronounced fractionation between LREE and HREE, positioning it within the field of volcanic arc granitoids (PEARCE et al. 1984) The whole-rock isotopic analysis indicates an initial εNd of -9.8 and initial $^{87}Sr/^{86}Sr$ ratio of 0.714438 ± 0.000498 (U, k = 2). The apatite $^{87}Sr/^{86}Sr$ ratios vary between 0.715920 and 0.717079, with

an average isotopic composition of 0.716527 ± 0.000653 (2s, n = 14), a RSD of 0.07 %, and [Sr_{ap}] of 233 ppm.

3.2.4.5.3 Sample BG-14B

The BG-14B sample, located at coordinates -22,603914 and -43,28459 (WGS84), is a post-collisional intruded in the Rio Negro Complex (TUPINAMBÁ et al. 2000; 2012). It yielded a U-Pb zircon crystallization age of 518.3 ± 1.9 Ma. The observations microphotographs show fine- to medium-grained with a hypidiomorphic inequigranular texture and the mineral assemblages of this sample include quartz, plagioclase, biotite, and accessory minerals such as hornblende, zircon, and apatite (Figure 13C). Apatite grains typically occur either individually or in groups, predominantly displaying euhedral to subhedral crystal forms, with faces often recognizable by their hexagonal shapes and relief. They are found in the interstitial of rock-forming minerals, mainly in association with plagioclase and biotite (Figure 13F). It is characterized by a diorite chemical composition, with low SiO_2 content 56.2 wt % and Na_2O + K_2O totaling 5.5 wt %, and exhibits a metaluminous, calc-alkaline affinity. The sample shows weak fractionation between LREE and HREE and plots within the field of volcanic arc granitoids (PEARCE et al. 1984). The whole rock isotopic data provide an initial εNd of -7.2 and initial $^{87}Sr/^{86}Sr$ ratios of 0.711182 ± 0.000420 (U, k = 2). The average of the $^{87}Sr/^{86}Sr$ isotopic ratios measured in apatite grains in sample BG-14B is 0.712937 ± 0.000344 (2s, n = 12), ranging from 0.712656 to 0.713222, with a RSD of 0.02% and an apatite Sr content of 83 ppm.

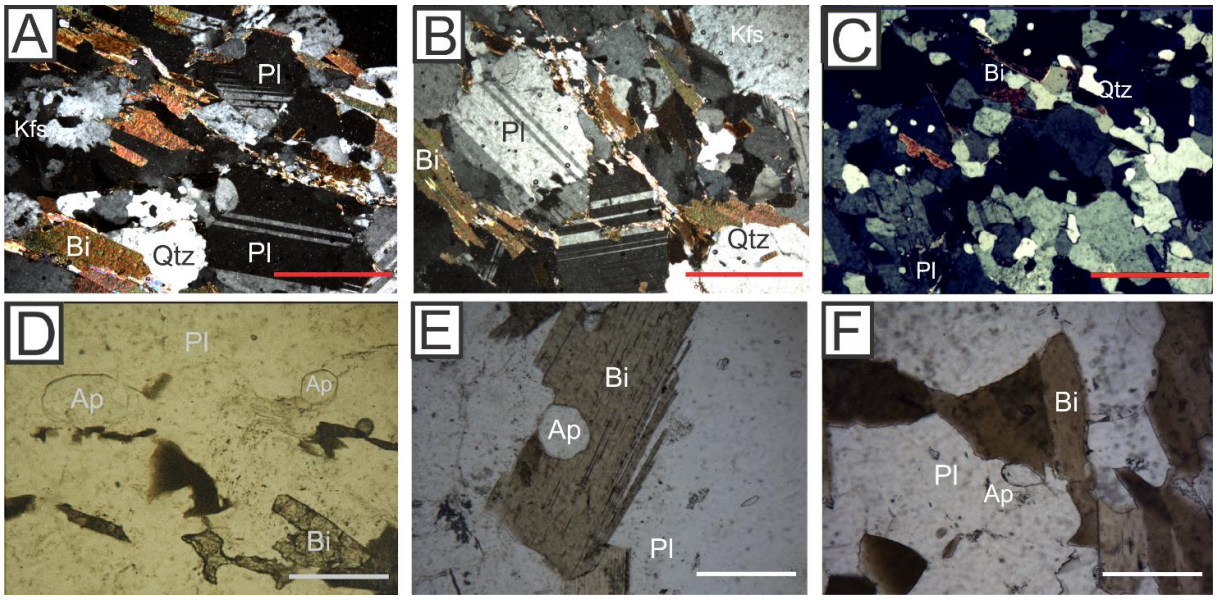

Figure 13 - Thin-section photographs under cross-polarized light of major mineral assemblages of the (A) SMM-CMM-172, (B) BG-200, (C) BG-14B. Thin-section photographs under plane-polarized light showing (D) euhedral prismatic apatite of the SMM-CMM-172 with apatite inclusions in the phenocrysts, (E) BG-200 and (F) BG-14B. Kfs = K-feldspar; Pl = plagioclase; Qtz = quartz; Bi = biotite; Ap = apatite. Red scale bar equal to 1 mm and white scale bar equal to 0.5 mm.

All raw data on the chemical and isotopic composition of the whole-rock are provided in Figure S1 and Tables S.5 and S.6 of the Supplementary Material.

3.2.5 Discussion

3.2.5.1 Relationship between $^{87}Sr/^{86}Sr$ isotopic fractionation and the amount of Sr in the reference materials and samples

To evaluate possible significant isotopic fractionations of the $^{87}Sr/^{86}Sr$ ratios analyzed in the reference materials, based on the amount of Sr (ng) loaded on the chromatographic column in different orders of magnitude (10^1, 10^0 and/or 10^{-1}), groups were formed with the individual values measured for comparison of the averages that will be described below.

The "LAGIR values" group encompasses all the individual $^{87}Sr/^{86}Sr$ ratios from reference materials, while the other groups are subsets derived from this main group, composed of the individual values corresponding to the different orders of magnitude of the Sr mass (ng), loaded on the column (10^1, 10^0 and/or 10^{-1}). Finally, the last group represents the average of the reference value based on the literature of EN-1 (Figure 14A) and Durango Apatite (Figure 14B). The variability between the averages of these groups for each reference material was less than 0.0005 %, and the statistical tests comparing the averages are presented below and reinforce the robustness of this assessment. The good reproducibility of the RMs EN-1 and Durango Apatite, used in the development of the technique presented in this work, ensures the reliability of the obtained results.

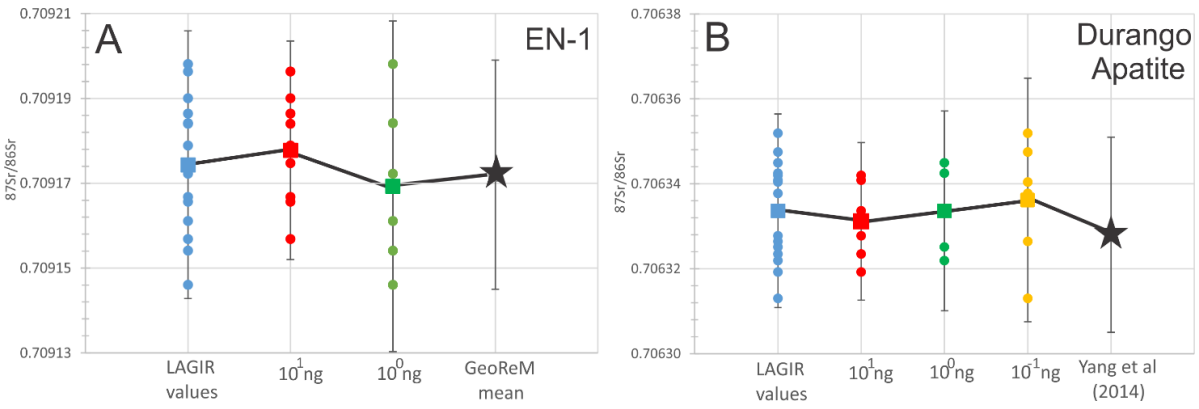

Figure 14 - Comparison of groups separated by Sr mass according to their order of magnitude, the average of all values measured in LAGIR and literature data average. (A) EN-1 and (B) Durango Apatite.

For both the EN-1 ($F(2,27) = 0.518$, $p = 0.602$) and Durango Apatite ($F(3,28) = 0.185$, $p = 0.906$), the one-way ANOVA Fisher test showed no significant statistical difference observed between the Sr results and the average Sr composition for 10^1, 10^0 and/or 10^{-1} orders of magnitude. The Student test also showed no significant difference for both EN-1 ($t(14) = 0.576$, $p = 0.572$) and Durango Apatite ($t(15) = 1.990$, $p = 0.066$) when comparing the measured values with values from the GeoReM and YANG et al. (2014), respectively.

As demonstrated, when considering variations in the range of two orders of magnitude for Sr masses, no significant fractionation was observed in the Sr isotopic composition obtained in the averages of the reference materials, which can be extended to studies of samples with grains from the same population, ensuring that the mass variation remains within an adequate range, providing reliable isotopic compositions. Grain mass control, whether by means of analytical balances or by estimating its dimensions, should always be prioritized to ensure that the maximum Sr mass loading in the chromatographic column does not exceed the limit of 100 ng, as established by CHARLIE et al. (2006).

The evaluation and comparison between the averages of the $^{87}Sr/^{86}Sr$ ratio performed in single-grain and multi-grain samples of SMM-CMM-172, BG-200, and BG-14B confirm the homogeneity of the population of selected grains, in addition to corroborating the excellent results of variation of the Sr mass performed in the reference materials. Although the single grains present relatively uniform estimated masses, the amounts of Sr exhibit significant variations, reaching up to an order of magnitude, a behavior also observed in the multi-grains batches. These differences are directly related to the Sr contents in the analyzed grains.

For the proposed technique, to obtain $^{87}Sr/^{86}Sr$ isotopic ratios in apatite grains, chemical analysis is not essential. However, to evaluate the variability and homogeneity of granitoid rocks samples and validate the technique regarding its analytical rigor, Sr concentrations were determined by chemical analysis. The results showed absolute differences of one order of magnitude between samples SMM-CMM-172, BG-200, and BG-14B, whose Sr contents were 945, 233, and 83 ppm, respectively. These data, combined with the estimated grain mass for single-grain or multi-grain analyses, allowed the calculation of the mass of Sr loaded on the chromatographic column.

Among the samples studied, the amounts of Sr varied by up to two orders of magnitude. In single-grain samples with a mass of approximately 3 µg, the amounts of Sr

varied between 0.2 and 3 ng, while in multi-grain batches (composed of 5 to 10 grains) they presented values that reached 30 ng (See Table S7 of Supplementary Material). Statistical tests for comparison of averages were performed between the group containing all values and the single-grain and multi-grain subgroups. The results indicated that there were no significant differences between the values, as illustrated in Figure 15.

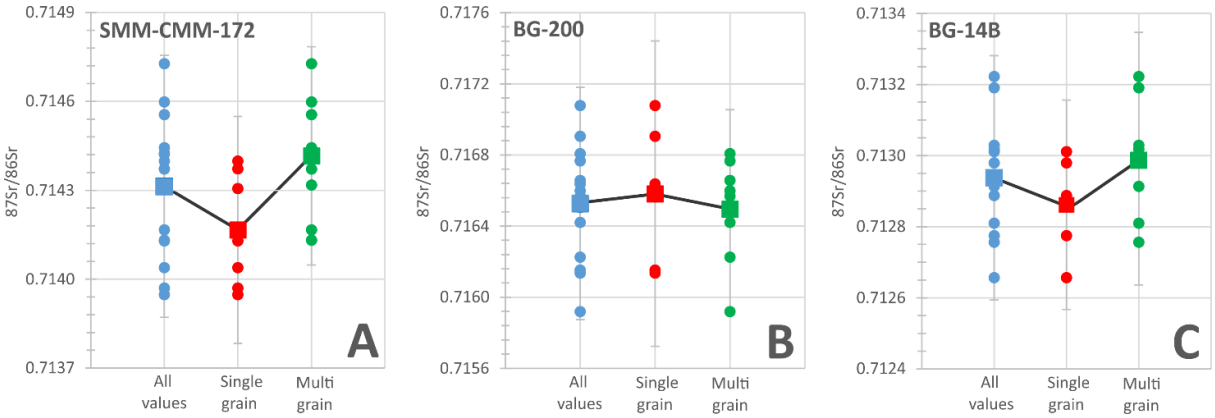

Figure 15 - The blue circle represents the individual values of the "All values" group (complete set of isotopic measurements). The red and green circles correspond to the values of the "Single-grain" and "Multi-grain" subgroups (derived from the complete set), respectively. The squares indicate the average or central values of each group.

One-way ANOVA (Fisher) revealed no statistically significant differences among the groups “all values,” “single-grains,” and “multi-grains” for the SMM-CMM-172, BG-200, and BG-14B samples: $F(2,31) = 3.039$, $p = 0.062$; $F(2,25) = 0.107$, $p = 0.899$; and $F(2,21) = 0.853$, $p = 0.440$, respectively.

Since chemical analysis is not essential, researchers that may adopt this technique are encouraged to estimate the Sr concentration based on diagrams described by CHU et al. (2009), JIA et al. (2020), and YAN et al. (2024). These estimates can be based on available data, such as chemical analyses of Sr in whole rock, SiO_2 contents (% wt), or tectonic classification, in addition to the simple petrographic classification of granitoid rocks. In general, the Sr contents in apatite grains tend to be restricted to the range $0.25 \leq Sr_{apatite}/Sr_{whole\text{-}rock} \leq 1$ (CHU et al., 2009).

3.2.5.2. Variability of $^{87}Sr/^{86}Sr$ ratios between apatite grains and whole-rock analysis

The variability of the RSD for the individual values of the apatite grains of the samples SMM-CMM-172, BG-200, and BG-14B is less than 0.05 % (Figure 16). When comparing the RSD of the individual values of the analyzed reference materials (0.002 %)

with the variability of the measurements in the apatite grains of the samples, a reduction of one order of magnitude is observed. This indicates that the variation observed in the RSD in the apatite grains of the samples probably does not result from analytical problems intrinsic to the procedures of the presented technique but may be related to sources of variability of a geological nature.

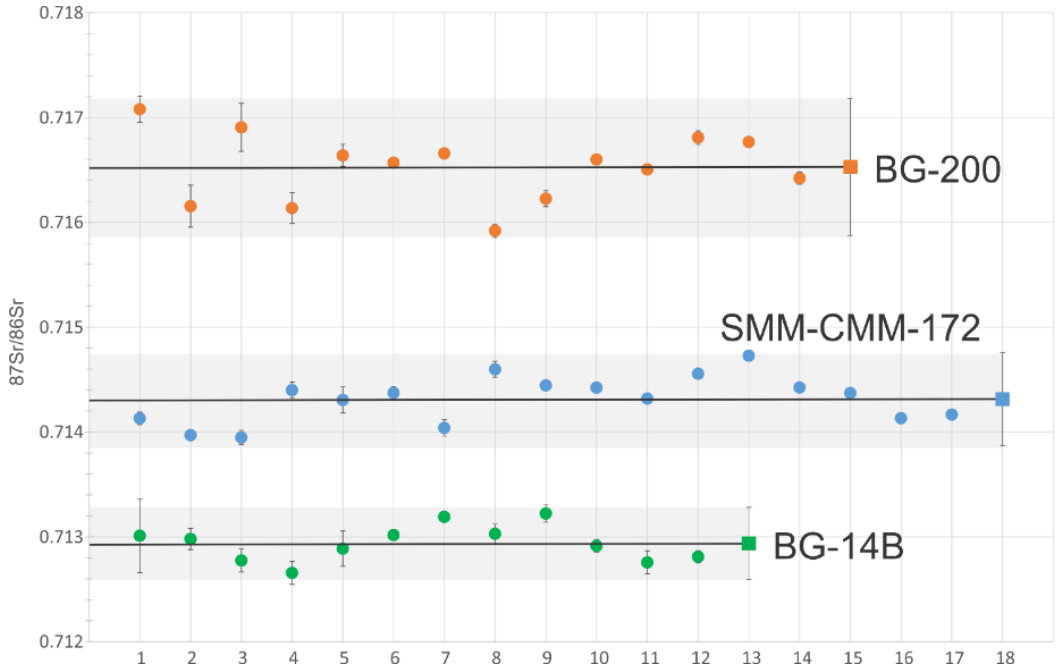

Figure 16 - The variability of the individual values of the apatite grains of the samples SMM-CMM-172, BG-200, and BG-14B with their respective uncertainties under repeatability conditions (2s) and the average of all the values and their uncertainties (2s) under intermediate precision conditions.

In several studies, the Sr isotopic compositions in granitoid rocks present RSD varying between the individual apatite values. SUN et al. (2021) considered the initial $^{87}Sr/^{86}Sr$ ratios in apatite grains from group 1 (G1) in their research as having low variability (= 0.2 %). ZHOU et al. (2023) found, in their studies with alkaline rocks, relatively low initial $^{87}Sr/^{86}Sr$ ratios, with RSD of 0.2 %. LINGHU et al. (2023) performed Sr isotope analyses on apatite grains from two granitoid rocks derived from a pluton and identified in situ $^{87}Sr/^{86}Sr$ values with RSD lower than 0.19 %, reporting that these values did not present significant differences within the margins of error. Thus, it is inferred that there is a low variability in the samples from this study, with RSD below 0.05 % (Figure 17).

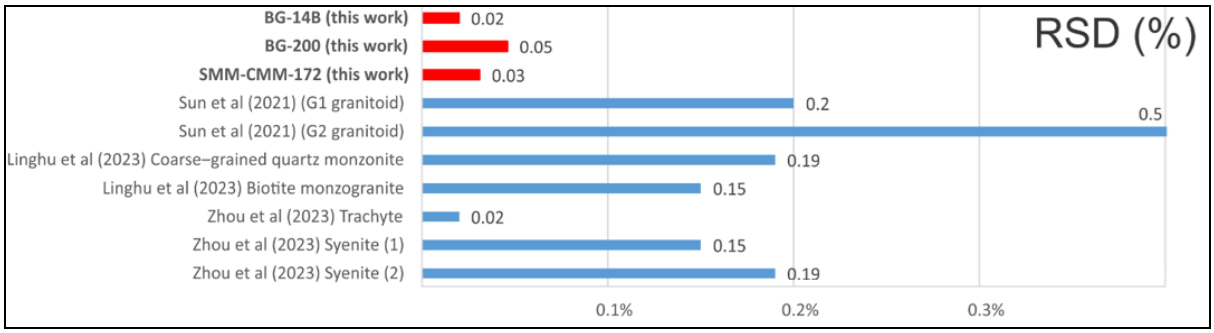

Figure 17 - Comparison of the RSDs (relative standard deviations) of the $^{87}Sr/^{86}Sr$ ratios of the apatite grains in this work with the literature.

The relative percentage difference (RPD) between the whole-rock ($^{87}Sr/^{86}Sr$ (t) ratio calculated and the average ratio in the apatite grains is 0.5 %, 0.3 %, and 0.2 % for the SMM-CMM-172, BG-200 and BG-14B samples, respectively. Figure 18 presents the individual $^{87}Sr/^{86}Sr$ ratios obtained in apatite grains, as well as the initial $^{87}Sr/^{86}Sr$ ratios calculated from the whole-rock analyses for each of the studied samples in combination with the initial εNd values, assuming approximately that the initial εNd from whole-rock is equivalent to that of the apatite grains, based on LINGHU et al. (2023). Figure 18 and Table 9 also show the relationship between $\varepsilon Nd_{(t)}$ and $^{87}Sr/^{86}Sr_{(t)}$ and reinforce the agreement by demonstrating that the Sr isotopic data of the apatite grains and the whole-rocks are within the regional fields of the samples SMM-CMM-172, BG-200 and BG-14B previously defined for granitoid rocks associated with the pre-, syn- and post-collisional Ribeira Orogeny, respectively. These results confirm the robustness of the isotopic analyses performed by the proposed technique, demonstrating that the apatite grains reliably preserve the initial isotopic signature of the source rocks. Thus, they contribute to the understanding of the isotopic evolution of the studied rocks and reinforce their relevance as tools for geological reconstruction studies.

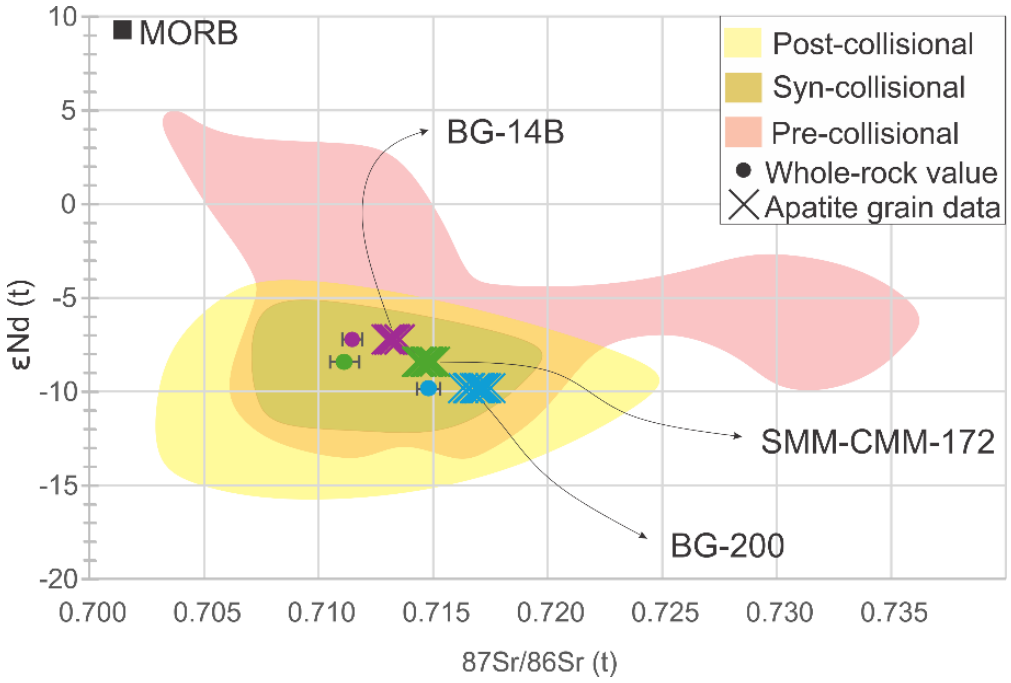

Figure 18 - εNd vs. $^{87}Sr/^{86}Sr$ diagram, considering that εNd values of whole-rock and apatite grains are equivalent. Data in plotted fields for pre-, syn- and post-collisional granitoid rocks are from MEDEIROS et al. (2000); SILVA (2011); MACHADO et al. (2016); PEIXOTO et al. (2017); HEILBRON et al. (2020); COELHO et al. (2023), POTRATZ et al. (2025).

Table 9 – Summary of isotopic data from granitoid rocks samples

Sample	Rock type	Collisional stage [a]	Unit	Age (Ma)	$^{87}Sr/^{86}Sr_{(b)}$ [c]	$^{87}Sr/^{86}Sr_{(apatite)}$ [c] [d]	RPD (%) [e]
SMM-CMM-172	granodiorite	pre	Rio Negro	629 ± 10	0.710833 ± 628	0.714313 ± 442	0.5
BG-200	granite	syn	Bingen	602.2 ± 4.9	0.714438 ± 498	0.716527 ± 653	0.3
BG-14B	diorite	post	Bingen	518.3 ± 1.9	0.711182 ± 420	0.712937 ± 344	0.2

Note: (a) Collisional stage of the Brasiliano orogen; (b) calculated initial ratio from whole-rock; (c) Expanded uncertainty (U) with coverage factor (k = 2) 95 % confidence interval; (d) Average ratio in the apatite grains; (e) Relative percentage difference between the calculated initial ratio and the average ratio in the apatite grains.

3.2.5.3 Advantages and limitations of the technique

The technique developed for the analysis of $^{87}Sr/^{86}Sr$ isotopic ratios in apatite grains presents advantages that make it a viable alternative tool for large-scale studies in different geological contexts and in petrogenetic investigations. Among its main advantages are the reduction of costs and time required for analysis, without compromising the accuracy of the results. The optimized use of reagents and the simplification of chemical procedures contribute to the reduction of laboratory blanks and isobaric interferents, ensuring greater reliability in the data obtained. Furthermore, the technique allows analyses on microanalytical scales, with samples containing as low as 0.5 ng of Sr.

Despite these advantages, the technique has some limitations. In samples with very small grains and/or low apatite content, it can be challenging to obtain sufficient Sr material for isotopic analysis, especially in single grains, which can compromise the precision of the results. The presence of grains with complex internal structures and/or mineral inclusions not identified by binocular magnifying glass can also negatively affect the quality of the results. In addition, the interpretation of isotopic data can be complex in environments where apatite undergoes secondary chemical or isotopic alteration, such as metasomatism, or when there is the presence of inherited grains. Under these conditions, the isotopic ratios obtained may not reflect the initial composition of the magmatic system, requiring a careful analysis of the results, and integrating them with other evidence, such as petrographic and geochemical studies. Therefore, although the technique demonstrates high efficiency in several situations, its application depends on well-preserved samples and an adequate geological context.

3.2.6 Conclusions

The TIMS technique presented here combines detailed chemical and spectrometric procedures for the analysis of Sr isotopes in apatite grains with low variability (< 0.05%). The developed method validates the use of Sr isotopic composition in apatite as a proxy to estimate the initial ratio $^{87}Sr/^{86}Sr$ in granitoid rocks. This approach stands out for its efficiency in reducing costs and analysis time while maintaining high analytical precision.

The reliability of the technique is corroborated by the reproducibility obtained from reference materials, such as EN-1 (USGS) and Durango Apatite, which prove the robustness of the method. Furthermore, the initial $^{87}Sr/^{86}Sr$ isotopic ratios, calculated both from whole-rock and apatite grains from representative samples of pre-, syn- and post-collisional magmatism of the Ribeira Orogeny, consistently reflect the initial Sr isotopic composition of the magmatic system, within an uncertainty of 0.5 %.

CONSIDERAÇÕES FINAIS

A presente tese abordou o desenvolvimento de procedimentos analíticos utilizando a técnica de espectrometria de massas por termo-ionização (TIMS), em amostras de rocha total e apatita fornecendo composições isotópicas precisas e confiáveis para estudos petrogenéticos.

O principal objetivo foi desenvolver e otimizar procedimentos analíticos para a medição das razões isotópicas Sm-Nd e Sr-Sr, avaliando sua aplicabilidade na caracterização de estudos petrogenéticos e na obtenção de medições mais precisas e reprodutíveis. Esse objetivo foi alcançado, como demonstrado pelos dados obtidos e sua coerência com a literatura existente.

Os dois manuscritos apresentados como produto desta pesquisa evidenciam a importância, eficácia e aplicabilidade das metodologias laboratoriais em petrogênese e evolução crustal de relevância regional. Os resultados indicaram que os procedimentos químicos e analíticos em TIMS apresentam elevada robustez e precisão, validando a abordagem metodológica adotada e evidenciando seu potencial para aplicações em estudos geológicos. As etapas de coleta das amostras, purificação química, separação dos elementos por cromatografia de troca iônica e análise espectrométrica por TIMS mostraram-se adequadas aos objetivos do estudo. Além disso, a calibração rigorosa dos equipamentos e os testes de reprodutibilidade foram fundamentais para assegurar a confiabilidade dos resultados.

O primeiro artigo focou na composição isotópica de Nd e Sr em rocha total do material de referência BRP-1, um basalto Cretáceo da Bacia do Paraná, destacando a importância de materiais de referência bem caracterizados para a obtenção de dados isotópicos precisos e reprodutíveis. A análise da consistência dos resultados ao longo de doze anos no LAGIR, sob diferentes condições de digestão, confirmou a confiabilidade dos dados, reforçando o uso do BRP-1 como referência para estudos isotópicos.

O segundo artigo destacou a análise isotópica de Sr em grãos de apatita por TIMS como uma ferramenta eficiente e de menor custo para identificar assinaturas isotópicas iniciais, permitindo a distinção entre fontes. A implementação de uma metodologia otimizada para a determinação da razão $^{87}Sr/^{86}Sr$ em grãos de apatita representou um avanço significativo, reduzindo o tempo e os custos analíticos em comparação com o procedimento padrão utilizado no primeiro artigo, sem comprometer a qualidade dos dados. Além disso, a alta precisão na identificação de fontes magmáticas mantélicas ou crustais amplia as

possibilidades de aplicação da metodologia, incluindo a compreensão dos processos magmáticos, como também amplia a aplicabilidade em estudos de proveniência sedimentar e evolução crustal. A eficácia deste método, em comparação com análises convencionais de rocha total, destaca o potencial da apatita como um proxy valioso para investigações geológicas detalhadas, reforçando a relevância desses procedimentos em diferentes contextos, desde estudos regionais até investigações globais sobre a história da Terra.

Ambos os artigos convergem para a consolidação de técnicas analíticas robustas, fornecendo subsídios para a interpretação dos processos geológicos, apoiados por metodologias bem aplicadas e materiais de referência adequados.

Os desafios inerentes à condução da pesquisa foram evidenciados pela complexidade na preparação das amostras e a necessidade de ajustes nos procedimentos analíticos, que demandaram tempo e repetição de experimentos, bem como revisão sistemática da literatura recente. Além disso, a quantidade limitada de Sr em alguns grãos de apatita com baixo teor desse elemento representou um desafio para a obtenção de dados precisos e acurados.

Nesse sentido, recomenda-se como futuras pesquisas, a aplicabilidade do método aqui apresentado em diferentes contextos geológicos, ampliando a base de dados para diversas formações geológicas. A redução do tamanho e do volume das etapas de digestão de amostras e eluição dos elementos químicos pode tornar os procedimentos ainda mais rápidos, eficientes e com menor consumo de reagentes, reduzindo custos e minimizando erros experimentais. Ademais, o desenvolvimento ou a otimização dos componentes do espectrômetro de massas pode aumentar sua capacidade de detectar e medir quantidades extremamente baixas, na ordem de $<< 10^{-1}$ ng de Sr com maior precisão isotópica. Isso é particularmente relevante para amostras com baixas concentrações dos elementos de interesse, como Sr em apatita. Essas melhorias podem contribuir significativamente para o avanço dessa linha de pesquisa.

A principal contribuição original desta tese foi o refinamento metodológico para a análise de razões isotópicas de Sm-Nd e Sr-Sr em rocha total e apatita, resultando em procedimentos analíticos otimizados e validados.

Por fim, esta jornada de pesquisa foi marcada por desafios metodológicos e ajustes científicos enriquecedores. O desenvolvimento deste estudo proporcionou um aprendizado profundo sobre a complexidade das análises isotópicas e sua relevância para as geociências, além de evidenciar seu potencial para aplicações em diversas áreas de estudo.

REFERÊNCIAS

AGGARWAL, SK. Thermal ionisation mass spectrometry (TIMS) in nuclear science and technology – a review. **Analytical Methods**. v. 8:942, 2016

AHMAD, S., DAYAL, A., PADMAKUMARI, VM., GOPALAN, K. Evolution of strontium isotopes in seawater during the middle Miocene: New results from ODP site 758A. **Journal of the Geological Society of India**. v. 55, 2000

ALI, K.; JEON, H.; ANDRESEN, A.; LI, S. Q.; HARBI, H.; HEGNER, E. U-Pb zircon geochronology and Nd-Hf-O isotopic systematics of the Neoproterozoic Hadb adh Dayheen ring complex, Central Arabian Shield, Saudi Arabia. **Lithos**, v. 206, p. 348-360, 2014.

ALLÈGRE, C. J. **Isotope Geology**. Nova York: Cambridge University Press, 2008.

ALMEIDA, F. F. M. O Craton do São Francisco. *Revista Brasileira de Geociências*, v. 7, p. 349–364, 1977.

ALMEIDA, F. F. M.; DE HASUI, Y.; DE BRITO-NEVES, B. B. Brazilian structural provinces: an introduction. **Earth Science Reviews**, v. 17, p. 1–29, 1981.

ALMEIDA, R., ELIZEU, V. H. BRUNO, BERSAN, S.M., ARAUJO, L.E.D.A.B., DUSSIN, I., VALERIANO, C.M., NETO, C., HEILBRON, M. Rhyacian-Orosirian tectonic history of the Juiz de Fora Complex: Evidence for an Archean crustal reservoir within an island-arc system. **Geoscience Frontiers**, v.13 (5), 101292, 2022

ALTHERR, R.; HOLL, A.; HEGNER, E.; LANGER, C.; KREUZER, H. High-potassium, calc-alkaline I-type plutonism in the European Variscides: Northern Vosges (France) and northern Schwarzwald (Germany). **Lithos**, v. 50, p. 51-73, 2000.

AOKI, J., TAKAGAI, Y. Direct quantification of femtogram per liter (fg L−1) level 90Sr in rainwater using thermal ionization mass spectrometry. **Journal of Analytical Atomic Spectrometry**. v.39, p. 408-413, 2024

AWADH S. M. **Geochemistry of Radioactive Isotopes** IN: RENÉ, M., GEMMA AIELLO, G., EL BAHARIYA, G. eds. **Geochemistry**. IntechOpen. 314pp, 2021

BABINSKI, M.; PETRONILHO, L. A.; MAGDALENO, G. B.; SILVA, R. A.; RUIZ, I. R.; ENZWEILER, J. Reference Material BRP-1 (Basalt Ribeirão Preto): can it be used as an isotope standard? *Anais*. Prague: **European Association of Geochemistry**, 2014. p. 91
.

BAO Z.A., ZONG C.L., FANG L.R., YUAN H.L., CHEN K.Y., DAI M.N. Determination of Hf–Sr–Nd isotopic ratios by MC-ICP-MS using rapid acid digestion after flux-free fusion in geological materials. **Acta Geochimica**, v. 37, p. 244–256, 2018

BEARD, B. L.; GLAZNER, A. F. Trace element and Sr and Nd isotopic composition of mantle xenoliths from the Big Pine Volcanic Field, California. **Journal of Geophysical Research**, v. 100, n. B3, p. 4169–4179, 1995.

BELLUCCI, J.J., NEMCHIN, A.A., WHITEHOUSE, M.J., HUMAYUN, M., HEWINS, R., ZANDA, B. Pb-isotopic evidence for an early, enriched crust on Mars. **Earth and Planetary Science Letters**, v. 410, p. 34–41, 2015

BELOUSOVA, E. A.; WALTERS, S.; GRIFFIN, W. L.; O'REILLY, S. Y. Trace-element signatures of apatites in granitoids from the Mt Isa Inlier, northwestern Queensland. **Australian Journal of Earth Sciences**, v. 48, p. 603–619, 2001.

BELOUSOVA, E. A.; GRIFFIN, W. L.; O'REILLY, S. Y.; FISHER, N. I. Apatite as an indicator mineral for mineral exploration: trace-element compositions and their relationship to host rock type. **Journal of Geochemical Exploration**, v. 76, p. 45–69, 2002.

BENTLEY, R. A. Strontium isotopes from the earth to the archaeological skeleton: A review. **Journal of Archaeological Method and Theory**. v. 9(3), p. 103-132, 2002

BIRCK, J. L. The precision and sensitivity of thermal ionisation mass spectrometry (TIMS): an overview of the present status. **Geostandards and Geoanalytical Research**, v. 25, p. 253–259, 2001

BOELRIJK, N. A. I. M. A general formula for "double" isotope dilution analysis. **Chemical Geology - Short Communication**, v. 3, p. 323-325, 1968.

BRITO NEVES, B. B.; FUCK, R. A. Neoproterozoic evolution of the basement of the South-American platform. **Journal of South American Earth Sciences**, v. 47, p. 72–89, 2013.

BRUAND, E., STOREY, C., FOWLER, M. Accessory mineral chemistry of high Ba-Sr granites from Northern Scotland: constraints on petrogenesis and records of whole-rock Signature. **Journal of Petrology**. v. 55(8), p. 1619–1651, 2014

BRUAND, E. et al. Accessory mineral constraints on crustal evolution: Elemental fingerprints for magma discrimination. **Geochemical Perspectives Letters**, v. 13, p. 7–12, 2020.

BRUNO, H., ELIZEU, V., HEILBRON, M., VALERIANO, C.M., STRACHAN, R., FOWLER, M., BERSAN, S. MOREIRA, H., DUSSIN, I., SILVA, L.G.E., TUPINAMBÁ, M., ALMEIDA, J., NETO, C., STOREY, C. Neoarchean and Rhyacian TTG-Sanukitoid suites in the southern São Francisco Paleocontinent, Brazil: evidence for diachronous change towards modern tectonics **Geoscience Frontiers**. v. 11, p. 1763-1787, 2020

BURKE, W. H., DENISON, R. E., HETHERINGTON, E. G., KOEPNICK, R. B., NELSON, H. F., OTTO, J. B. Variations of seawater 87Sr/86Sr throughout Phanerozoic time. **Geology**, v. 10, p. 516–519, 1982.

BÜRGER, S., VOGL, J., KLOETZLI, U., NUNES, L. AND LAVELLE, M. Thermal Ionisation Mass Spectrometry. In: PROHASKA, T., IRRGEHER, J., A ZITEK, N. JAKUBOWSKI (Hrsg.), Sector Field Mass Spectrometry for Elemental and Isotopic Analysis. 3 Aufl., **New Developments in Mass Spectrometry, Royal Society of Chemistry**, p. 381-438, 2015

BUZENCHI A, MOREIRA H, BRUGUIER O, BOSCH D, DHUIME B. High spatial resolution (10-50 μm) analysis of Sr isotopes in rock-forming apatite by LA-MC-ICP-MS. **Journal of Analytical Atomic Spectrometry.** v. 38(10), p. 2113-2126, 2023

CAMPOS NETO, M. C.; CABY, R. Lower crust extrusion and terrane accretion in the Neoproterozoic nappes of southeast Brazil. **Tectonics**, v. 19, p. 669–687, 2000.

CAMPOS NETO, M. C. Orogenic systems from southwestern Gondwana, an approach to Brasiliano-Pan African cycle and orogenic collage in southeastern Brazil. In: CORDANI, U. G.; MILANI, E. J.; THOMAZ FILHO, A.; CAMPOS, D. A. (Eds.). **Tectonic Evolution of South America**. 31st International Geological Congress, Rio de Janeiro, 2000. p. 335–365.

CAPO, R. C., DEPAOLO, D. J. Homogeneity of Sr Isotopes in the Oceans, **Eos Trans. AGU**, v.73, p. 272, 1992

CAPISTRANO, G. G.; SCHMITT, R. S.; MEDEIROS, S. R.; FERNANDES, G. L. F. Evidence of a Neoproterozoic active continental margin - Geochemistry and isotope geology of high-grade paragneiss from the Ribeira Orogen, SE Brazil. **Journal of South American Earth Sciences**, v. 77, p. 170–184, 2017.

CARLSON, R.W. **Thermal Ionization Mass Spectrometry**. Treatise on Geochemistry, 15, p. 337-354, 2014

CARVALHO, M.O., MOTTRAM, C.M., VALERIANO, C.M., RAMOS, R.R.C., PARRISH, R., DUNLOP, J., COTA, N., PARAVIDINI, G., NETO, C.C.A., HEILBRON, M., STOREY, C. Sedimentary provenance in continental rifts: U–Pb detrital zircon, Nd and Sr isotopes and lithogeochemistry of the Eocene alluvial sandstones of the Resende Basin, SE–Brazil, **Sedimentary Geology**. v. 453, 106452, 2023

Charlier, B.L.A., Ginibre, C., Morgan, D., Nowell, G.M., Pearson, D.G ., Davidson, J.P. and Ottley, C.J. (2006) Methods for the microsampling and high-precision analysis of strontium and rubidium isotopes at single crystal scale for petrological and geochronological applications. **Chemical Geology, 232**,114–133.

CHEN, W.; SIMONETTI, A. Evidence for the Multi-Stage Petrogenetic History of the Oka Carbonatite Complex (Québec, Canada) as Recorded by Perovskite and Apatite. **Minerals**, v. 4, p. 437-476, 2014

CHENG, T., NEBEL, O., SOSSI, P., CHEN, F. Assessment of hafnium and iron isotope compositions of Chinese national igneous rock standard materials GSR-1 (granite), GSR-2 (andesite), and GSR-3 (basalt). **International Journal of Mass Spectrometry**, v. 386, p. 61–66, 2015

CHERNIAK D.J., RYERSON F.J. A study of strontium diffusion in apatite using Rutherford backscattering spectroscopy and ion implantation. **Geochimica et Cosmochimica Acta,** v. 57, p. 4653–4662, 1993

CHU, M.F., WANG, K.L., GRIFFIN, W.L., CHUNG, S.L., O'REILLY, S.Y., PEARSON, N.J., IIZUKA, Y. Apatite Composition: Tracing Petrogenetic Processes in Transhimalayan Granitoids. **Journal of Petrology**. v. 50(10), p. 1829-1855, 2009

COELHO, V. S. A.; MENDES, J. C.; LUDKA, I. P.; VALERIANO, C. M. Age and petrogenetic constraints of the post-collisional Parati Granite, southeast Brazil. **Journal of South American Earth Sciences**, v. 132, p. 104595, 2023.

CORDANI, U. G.; COUTINHO, J. M. V.; NUTMAN, A. P. Geochronological constraints on the evolution of the Embu Complex. **Journal of South American Earth Sciences**, v. 14, p. 903–910, 2002.

CORRALES, F. F. P.; DUSSIN, I. A.; HEILBRON, M.; BRUNO, H.; BERSAN, S.; VALERIANO, C. M.; PEDROSA-SOARES, A. C.; TEDESCHI, M. Coeval high Ba-Sr arc-related and OIB Neoproterozoic rocks linking pre-collisional magmatism of the Ribeira and Araçuaí orogenic belts, SE-Brazil. **Precambrian Research,** v. 337, p. 105476, 2020.

COTTA, A.J.B, ENZWEILER, J., WILSON, SA, PEREZ, CA, NARDY, AJR, LARIZZATTI, JH. Homogeneity of the geochemical reference material BRP-1 (Paraná Basin Basalt) and assessment of minimum mass. **Geostandards and Geoanalytical Research**, v. 31(4), p. 379-393, 2007

COTTA A.J.B., ENZWEILER J. Certificate of Analysis of the Reference Material BRP-1 (Basalt Ribeirão Preto). **Geostandards and Geoanalytical Research,** v. 32(2), p. 231-235, 2008

CREASER, R. A., GRAY, C. M. Preserved Initial 87Sr/86Sr in Apatite from Altered Felsic Igneous Rocks: A Case Study from the Middle Proterozoic of South Australia. **Geochimica et Cosmochimica Acta**, v. 56(7), p. 2789–2795, 1992

CRUMMY, J. M.; SAVOV, I. P.; NAVARRO-OCHOA, C.; MORGAN, D. J.; WILSON, M. High-K Mafic Plinian Eruptions of Volcán de Colima, Mexico. **Journal of Petrology**, v. 55, n. 11, p. 2155-2192, 2014.

DANESHVAR, N.; AZIZI, H.; ASAHARA, Y.; TSUBOI, M.; HOSSEINI, M. Rare Earth Elements and Sr Isotope Ratios of Large Apatite Crystals in Ghareh Bagh Mica Mine, NW Iran: Tracing for Petrogenesis and Mineralization. **Minerals.** v. 10, 833, 2020

DEER, W.A., HOWIE, R.A., ZUSSMAN, J. Minerais constituintes das rochas: uma introdução**.** Tradução de Carlos António Regêncio Macedo. **Lisboa/POR: Fundação Calouste Gulbenkian,** 727 pp., 2014

DECOL, J.; HEILBRON, M.; PEIXOTO, C.; BRUNO, H.; BERSAN, S. M.; RODRIGUES, S. W. O.; CORRALES, F.; EIRADO, L. G.; TUPINAMBÁ, M. Adakites and associated granitoids from the Serra da Prata Arc: Evidence for a Tonian subduction setting within the Araçuaí-Ribeira orogenic system (AROS), SE Brazil. **Journal of South American Earth Sciences**, v. 111, p. 103481, 2021.

DE PAOLO, D. J.; WASSERBURG, G. J. Nd Isotopic variations and petrogenetic models. **Geophysical Research Letters**, v. 3, n. 5, p. 249-252, 1976.

DE PAOLO, D. J. Trace element and isotopic effects of combined wallrock assimilation and fractional crystallization. **Earth and Planetary Science Letters**, v. 53, p. 189–202, 1981.

De PAOLO, D.J. **Neodymium Isotope Geochemistry: An Introduction.** Springer, Berlin, 187 pp, 1988

DICKIN, A. P. Radiogenic Isotope Geology. 2. Ed. Nova York: **Cambridge University Press**, 490 pp., 2005

DOROSHKEVICH, A.; RIPP, G.; IZBRODIN, I.; SAVATENKOV, V. Alkaline magmatism of the Vitim province, West Transbaikalia, Russia: Age, mineralogical, geochemical and isotope (O, C, D, Sr and Nd) data. **Lithos**, v. 152, p. 157-172, 2012.

DU, Q.; MENG, F.; KERR, A. C.; CHEN, Y.; TIAN, Y.; WU, Z.; ZHOU, Y. Elemental and Sr–Nd–Pb–Hf isotope signatures of Early Cretaceous magmatic rocks in the Wulian area, Eastern Shandong: Implications for crust–mantle interaction at the edge of the Sulu collisional orogenic belt. **Lithosphere**, v. 2022, n. 1, p. 3296117, 2022.

EVANGELISTA, H., VALERIANO, C.M., PARAVIDINI, G., GONÇALVES JUNIOR, S.J., EDUARDO, D., SODRÉ, E.D., NETO, C.C.A., SANTOS, E.A., NETO, N.M., PEIXOTO, C., LICINIO, M.V.V.J., RIBEIRO, J.R., FLORES, A.F., PEREIRA, M.G., BARBOSA, C.F., BARCELLOS, J.R.C., OLIVEIRA, B.V.X., GUEBERT, F., NEGRÃO, F., ANJOS, M.J., SANTOS, R.S., SEOANE, J.C., CORDEIRO, J.C., HEILBRON, M. Using Nd-Sr isotopes in suspended sediments in the Abrolhos coral-reef (SW Atlantic, Brazil) to assess potential contamination from the 2015 Fundão dam collapse. **Science of The Total Environment**, v. 807, 151231, 2022

ERBAN, K.; KOCHERGINA, Y. V.; ERBAN, V.; HORA, J. M. Sample preparation and chromatographic separation for Sr, Nd, and Pb isotope analysis in geological, environmental, and archaeological samples. **Journal of Geosciences**, v. 67, p. 273–285, 2022.

FAURE, G., POWELL, J.L. Strontium Isotope Geology. **Springer-Verlag**, 188 pp., 1972

FAURE, G. **Principles of Isotope Geology**. 2. Ed. Nova York: John Wiley & Sons, Inc. 1986, 589 p.

FAURE, G., MENSING, T.M. Isotopes: Principles and applications. **Wiley-Blackwell, New Jersey**, 897pp., 2005

FICHTNER, V.; STRAUSS, H.; IMMENHAUSER, A.; BUHL, D.; NEUSER, R. D.; NIEDERMAYR, A. Diagenesis of carbonate-associated sulfate. **Chemical Geology**, v. 463, p. 61–75, 2017.

FISHER, C. Sm–Nd isotope systematics by laser ablation-multicollector-inductively coupled plasma mass spectrometry: Methods and potential natural and synthetic reference materials. **Chemical Geology.** v. 284(1–2), p. 1-20, 2011

FLANAGAN, F.J. Reference samples in geology and geochemistry. **Geostandards Newsletter**, 10(2), 195-264, 1986

FLOWERS, R.M., KETCHAM, R.A., SHUSTER, D.L., FARLEY, K.A. Apatite (U-Th)/He thermochronometry using a radiation damage accumulation and annealing model. **Geochimica et Cosmochimica Acta**, v. 73, p. 2347-2365, 2009

FOURNY, A., WEIS, D., SCOATES, J. S. Comprehensive Pb-Sr-Nd-Hf isotopic, trace element, mineralogical characterization of mafic to ultramafic rock reference materials, **Geochemistry, Geophysics, Geosystems**. V.17, p.739–773, 2016

FREITAS, N. C.; HEILBRON, M.; ALMEIDA, J.; DUSSIN, I.; CUTTS, K.; CARVALHO, M.; MOTTRAM, C.; STOREY, C.; CHAPMAN, G. New U-Pb and Hf data of the contact region between the Oriental and Cabo Frio terranes, Central Ribeira Belt, Brazil: Implications for the closure of the Ediacaran-Cambrian oceanic space. **Precambrian Research**, v. 401, p. 107272, 2024.

GILLESPIE, J., GLORIE, S., KHUDOLEY, A., COLLINS, A.S. Detrital apatite U-Pb and trace element analysis as a provenance tool: Insights from the Yenisey Ridge (Siberia), **Lithos**, v. 314–315, p. 140-155, 2018

GILLESPIE, J., NEMCHIN, A. A., KINNY, P. D., MARTIN, L., ALESHIN, M., ROBERTS, M. P., IRELAND, T. R., WHITEHOUSE, M. J., JEON, H., CAVOSIE, A. J., KIRKLAND, C. L. Strontium isotope analysis of apatite via SIMS. **Chemical Geology**, v.559, 119979, 2021

GIOIA, S.; PIMENTEL, M. M. The Sm-Nd isotopic method in the geochronology laboratory of the University of Brasília. **Anais da Academia Brasileira de Ciências**, v. 72, p. 219-245, 2000.

GIOIA, S.M.C.L., BABINSKI, M., WEISS, D.J., SPIRO, B., KERR, A.A.F.S., VERÍSSIMO, T.G., RUIZ, I., PRATES, J.C.M. An isotopic study of atmospheric lead in a megacity after phasing out of leaded gasoline, **Atmospheric Environment**, v. 149, p. 70-83, 2017

GLEASON, J. D., BERSHAW, J., WOODEN, J. L. Detrital Apatite U–Pb Geochronology by LA-ICPMS: Methods and Data Quality. **Chemical Geology**. v. 280(3-4), p. 213-225, 2011

GRANGE, M., NEMCHIN, A. PIDGEON, R. The effect of 1.9 and 1.4 Ga impact events on 4.3 Ga zircon and phosphate from an Apollo 15 melt breccia. **Journal of Geophysical Research, Planets.** v.118, p. 2180–2197, 2013

GRAY, D. R.; FOSTER, A.; MEERT, J. G.; GOSCOMBE, D.; ARMSTRONG, R.; TROUW, R. J. A.; PASSCHIER, C. W. A Damara orogen perspective on the assembly of southwestern Gondwana**. Geological Society, London, Special Publications**, v. 294, n. 1, p. 257–278, 2009.

GRUBBS, F. E.; BECK, G. Extension of Sample Sizes and Percentage Points for Significance Tests of Outlying Observations. **Technometrics**, v. 14, n. 4, p. 847-854, 1972.

GOSWAMI, P., PAUL, S., BHUSHAN, K.S., JAISON, P. G. Rapid and precise determination of the 238Pu/239Pu isotope ratio using thermal ionization mass spectrometry. Journal of Analytical Atomic Spectrometry. v. 39, p. 500-507, 2024

GUO, K., YU, J., FAN, D., HU, Z., LIU, Y., ZHANG, X, ZHANG, Y. Precise determination of Sr and Nd isotopic compositions of Chinese Standard Reference samples GSR-1, GSR-2, GSR-3 and GBW07315 by TIMS. **Geosystems and Geoenvironment,** v. 2 (4), 100206, 2023

HARLOV, D. E. Apatite: A fingerprint for metasomatic processes. **Elements**, v. 11, p. 171–176, 2015.

HAMMOUDA, T., CHANTEL, J., DEVIDAL, J.-L. Apatite solubility in carbonatitic liquids and trace element partitioning between apatite and carbonatite at high pressure. **Geochimica et Cosmochimica Acta**, v. 74, p. 7220-7235, 2010

HASEBE, N., BARBARAND, J., JARVIS, K., CARTER, A., HURFORD, A.J. Apatite fission-track chronometry using laser ablation ICP-MS. **Chemical Geology**, v. 207 (3–4), 2004

HE, Y.; ZHAO, G.; SUN, M.; WILDE, S. A. Geochemistry, isotope systematics and petrogenesis of the volcanic rocks in the Zhongtiao Mountain: An alternative interpretation for the evolution of the southern margin of the North China Craton. **Lithos**, v. 102, n. 1-2, p. 158-178, 2008.

HEGNER, E.; WALTER, H.; SATIR, M. Pb-Sr-Nd isotopic compositions and trace element geochemistry of megacrysts and melilitites from the Tertiary Urach volcanic field: source composition of small volume melts under SW Germany. **Contributions to Mineralogy and Petrology**, v. 122, p. 322–335, 1995.

HEILBRON, M.; MACHADO, N. Timing of terrane accretion in the Neoproterozoic–Eopaleozoic Ribeira Belt (SE Brazil). **Precambrian Research**, v. 125, p. 87–112, 2003.

HEILBRON, M.; SOARES, A. C. P.; CAMPOS, N.; SILVA, L. C.; TROUW, R.; JANASI, V. Província Mantiqueira. In: MANTESSO-NETO, V.; BARTORELLI, A.; DAL RÉ CARNEIRO, C.; BLEY DE BRITO NEVES, B. (Eds.), **Geologia do Continente Sul-Americano: Evolução da Obra de Fernando Flávio Marques de Almeida**. Beca Produções Culturais Ltda, São Paulo, p. 203–234, 2004.

HEILBRON, M.; VALERIANO, C.; TUPINAMBÁ, M.; ALMEIDA, J. C. H.; DUARTE, B. P.; VALLADARES, C.; SCHMITT, R.; GERAALDES, M.; RAGATKY, D.; PALERMO, N.; GONTIJO, A. Tectonic episodes related to West Gondwana amalgamation in the Ribeira Orogen. In: 1st Symposium on Neoproterozoic-Early Paleozoic Events in SW-Gondwana, **IGCP-Project** 478. Extended Abstracts, São Paulo, v. 1, p. 36–38, 2004.

HEILBRON, M.; VALERIANO, C. M.; TASSINARI, C. C. G.; ALMEIDA, J. C. H.; TUPINAMBÁ, M.; SIGA JR., O.; TROUW, R. Correlation of Neoproterozoic terranes between the Ribeira Belt, SE Brazil, and its African counterpart: Comparative tectonic evolution and open questions. **Geological Society of London, Special Publication**, v. 294, p. 1–22, 2008.

HEILBRON, M.; TUPINAMBÁ, M.; VALERIANO, C.; ARMSTRONG, R.; SILVA, L. G. E.; MELO, R. S.; SIMONETTI, A.; PEDROSA SOARES, A. C.; MACHADO, N. The Serra da Bolívia complex: The record of a new Neoproterozoic arc-related unit at Ribeira Belt. **Precambrian Research**, v. 238, p. 158–175, 2013.

HEILBRON, M.; VALERIANO, C. de M.; PEIXOTO, C.; TUPINAMBÁ, M.; NEUBAUER, F.; DUSSIN, I.; CORRALES, F.; BRUNO, H.; LOBATO, M.; ALMEIDA, J. C. H.; DO EIRADO SILVA, L. G. Neoproterozoic magmatic arc systems of the central Ribeira Belt, SE Brazil, in the context of the West-Gondwana pre-collisional history: A review. **Journal of South American Earth Sciences**, v. 105, p. 105400, 2020.

HEILBRON, M.; JANASI, V.; ARAÚJO, C. S.; PEIXOTO, C.; TOLEDO, B. B.; SANTIAGO, R.; MAURI, S.; ALVES, A.; CAXITO, F.; TUPINAMBÁ, M.; DECOL, J.; LOBATO, M.; CORRALES, F.; BRUNO, H.; PEDROSA SOARES, A. C. Neoproterozoic magmatic arcs of the Araçuaí-Ribeira Orogenic System (AROS), Brazil. **Journal of South American Earth Sciences**, v. 105400, 2025.

HUGHES, J.M., RAKOVAN, J.F. Structurally Robust, Chemically Diverse: Apatite and Apatite Supergroup Minerals. **Elements.** v.11 (3), p. 165–170, 2015

JACKSON, S. E., PEARSON, N. J., GRIFFIN, W. L., BELOUSOVA, E. A. The application of laser ablation-inductively coupled plasma-mass spectrometry to in situ U-Pb zircon geochronology. **Chemical Geology**, v. 211(1-2), p. 47-69, 2004

JAGER, E., HUNZIKER, J.C. (eds.), **Lectures in isotope geology**. Springer-Verlag, New York, 1977

JAHN, B.-M.; WU, F.; LO, C.-H.; TSAI, C.-H. Crust–mantle interaction induced by deep subduction of the continental crust: Geochemical and Sr–Nd isotopic evidence from post-collisional mafic–ultramafic intrusions of the northern Dabie complex, central China. **Chemical Geology**, v. 157, n. 1-2, p. 119–146, 1999.

JANASI, V. A.; ULBRICH, H. H. G. J. Late Proterozoic granitoid magmatism in the state of São Paulo, southeastern Brazil. **Precambrian Research**, v. 51, n. 1, p. 351–374, 1991.

JANASI, V. A.; LEITE, R. J.; VAN SCHMUS, W. R. U-Pb chronostratigraphy of the granitic magmatism in the Agudos Grandes Batholith (west of São Paulo, Brazil)— Implications for the evolution of the Ribeira Belt. **Journal of South American Earth Sciences**, v. 14, n. 4, p. 363–376, 2001.

JANOUŠEK, V.; FARROW, C. M.; ERBAN, V. Interpretation of whole-rock geochemical data in igneous geochemistry: Introducing Geochemical Data Toolkit (GCDkit). **Journal of Petrology**, v. 47, n. 6, p. 1255–1259, 2006.

JIA, F.; ZHANG, C.; LIU, H.; MENG, X.; KONG, Z. In situ major and trace element compositions of apatite from the Yangla skarn Cu deposit, southwest China: Implications for petrogenesis and mineralization. **Ore Geology Reviews**, v. 127, p. 103360, 2020.

JOCHUM, K. P., NOHL, U., HERWIG, K., LAMMEL, E., STOLL, B., & HOFMANN, A. W. GeoReM: A new geochemical database for reference materials and isotopic standards. **Geostandards and Geoanalytical Research**, v. 29(3), p. 333-338, 2005

JOCHUM, K.P., ENZWEILER, J. Reference materials in geochemical and environmental research. In: K. Turekian and H. Holland (ed.), **Treatise in geochemistry** (2nd edition), 15. Elsevier (Oxford), p. 43– 70, 2014

JOCHUM, K.P., WEIS, U., SCHWAGER, B., STOLL, B., WILSON, S.A., HAUG, G.H., ANDREAE, M.O. AND ENZWEILER, J. Reference Values Following ISO Guidelines for Frequently Requested Rock Reference Materials. **Geostandards and Geoanalytical Research**, v. 40, p. 333-350, 2016

JWEDA, J., BOLGE, L., CLASS, C., GOLDSTEIN, S.L. High Precision Sr-Nd-Hf-Pb Isotopic Compositions of USGS Reference Material BCR-2. **Geostandards and Geoanalytical Research**, v.40, p. 101-115, 2016

KAMENOV, G.; PERFIT, M.; MUELLER, P.; JONASSON, I. Controls on magmatism in an island arc environment: Study of lavas and sub-arc xenoliths from the Tabar-Lihir-Tanga-Feni island chain, Papua New Guinea. **Contributions to Mineralogy and Petrology**, v. 155, p. 635–656, 2008.

KANE, J. S., POTTS, P. J., WIEDENBECK, M., CARIGNAN, J., WILSON, S. International Association of Geoanalysts' Protocol for the certification of geological and environmental reference materials. **Geostandards Newsletter**, v. 27, p. 227-244, 2003

KANE, J. S., POTTS, P. J., MEISEL, T., WIEDENBECK, M. International Association of Geoanalysts' Protocol for the certification of geological and environmental reference materials: a supplement. **Geostandards and Geoanalytical Research**, v. 31, p. 285-288, 2007

KANI T., ISOZAKI, Y. The Capitanian Minimum: A Unique Sr Isotope Beacon of the Latest Paleozoic Seawater. **Frontiers in Earth Science.** v. 9, 662581, 2021

KENNEDY, A.K., WOTZLAW, J.-F., CROWLEY, J.L., SCHMITZ, M., SCHALTEGGER, U., WADE, B., MARTIN, L., TALAVERA, C., WARE, B. AND BUI, T.H. Apatite Reference Materials for SIMS Microanalysis of Isotopes and Trace Elements. **Geostandards and Geoanalytical Research**. v. 47, p. 373-402, 2023

KÖKSAL, S.; TOKSOY-KÖKSAL, F.; GÖNCÜOGLU, M. C. Petrogenesis and geodynamics of plagiogranites from Central Turkey (Ekecikdağ/Aksaray): new geochemical and isotopic data for generation in an arc basin system within the northern branch of Neotethys. **International Journal of Earth Sciences**, v. 106, n. 4, p. 1181–1203, 2017.

KOORNNEEF, J.; NIKOGOSIAN, I.; VAN BERGEN, M. J.; SMEETS, R.; BOUMAN, C.; DAVIES, G. TIMS analysis of Sr and Nd isotopes in melt inclusions from Italian potassium-rich lavas using prototype 1013 Ω amplifiers. **Chemical Geology**, v. 397, p. 14–23, 2015.

KENNEDY, A.K., WOTZLAW, J.-F., CROWLEY, J.L., SCHMITZ, M., SCHALTEGGER, U., WADE, B., MARTIN, L., TALAVERA, C., WARE, B. AND BUI, T.H. Apatite Reference Materials for SIMS Microanalysis of Isotopes and Trace Elements. **Geostandards and Geoanalytical Research**. v. 47, p. 373-402, 2023

LAHTINEN, M., ARPPE, L., NOWELL, G. Source of strontium in archaeological mobility studies marine diet contribution to the isotopic composition. **Archaeological and Anthropological Sciences**. v. 13, 1, 2021

LAN, T.-G. et al. Geochemistry and Sr–Nd–Pb–Hf isotopes of the Mesozoic Dadian alkaline intrusive complex in the Sulu orogenic belt, eastern China: Implications for crust–mantle interaction. **Chemical Geology**, v. 285, n. 1–4, p. 97–114, 2011.

LANA C., GONÇALVES O., MAZOZ A., BUICK I., KAMO S., SCHOLZ R., WANG H., MOREIRA H., BABINSKY M. AND QUEIROGA G. Assessing the U-Pb, Sm-Nd and Sr-Sr isotopic compositions of Sumé apatite as a reference material for LA-ICP-MS analyses. **Geostandards and Geoanalytical Research,** v.46, p. 71–95, 2021

LANE, K. L.; LITTLE, R. J. A.; TAYLOR, J. M. G. Robust statistical modeling using the t distribution. **Journal of the American Statistics**, v. 84, n. 408, p. 881–896, 1989.

LAPEN, T.; MEDARIS, L.; BEARD, B.; JOHNSON, C. The Sandvik peridotite, Gurskøy, Norway: Three billion years of mantle evolution in the Baltica lithosphere. **Lithos**, v. 109, p. 145–154, 2009.

LEVENE, H. Robust tests for equality of variances. In: OLKIN, I. (Ed.). **Contributions to Probability and Statistics**. Palo Alto: Stanford Univ. Press, 1960. p. 278–292.

LI, Z. et al. Geochemistry and Sm–Nd and Rb–Sr isotopic composition of eclogite in the Lhasa terrane, Tibet, and its geological significance. **Lithos**, v. 109, p. 240–247, 2009.

LI, Z. et al. In situ analysis of major elements, trace elements and Sr isotopic compositions of apatite from the granite in the Chengchao skarn-type Fe deposit, Edong Ore District: Implications for petrogenesis and mineralization. **Journal of Earth Science**, v. 29, p. 295–306, 2018.

LI, Z. et al. Early Cretaceous crust–mantle interaction in the Middle-lower Yangtze River Metallogenic Belt, East China: Li–Nd–Sr isotopic and elemental constraints. **Lithos**, v. 398–399, 106308, 2021.

LINGHU, M. et al. Magma source and petrogenesis of the Early Cretaceous granites in the Liaodong Peninsula: Evidence from in situ apatite Sr-Nd and zircon Hf-O isotopes. **Minerals**, v. 13, 545, 2023.

LIU, Y. H. et al. Compositions of high Fe–Ti eclogites from the Sulu UHP metamorphic terrane, China: HFSE decoupling and protolith characteristics. *Chemical Geology*, v. 239, p. 64–82, 2007.

LYONS, J. Volcanogenic iron oxide deposits, Cerro de Mercado and vicinity, Durango, Mexico. **Economic Geology**, v. 83, n. 8, p. 1886–1906, 1988.

LI, Z., DUAN, D., JIANG, S., MA, Y., YUAN, H. In-situ analysis of major elements, trace elements and Sr isotopic compositions of apatite from the granite in the Chengchao skarn-type Fe deposit, Edong ore district: Implications for petrogenesis and mineralisation. **Journal of Earth Sciences**, v.29, p. 295-306, 2018.

LI, C.F., CHU, Z.Y., PENG, P. Low-cost and sensitive method for Pb isotope determination using a novel β-Si_3N_4 emitter by thermal ionization mass spectrometry. **Talanta**, v. 257, 124390, 2023

LYONS, 1988. Volcanogenic iron oxide deposits, Cerro de Mercado and vicinity, Durango, Mexico. **Economic Geology.** v. 83(8), p. 1886–1906, 1988

MACHADO, N.; BROOKS, C.; HART, S. R. Determination of initial 87Sr/86Sr and 143Nd/144Nd in primary minerals from mafic and ultramafic rocks: Experimental procedure and implications for the isotopic characteristics of the Archean mantle under the Abitibi greenstone belt, Canada. **Geochimica et Cosmochimica Acta**, v. 50, p. 2335–2348, 1986.

MACHADO, N.; VALLADARES, C.; HEILBRON, M.; VALERIANO, C. U-Pb geochronology of the central Ribeira Belt (Brazil) and implications for the evolution of the Brazilian Orogeny. **Precambrian Research**, v. 79, p. 347–361, 1996.

MACHADO, N.; GAUTHIER, G. Determination of 207Pb/206Pb ages on zircon and monazite by laser ablation ICP-MS and application to a study of sedimentary provenance and metamorphism in southeastern Brazil. **Geochimica et Cosmochimica Acta**, v. 60, p. 5063–5073, 1996.

MACHADO, R.; PHILIPP, R. P.; McREATH, I.; PEUCAT, J. J. Geochemical and isotopic evidence for the petrogenesis and emplacement tectonics of the Serra dos Órgãos batholith in the Ribeira belt, Rio de Janeiro, Brazil. **Journal of South American Earth Sciences**, v. 68, p. 187–204, 2016.

MAKISHIMA, A. Thermal Ionization Mass Spectrometry (TIMS): Silicate Digestion, Separation, and Measurement. **Weinheim: Wiley-VCH. OCLC,** 2016

MARTYNOV, Y. A.; KHANCHUK, A. I.; GREBENNIKOV, A. V.; CHASHCHIN, A. A.; POPOV, V. K. Late Mesozoic and Cenozoic volcanism of the East Sikhote-Alin area (Russian Far East): a new synthesis of geological and petrological data. **Gondwana Research**, v. 47, p. 358-371, 2017.

McCULLOCH, M.T., WASSERBURG, G.J. Sm-Nd and Rb-Sr chronology of continental crust formation. **Science**, v. 200, p. 1003- 1011, 1978

MCDERMOTT, F.; HAWKESWORTH, C. The evolution of strontium isotopes in the upper continental crust. **Nature**, v. 344, p. 850-853, 1990.

MCLENNAN, S. M.; TAYLOR, S. R.; MCCULLOCH, M. T.; MAYNARD, J. B. Geochemical and Nd–Sr isotopic composition of deep-sea turbidites: crustal evolution and plate tectonic associations. **Geochimica et Cosmochimica Acta**, v. 54, p. 2015–2050, 1990.

MCLENNAN, S. M.; HEMMING, S. Samarium Neodymium Elemental and Isotopic Systematics in Sedimentary-Rocks. **Geochimica et Cosmochimica Acta**, v. 56, n. 3, p. 887-898, 1992.

MEDEIROS, S. R.; WIEDEMANN-LEONARDOS, C.; MENDES, J. C. Post-collisional multistage magmatism in the Ribeira Mobile Belt: geochemical and isotopic study of the

Varzea Alegre Intrusive Complex, Espírito Santo, Brazil. **Revista Brasileira de Geociências**, v. 30, p. 30–34, 2000.

MEERT, J. G.; LIEBERMAN, B. S. The Neoproterozoic assembly of Gondwana and its relationship to the Ediacaran-Cambrian radiation. **Gondwana Research**, v. 14, p. 5–21, 2008.

MEIJA, J.; COPLEN, T.; BERGLUND, M.; BRAND, W.; DE BIÈVRE, P.; GRÖNING, M.; HOLDEN, N.; IRRGHER, J.; LOSS, R.; WALCZYK, T.; PROHASKA, T. Atomic weights of the elements 2013 (IUPAC Technical Report). **Pure and Applied Chemistry**, v. 88, p. 265-291, 2016.

MORTON, A., YAXLEY, G. Detrital apatite geochemistry and its application in provenance studies. In: Sedimentary Provenance and Petrogenesis: Perspectives from Petrography and Geochemistry. ARRIBAS, J., JOHNSSON, M.J., CRITELLI, S. **Geological Society of America**, v 420, 2007

NETO, C. C. A.; VALERIANO, C. M.; PASSARELLI, C. R.; HEILBRON, M.; LOBATO, M. Monazite ID-TIMS U-Pb geochronology in the LAGIR laboratory, Rio de Janeiro State University: protocols and first applications to the assembly of the Gondwana supercontinent in SE-Brazil. **Anais da Academia Brasileira de Ciências**, v. 86, p. 171–186, 2014.

NETO, C., VALERIANO, C.M., ENZWEILER, J., PARAVIDINI, G., CARVALHO, M., HEILBRON, M., LANA, C., LARIZZATTI, J.H. ID-TIMS Sm-Nd and Sr Isotope Ratios of Reference Material Basalt Ribeirão Preto (BRP-1). **Geostandards and Geoanalytical Research**, v. 47, 12498, 2023

NIER, A. O. Isotopic Constitution of Strontium, Barium, Bismuth, Thallium and Mercury. **Physical Review**, v. 54, n. 4, p. 275–278, 1938.

NOGUEIRA, J., EVANGELISTA, H., VALERIANO, C.M., SIFEDDINE, A., NETO, C., VAZ, G., MOREIRA, L.S., CORDEIRO, R.C., TURCQ, B., ANICETO, K.C., NETO, A.B., MARTINS, G., BARBOSA, C.G.G., GODOI, R.H.M., SHIMIZU, M.H. Dust arriving in the Amazon basin over the past 7,500 years came from diverse sources. **Communications Earth & Environment**, 2(5), 2021.

OKUNO, E., YOSHIMURA, E. M. **Física das Radiações**. 1. ed. S. Paulo: Oficina de Textos, 296 pp. 2010

OLIVEIRA, I. Isótopos de Nd e Sr em minerais de diferentes séries petrogenéticas nos complexos alcalino-carbonatíticos de Salitre e Catalão I. 2015. Dissertação de Mestrado, nº 343. Universidade de Brasília, Brasília, DF.

PASSARELLI, C. R.; MAS, B.; Mc, C. N.; JR, S.; HJ, P. F. Geocronologia e geologia isotópica dos terrenos Pré-cambrianos da porção sul-oriental do Estado de São Paulo. **Geologia USP, Série Científica**, v. 4, p. 55–74, 2004.

PACHETT, P. J. Radiogenic isotope geochemistry of the rare earth elements. In: LIPIN, B. R.; McKAY, G. A. (eds). **Reviews in Mineralogy**, v. 21, p. 25-44, 1989. Geochemistry and Mineralogy of the Rare Earth Elements. Mineralogical Society of America (Washington, DC).

PAUL, A.N., SPIKINGS, R.A., GAYNOR, S.P. U-Pb ID-TIMS reference ages and initial Pb isotope compositions for Durango and Wilberforce apatites. **Chemical Geology,** v. 586, 2021

PEARCE, J. A.; HARRIS, N. B. W.; TINDLE, A. G. Trace element discrimination diagrams for the tectonic interpretation of granitic rocks. **Journal of Petrology**, v. 25, p. 956-983, 1984.

PEIXOTO, C. HEILBRON, M., RAGATKY, D., ARMSTRONG, R., DANTAS, E., VALERIANO, C. M., SIMONETTI, A. Tectonic evolution of the Juvenile Tonian Serra da Prata magmatic arc in the Ribeira Belt, SE Brazil: Implications for early west Gondwana amalgamation. **Precambrian Research.** v. 302, p. 221-254, 2017

PEIXOTO, C. A.; LOBATO, M.; FREITAS, N. C.; HEILBRON, M.; DUSSIN, I.; DANTAS, E. Geochronological constraints of high-grade metasedimentary rocks of the Italva and Costeiro basins: reconstructing the Outer Magmatic Arc System of the Ribeira Belt, SE Brazil. **Precambrian Research**, v. 382, p. 106879, 2022.

PENHA, H. M., FERRARI, A. L., RIBEIRO, A., AMADOR, E.S., PENTAGNA, F. V. P. JUNHO, M. C. B E BRENNER, T. L. A Geologia da Folha Petrópolis. **Anais do XXXI Congresso Brasileiro de Geologia**, Camboriú, v. 5, p. 2965-2974, 1980

PICCOLI, P.M., CANDELA, P.A. Apatite in Igneous Systems. **Reviews in Mineralogy and Geochemistry**. v. 48, p. 255-292, 2002

POTRATZ, G. L.; GERALDES, M.; MARTINS, M. V.; ALMEIDA, B. Sana granite, a post-collisional S-type magmatic suite of the Ribeira Belt (Rio de Janeiro, SE Brazil). **Lithos**, v. 388, p. 106067, 2021.

POTRATZ, G. L.; VALERIANO, C. M.; NETO, C. C. A. Contributions to understanding post-collisional magmatism in the Neoproterozoic of the Ribeira Belt, SE-Brazil: Sr-Sr and Sm-Nd isotopic composition of the Sana and Itaoca granites. Brazilian Journal of Geology, 2025.

PRICE, R. C.; GAMBLE, J. A.; SMITH, I. E. M.; MAAS, R.; WAIGHT, T.; STEWART, R. B.; WOODHEAD, J. The anatomy of an andesite volcano: a time-stratigraphic study of andesite petrogenesis and crustal evolution at Ruapehu Volcano, New Zealand. **Journal of Petrology**, v. 53, n. 10, p. 2139-2189, 2012.

PRICE, R. C.; NICHOLLS, I. A.; DAY, A. Lithospheric influences on magma compositions of late Mesozoic and Cenozoic intraplate basalts (The Older Volcanics) of Victoria, South-Eastern Australia. **Lithos**, v. 206, p. 179-200, 2014.

PTÁČEK P. Introduction to Apatites [Internet]. Apatites and their Synthetic Analogues - Synthesis, Structure, Properties and Applications. **InTech**, 2016

PUCHTEL, I. S. et al. The coupled 182W-142Nd record of early terrestrial mantle differentiation. **Geochemistry, Geophysics, Geosystems**, v. 17, p. 2168–2193, 2016.

R CORE TEAM. R: A language and environment for statistical computing (Version 3.6) [**Computer software**]. 2019. Disponível em: https://cran.r-project.org/.

RACZEK, I., JOCHUM, P., HOFMANN, A.W. Neodymium and strontium isotope data for USGS reference materials BCR-1, BCR-2, BHVO-1, BHVO-2, AGV-1, AGV-2, GSP-1, GSP-2 and eight MPI-DING reference glasses. **Geostandards Newsletter**, 27, p. 173–179, 2003

RAKOVAN, J., HUGHES, J. M. Apatite -A large and illustrious family. In Apatite: The great pretender, ed. J. Rakovan, G. A. Staebler, and D. A. Dallaire, 4–9. Mineral monograph 17. Denver, CO: **Lithographie**, Ltd., 2013

RAKOVAN, J., SCOVIL, J.A. **Apatite and the Apatite Supergroup, Rocks & Minerals**, v. 96:1, p. 13-19, 2021

RAMOS, F. C.; WOLFF, J. A.; TOLLSTRUP, D. L. Measuring 87Sr/86Sr variations in minerals and groundmass from basalts using LA-MC-ICPMS. **Chemical Geology**, v. 211, n. 1-2, p. 135–158, 2004.

ROBINSON, F. A.; FODEN, J. D.; COLLINS, A. S. Geochemical and isotopic constraints on island arc, synorogenic, post-orogenic and anorogenic granitoids in the Arabian Shield, Saudi Arabia. **Lithos**, v. 220–223, p. 97-115, 2015.

ROLLINSON, H. R. **Using geochemical data: evaluation, presentation, interpretation**. 1. ed. United Kingdom: PEARSON (Presentice Hall), 1993.

RUTHERFORD, E., SODDY, F. The cause and nature of radioactivity. **The Collected Papers of Lord Rutherford of Nelson**. p. 370−396, 1902

SANTOS A.R., AGEE C.B., MCCUBBIN F.M., SHEARER C.K., BURGER P.V., TARTÈSE R. AND ANAND M. Petrology of igneous clasts in Northwest Africa 7034: Implications for the petrologic diversity of the Martian crust. **Geochimica et Cosmochimica Acta**, v.157, p. 56–85, 2015

SANTOS, M.M., LANA, C., SCHOLZ, R., BUICK, I., SCHMITZ, M.D., KAMO, S.L., GERDES, A., CORFU, F., TAPSTER, S., LANCASTER, P., STOREY, C.D., BASEI, M.A.S., TOHVER, E., ALKMIM, A., NALINI, H., KRAMBROCK, K., FANTINI,

C. WIEDENBECK, M. A new appraisal of Sri Lankan BB zircon as a reference material for LA-ICP-MS U-Pb geochronology and Lu-Hf isotope tracing. **Geostandards and Geoanalytical Research**, v. 41, p. 335–358, 2017

SANTOS, E.A., EVANGELISTA, H., VALERIANO, C.M., NETO, C.C.A., CASTAGNA, A., HEILBRON, M. Origin and radiogenic isotope fingerprinting of aerosols over the Southwestern Atlantic and corresponding Southern Ocean Sector. **Aeolian Research**, v. 45, 100596, 2020

SCHMITT, R. S.; TROUW, R. A. J.; VAN SCHMUS, W. R.; PIMENTEL, M. M. Late amalgamation in the central part of Western Gondwana: new geochronological data and the characterization of a Cambrian collisional orogeny in the Ribeira Belt (SE Brazil). **Precambrian Research**, v. 133, p. 29–61, 2004.

SCHMITT, R. D. S.; TROUW, R.; VAN SCHMUS, W. R.; ARMSTRONG, R.; STANTON, N. S. G. The tectonic significance of the Cabo Frio Tectonic Domain in the SE Brazilian margin: a Paleoproterozoic through Cretaceous saga of a reworked continental margin. **Brazilian Journal of Geology**, v. 46, p. 37–66, 2016.

SCHMITZ, M. D.; SMITH, I. E. M. The Petrology of the Rotoiti Eruption Sequence, Taupo Volcanic Zone: an Example of Fractionation and Mixing in a Rhyolitic System. **Journal of Petrology**, v. 45, n. 10, p. 2045-2066, 2004.

SHAPIRO, S. S.; WILK, M. B. An analysis of variance test for normality (complete samples). **Biometrika**, v. 52, n. 3/4, p. 591–611, 1965.

SILVA, L. C.; ARMSTRONG, R.; NOCE, C. M.; CARNEIRO, M. A.; PIMENTEL, M.; PEDROSA-SOARES, A. C.; LEITE, C. A.; VIEIRA, V. S.; SILVA, M. A.; PAES, V. J. C.; CARDOSO, F. J. M. Reavaliação da evolução geológica em terrenos Pré-cambrianos brasileiros com base em novos dados U-Pb SHRIMP, parte II: Orógeno Araçuaí, Cinturão Mineiro. 2002.

SLÁMA, J., KOŠLER, J., CONDON, D. J., CROWLEY, J. L., GERDES, A., HANCHAR, J. M., HORSTWOOD, M. S. A., MORRIS, G. A., NASDALA, L., NORBERG, N.,

SCHALTEGGER, U., SCHOENE, B., TUBRETT, M. N., WHITEHOUSE, M. J. Plešovice zircon — A new natural reference material for U–Pb and Hf isotopic microanalysis. **Chemical Geology**, v. 249(1–2), p. 1-35, 2008

SLOVAK, N.M. Applications of Sr isotopes in archaeology. **Handbook of Environmental Isotope Geochemistry**. p. 743-768, 2012

SUN, J.-F., ZHANG, J.-H., YANG, J.-H., YANG, Y.-H., & CHEN, S. Tracing magma mixing and crystal–melt segregation in the genesis of syenite with mafic enclaves: Evidence from in situ zircon Hf–O and apatite Sr–Nd isotopes. **Lithos**, v. 334–335, p. 42–57, 2019

SUN, J. F.; YANG, J. H.; ZHANG, J. H.; YANG, Y. H.; ZHU, Y. S. Apatite geochemical and Sr–Nd isotopic insights into granitoid petrogenesis. **Chemical Geology**, v. 566, p. 120104, 2021.

SUO, Q., SHEN, P., LI, C., FENG, H., CHU, X. Mineral chemistry and apatite Sr isotope signatures record overprinting mineralization in the Duobaoshan porphyry Cu deposit, Heilongjiang Province, NE China. **Ore Geology Reviews**, v. 162, 2023

TANAKA, T., TOGASHI, S., KAMIOKA, H., AMAKAWA, H., KAGAMI, H., HAMAMOTO, T., YUHARA, M., ORIHASHI, Y., YONEDA, S.,SHIMIZU, H., KUNIMARU, T., TAKAHASHI, K., YANAGI, T., NAKANO, T., FUJIMAKI, H., SHINJO, R., ASAHARA, Y., TANIMIZU,M. AND DRAGUSANU, C. (2000). JNdi-1: a neodymium isotopic reference in consistency with LaJolla neodymium. **Chemical Geology, 168,** p. 279–281, 2000.

TERENTIEV, R.; KONSTANTIN, S.; SANTOSH, M. Paleoproterozoic crustal evolution in the East Sarmatian Orogen: Petrology, geochemistry, Sr-Nd isotopes and zircon U-Pb geochronology of andesites from the Voronezh massif, Western Russia. **Lithos**, v. 246-247, p. 61-80, 2016.

TESSALINA, S., JOURDAN, F., NUNES, L., KENNEDY, A., DENYSZYN, S., PUCHTEL, I., TOUBOUL ,M., CREASER , R., BOYET , M., BELOUSOVA , E., TRINQUIER, A. Application of Radiogenic Isotopes in Geosciences: Overview and

Perspectives. In: Principles and Practice of Analytical Techniques in Geosciences, Grice, K. (eds), **The Royal Society of Chemistry**, p. 49-93, 2014

THE JAMOVI PROJECT. Jamovi (Version 1.2) [**Computer Software**]. 2020. Disponível em: https://www.jamovi.org.

TRITON HARDWARE MANUAL. Triton Hardware Manual, Issue 12, **Thermo Finnigan**, 2002.

TROLL, V. R., WEIS, F. A., JONSSON, E., ANDERSSON, U. B., MAJIDI, S. A., HÖGDAHL, K., HARRIS, C., MILLET, M.-A., CHINNASAMY, S. S., KOOIJMAN, E., & NILSSON, K. P. Global Fe–O isotope correlation reveals magmatic origin of Kiruna-type apatite-iron-oxide ores. **Nature Communications**, v. 10, 1712, 2019

TROUW, R.A.; HEILBRON, M.; RIBEIRO, A.; PACIULLO, F.; VALERIANO, C.; ALMEIDA, J.H.; TUPINAMBÁ, M.; ANDREIS, R. The central segment of the Ribeira belt. In: CORDANI, U.G.; MILANI, E.J.; THOMAZ FILHO, A.; CAMPOS, D.A. (Eds.). **Geotectonics of South America**. Special Publication for the 31 IGC/2000. p. 297–310.

TSUBOI, M. The use of apatite as a record of initial 87Sr/86Sr ratios and indicator of magma processes in the Inagawa pluton, Ryoke belt, Japan. **Chemical Geology**, v. 221, p. 157–169, 2005

TUPINAMBÁ, M.; TEIXEIRA, W.; HEILBRON, M. Neoproterozoic western Gondwana assembly and subduction-related plutonism: the role of the Rio Negro complex in the Ribeira belt, southeastern Brazil. **Revista Brasileira de Geociências**, v. 30, p. 7–11, 2000.

TUPINAMBÁ, M.; HEILBRON, M.; DUARTE, B.P.; NOGUEIRA, J.R.; VALLADARES, C.; ALMEIDA, J.; SILVA, L.G.E.; MEDEIROS, S.R.; ALMEIDA, C.G.; MIRANDA, A.; RAGATKY, C.D.; MENDES, J.; LUDKA, I. Geologia da Faixa Ribeira Setentrional: estado da arte e conexões com a Faixa Araçuaí. **Geonomos**, v. 15, n. 1, p. 67–79, 2007.

TUPINAMBÁ, M.; HEILBRON, M.; VALERIANO, C.M.; PORTO JR., R.; DIOS, F.R.B.; MACHADO, N.; SILVA, L.G.E.; ALMEIDA, J.C.H. Juvenile contribution of the

Neoproterozoic Rio Negro magmatic arc (Ribeira belt, Brazil): implications for western Gondwana. **Gondwana Research**, v. 21, n. 2–3, p. 422–438, 2012.

VALERIANO, C.M., RAGATKY, D., GERALDES, M., C., HEILBRON, M., VALLADARES, C., SCHMITT, R., TUPINAMBÁ, M., PALERMO, N., ALMEIDA, J.C.H., DUARTE, B. P., MARTINS, JR. E., NOGUEIRA, J.R. A new TIMS laboratory under construction in Rio de Janeiro. Brazil. In: **Short Papers of the IV South American Symposium on Isotope Geology**, v. 1, p. 131-133, 2003

VALERIANO, C.M.; TUPINAMBÁ, M.; SIMONE, A.; HEILBRON, M.; ALMEIDA, J.; SILVA, L.G.E. U-Pb LA-MC-ICPMS geochronology of Cambro-Ordovician post-collisional granites of the Ribeira belt, southeast Brazil: terminal Brasiliano magmatism in central Gondwana supercontinent. **Journal of South American Earth Sciences**, v. 32, p. 416–428, 2011.

VALERIANO C.M., NEUMANN R., ALKMIM A.R., EVANGELISTA H., HEILBRON M., NETO C.C.A., SOUZA G.P. Sm–Nd and Sr isotope fingerprinting of iron mining tailing deposits spilled from the failed SAMARCO Fundão dam 2015 accident at Mariana, SE-Brazil. **Applied Geochemistry**. v. 106, p. 34-44, 2019

VAN KRANENDONK, M.; KRÖNER, A.; HEGNER, E.; CONNELLY, J. Age, lithology and structural evolution of the c. 3.53 Ga Theespruit Formation in the Tjakastad area, southwestern Barberton Greenstone Belt, South Africa, with implications for Archean tectonics. **Chemical Geology**, v. 261, p. 114-138, 2009.

VERMEESCH, P. IsoplotR: a free and open toolbox for geochronology. **Geoscience Frontiers**, v. 9, p. 1479-1493, 2018.

VIM. International vocabulary of metrology – Basic and general concepts and associated terms (VIM). **Joint Committee for Guides in Metrology**, Bureau International des Poids et Mesures, Sèvres, France, 2008. 90 p.

WALTHER, C.; WENDT, K. **Handbook of Radioactivity Analysis**. 4th ed. Chapter 8 - Radioisotope mass spectrometry, v. 1, p. 861-898, 2020.

WANG, H.; CAI, K.; SUN, M.; XIA, X.P.; LAI, C.K.; LI, P.; WAN, B.; ZHANG, Z. Apatite as a magma redox indicator and its application in metallogenic research. **Lithos**, v. 422–423, 2022.

WEIS, D., KIEFFER, B., MAERSCHALK, C., PRETORIUS, W., & BARLING, J. High-precision Pb-Sr-Nd-Hf isotopic characterization of USGS BHVO-1 and BHVO-2 reference materials. **Geochemistry, Geophysics, Geosystems**, 6, 2005.

WEIS, D., KIEFFER, B., MAERSCHALK, C., BARLING, J., DE JONG, J., WILLIAMS, G. A., HANANO, D., PRETORIUS, W., MATTIELLI, N., SCOATES, J. S., GOOLAERTS, A., Friedman, R. M. and Mahoney, J. B. High-precision isotopic characterization of USGS reference materials by TIMS and MC-ICP-MS. **Geochemistry Geophysics Geosystem**, 7(8), 2006

WEIS D., KIEFFER B., HANANO D., NOBRE SILVA I., BARLING J., PRETORIUS W., MAERSCHALK C., MATTIELLI N. Hf isotopic composition of USGS reference materials. **Geochemistry Geophysics Geosystem**. v.8, 2007

WEIS, U., STOLL, B., FÖRSTER, M. W., HELL, K., KAISER, V., OTTER, L. M., JOCHUM, K.P. Geostandards and Geoanalytical Research Bibliographic Review 2020. **Geostandards and Geoanalytical Research,** v. 46(1), p. 129-134, 2022

WHITE, W.M. **Geochemistry**. On-line textbook, Cornell University, New York. 700 pp., 2005

WONG, J., SUN, M., XING, G. F., LI, X. H., ZHAO, G. C., WONG, K., YUAN, C., XIA, X. P., LI, L. M., WU, F. Y. Geochemical and zircon U-Pb and Hf isotopic study of the Baijuhuajian metaluminous A-type granite: Extension at 125-100 Ma and its tectonic significance for South China. **Lithos**, v. 112(3–4), p. 289-305, 2009

WU, F.Y. Geochemical applications of in situ isotopic analyses by laser ablation. Geochemical News. 143p., 2010

YAN, H.; XU, Z.; LI, G.; ZHENG, B.; GAO, J.; LONG, X. Whole-Rock and Apatite Geochemistry of Late Triassic Plutonic Rocks in the Eastern Songpan-Ganzi Orogenic Belt: Petrogenesis and Implications for Tectonic Evolution. **Lithosphere**, v. 2024, p. 1, lithosphere_2023_284, 2024.

YANG, Y., WU, F.-Y., YANG, J.-H., CHEW, D., XIE, L., CHU, Z.-Y., ZHANG, Y.-B., & HUANG, C. Sr and Nd isotopic compositions of apatite reference materials used in U–Th–Pb geochronology. **Chemical Geology**, v. 385, p. 35–55, 2014.

YOBREGAT, E.; FITOUSSI, C.; BOURDON, B. A new method for TIMS high precision analysis of Ba and Sr isotopes for cosmochemical studies. **Journal of Analytical Atomic Spectrometry**, v. 32, p. 1388-1399, 2017

YOKOYAMA, T., OHKUMA, Y., NISHIKAWA, K., SUMIYA, K., GAUTAM, I. Evaluation of the Residual Mass Fractionation in High-Precision Cr Isotopic Analysis with TIMS. **Geostandards and Geoanalytical Research.** v. 47(2), p.415-435, 2023

ZHANG, G. L., ZONG, C. L., YIN, X. B., LI, H. Geochemical constraints on a mixed pyroxenite-peridotite source for East Pacific Rise basalts. **Chemical Geology**, v. 330, p. 176-187, 2012

ZHAO, X.-F., ZHOU, M.-F., GAO, J.-F., LI, X.-C., LI, J.-W. In situ Sr isotope analysis of apatite by LA-MC-ICPMS: constraints on the evolution of ore fluids of the Yinachang Fe-Cu-REE deposit, Southwest China. **Mineralium Deposita**, v. 50(7), p. 871-884, 2015

ZHOU, B.Q., YANG, J.H., SUN, J.F., WANG, H., ZHU, Y.S., WU, Y.D., XU, L. Apatite geochemical and Sr-Nd isotopic constraints on the source and petrogenesis of alkaline volcanic-plutonic ring complex. Lithos 456–457, 107334. **Lithos**, v. 456-457, p. 107334, 2023.

APÊNDICE A – Material suplementar do 1º artigo

Table S1.1 - Main basalts RMs, Provider, mass fractions (Nd and Sr), age and tectonic context

Reference material - basalt	Suplier	Name/site	Age (Ma)	Sr (µg g^{-1})	Nd (µg g^{-1})	Tectonic context
BHVO-1	USGS	Hawaiian Volcano Observatory Basalt	0.210–0.280	399.2	24.8	Oceanic within plate
BHVO-2	USGS	Hawaiian Volcano Observatory Basalt	0.210–0.280	394.1	24.3	Oceanic within plate
BCR-1	USGS	Columbia River Basalt	17	334.9	28.7	Continental within plate
BCR-2	USGS	Columbia River Basalt	17	337.4	28.3	Continental within plate
BIR-1	USGS	Reykjavik Iceland Basalt	0.01	108.6	2.4	mid-Atlantic ridge
BEM (GBW07126) (a) (b)	Chinese	Emeishan Basalt, Sichuan, China	265	536	57.4	Continental within plate
BE-N	GIT-IWG	Basalte d'Essey-la-Côte, old volcano near Nancy, France	27.6	1392	66.4	Continental within plate
JB-1	GSJ	Kitamatsuura basalt, Sasebo	7.6	440	26.2	Oceanic within plate
JB-1b	GSJ	Kitamatsuura basalt, Sasebo	8.6–6.0	439	26.1	Oceanic within plate
JB-2	GSJ	Oshima volcano	0.01	178.2	6.4	arc volcanism

Note:

(a) Tong C., Zhou S., Li J., Liu X. and Wu J. (2005) The Preparation and Characteristics of the Geochemical Certified Reference Material BEM (Emeishan Basalt). Geostandards and Geoanalytical Research, 29(2), 225–231.

(b) Lo C.H., Chung S.L., Lee T.Y. and Wu G. (2002) Age of the Emeishan flood magmatism and relations to Permian-Triassic boundary events. Earth and Planetary Science Letters. 198, 449–458

Table S1.2. Mass fractions USGS RMs and LAGIR

			certified values (µg g-1)						LAGIR values (µg g-1)			
USGS RM	Rock type	Name/site	Sr	U	Nd	U	Sm	U	Nd	U	Sm	U
AGV-1	andesite	Guano Valley, Lake County, Oregon, USA	661.0	3.7	32.1	0.3	5.8	0.1	32.4	0.9	5.9	0.1
BCR-1	basalt	Columbia River Group basalt, Bridal Veil Flow Quarry, Washington, USA	334.9	3.5	28.7	0.1	6.6	0.0	29.3	0.8	6.6	0.4
G-2	granite	Westerly granite, from Sullivan quarry, Bradford, Rhode Island, USA	474.9	6.1	53.8	0.7	7.2	0.1	51.5	2.4	6.9	0.4
GSP-1*	granodiorite	Silver Plume, Colorado, USA	234.0	5.4	196.0	3.3	26.3	5.5	191.5	11.4	24.5	1.4
BHVO-1	basalt	Kilauea caldera, Kilauea volcano, Hawaii, USA	399.2	5.0	24.3	0.3	6.2	0.1				

Note

(1) RM - Reference materials

(2) U- 2s - measurement reproducibility

(3) Reference: Jochum, K.P., Weis, U., Schwager, B., Stoll, B., Wilson, S.A., Haug, G.H., Andreae, M.O. and Enzweiler, J. (2016),
Reference Values Following ISO Guidelines for Frequently Requested Rock Reference Materials. Geostand Geoanal Res, 40: 333-350.

(4) * Reference: Barth, M.G., McDonough, W.F., Rudnick, R.L. (2000). Tracking the budget of Nb and Ta in the continental crust. Chemical Geology, 165, 197-213

Table S.1.3.1 - Tests of Normality (Nd)

Nd	Test	statistic	p
AGV-1 (Nd)	Shapiro-Wilk	0.977	0.292
AGV-1 (Sr)	Shapiro-Wilk	0.112	0.347
G-2 (Nd)	Shapiro-Wilk	0.925	0.328
G-2 (Sr)	Shapiro-Wilk	0.940	0.321
BCR-1 (Nd)	Shapiro-Wilk	0.952	0.260
BCR-1 (Sr)	Shapiro-Wilk	0.849	0.131
BHVO-1 (Sr)	Shapiro-Wilk	0.942	0.345

Note. A low p-value suggests a violation of the assumption of equal variances (<0.05)

df - degrees of freedom

p - p-value probability

Table S1.3.2 - Homogeneity of Variances Test (Levene's)

Nd	F	df	df2	p
AGV-1 (Nd)	0.153	1	59	0.697
AGV-1 (Sr)	1.637	2	67	0.202
G-2 (Nd)	0.042	1	10	0.842
G-2 (Sr)	0.128	2	14	0.881
BCR-1 (Nd)	2.032	3	22	0.139
BCR-1 (Sr)	2.304	1	14	0.151
BHVO-1 (Sr)	1.327	1	15	0.267

Table S1.3.3 - Independent Samples T-Test

Nd		Statistic	df	p
AGV-1 (Nd)	Student's t	4.204	59	9.03E-05
G-2 (Nd)	Student's t	-0.703	10	0.498
BCR-1 (Sr)	Student's t	-0.584	14	0.569

Table S1.3.4 - One-Way ANOVA (Fisher's)

Nd	F	df1	df2	p
G-2 (Sr)	3.083	2	14	0.078
AGV-1 (Sr)	11.445	2	67	5.30E-05
BCR-1 (Nd)	59.716	3	5	1.56E-04
BHVO-1 (Sr)	0.037	2	21	0.964

Table S1.3.5 - Tukey Post-Hoc Test – BCR-1 (Nd)

		LAGIR	Weis et al 2006	Puchtel et al 2013	Ali et al 2014
LAGIR	Mean difference	—	6.59E-02	2.10E-03	2.02E-01
	p-value	—	0.160	1.000	< .001
Weis et al 2006	Mean difference		—	-6.3846e−6	1.36E-01
	p-value		—	0.142	0.003
Puchtel et al 2013	Mean difference			—	2.00E-01
	p-value			—	< .001
Ali et al 2013	Mean difference				—
	p-value				—

Table S1.3.6 - Tukey Post-Hoc Test – G-2 (Sr)

		LAGIR	Weis et al 2006	Yobregat et al. 2017
LAGIR	Mean difference	—	-1.08E-05	-6.22E-06
	p-value	—	0.065	0.374
Weis et al 2006	Mean difference		—	4.57E-06
	p-value		—	0.483
Yobregat et al. 2017	Mean difference			—
	p-value			—

Table S1.3.7 - Tukey Post-Hoc Test – AGV-1 (Sr)

		LAGIR	Weis et al 2006	Yobregat et al 2017
LAGIR	Mean difference	—	-1.094e−5	-8.744e−6
	p-value	—	1.57e-4	0.355
Weis et al 2006	Mean difference		—	2.20E-03
	p-value		—	0.850
Yobregat et al 2017	Mean difference			—
	p-value			—

Table S1.4 - USGS Reference Materials (RMs) in LAGIR

RM	#LAGIR	Sm (µg g-1)	Nd (µg g-1)	143Nd/144Nd (m)	(2s)	143Nd/144Nd (m)*	RM	#LAGIR	Sm (µg g-1)	Nd (µg g-1)	143Nd/144Nd (m)	(2s)	143Nd/144Nd (m)*	RM	#LAGIR	Sm (µg g-1)	Nd (µg g-1)	143Nd/144Nd (m)	(2s)	143Nd/144Nd (m)*	RM	#LAGIR	Sm (µg g-1)	Nd (µg g-1)	143Nd/144Nd (m)	(2s)	143Nd/144Nd (m)*
AGV-1	1			0.512783	0.000004	0.512798	**BCR-1**	10	6.2	28.7	0.512639	0.000004	0.512654	**G-2**	2	7.1	52.2	0.512215	0.000003	0.512230	**GSP-1**	614	24.3	189.8	0.511355	0.000006	0.511370
AGV-1	9			0.512789	0.000005	0.512804	**BCR-1**	170	6.8	30.0	0.512631	0.000002	0.512646	**G-2**	5	7.0	52.4	0.512209	0.000004	0.512224	**GSP-1**	616	23.9	186.9	0.511359	0.000009	0.511374
AGV-1	21			0.512779	0.000004	0.512794	**BCR-1**	968	6.7	29.5	0.512629	0.000002	0.512644	**G-2**	557	6.7	49.8	0.512211	0.000007	0.512226	**GSP-1**	617	25.2	197.9	0.511360	0.000004	0.511375
AGV-1	108			0.512786	0.000002	0.512801	**BCR-1**	1254	6.6	29.1	0.512617	0.000010	0.512632										24.5	191.5			
AGV-1	116			0.512785	0.000003	0.512800	**BCR-1**	1266	6.7	29.1	0.512629	0.000005	0.512644										0.7	5.7			
AGV-1	169			0.512787	0.000003	0.512802	**BCR-1**	436			0.512633	0.000010	0.512648										1.4	11.4			
AGV-1	222			0.512781	0.000004	0.512796	**BCR-1**	437			0.512623	0.000010	0.512638														
AGV-1	428			0.512791	0.000021	0.512806	**BCR-1**	1964	6.7	29.2	0.512633	0.000004	0.512648														
AGV-1	520			0.512779	0.000003	0.512794																					
AGV-1	521			0.512789	0.000003	0.512804																					
AGV-1	542			0.512777	0.000004	0.512792																					
AGV-1	545	5.9	32.6	0.512790	0.000012	0.512805																					
AGV-1	554	5.9	32.6	0.512787	0.000008	0.512802																					
AGV-1	555	6.0	32.9	0.512780	0.000003	0.512795																					
AGV-1	584	5.8	32.2	0.512782	0.000007	0.512797																					
AGV-1	595	5.8	32.3	0.512786	0.000008	0.512801																					
AGV-1	692	6.0	32.9	0.512785	0.000007	0.512800																					
AGV-1	786	6.0	33.1	0.512776	0.000013	0.512791																					
AGV-1	724	5.9	32.6	0.512792	0.000008	0.512807																					
AGV-1	915	5.9	32.4	0.512777	0.000010	0.512792																					
AGV-1	940	5.9	32.7	0.512793	0.000008	0.512808																					
AGV-1	1065	6.0	33.0	0.512780	0.000009	0.512795																					
AGV-1	1136		33.4	0.512778	0.000007	0.512793																					
AGV-1	1147	5.7	31.7	0.512795	0.000009	0.512810																					
AGV-1	1149	5.8	31.9	0.512781	0.000008	0.512796																					
AGV-1	1150	5.9	32.6	0.512788	0.000005	0.512803																					
AGV-1	1152	5.8	31.9	0.512776	0.000004	0.512791																					
AGV-1	1153	5.9	32.5	0.512790	0.000003	0.512805																					
AGV-1	1154	5.8	32.3	0.512786	0.000007	0.512801																					
AGV-1	1171	5.8	32.2	0.512790	0.000005	0.512805																					
AGV-1	1274			0.512785	0.000003	0.512800																					
AGV-1	1282	5.8	32.1	0.512776	0.000003	0.512791																					
AGV-1	1344	5.8	32.2	0.512786	0.000004	0.512801																					
AGV-1	1358	6.0	33.3	0.512787	0.000009	0.512802																					
AGV-1	1360	5.8	32.3	0.512786	0.000004	0.512801																					
AGV-1	1371	5.9	32.4	0.512786	0.000006	0.512801																					
AGV-1	1415	5.8	32.0	0.512775	0.000007	0.512790																					
AGV-1	1424	5.8	32.1	0.512784	0.000003	0.512799																					
AGV-1	1524	5.9	32.5	0.512789	0.000007	0.512804																					
AGV-1	1537	5.8	32.1	0.512792	0.000003	0.512807																					
AGV-1	1558	5.8	32.3	0.512776	0.000009	0.512791																					
AGV-1	1568	5.8	32.0	0.512783	0.000004	0.512798																					
AGV-1	1589	5.8	32.3	0.512780	0.000005	0.512795																					
AGV-1	1611	5.8	32.1	0.512780	0.000005	0.512795																					
AGV-1	1623	5.8	32.3	0.512787	0.000004	0.512802																					
AGV-1	1635	5.8	32.3	0.512788	0.000005	0.512803																					
AGV-1	1090			0.512779	0.000012	0.512794																					
AGV-1	1210			0.512783	0.000005	0.512798																					
AGV-1	1960	5.7	31.8	0.512779	0.000003	0.512794																					
AGV-1	2027	5.7	31.4	0.512790	0.000009	0.512805																					
AGV-1	2029	5.8	32.1	0.512780	0.000009	0.512795																					
Mean		5.9	32.4	**0.512784**		**0.512799**			6.6	29.3	**0.512629**		**0.512644**			6.9	51.5	**0.512212**		**0.512227**			24.5	191.5	**0.511358**		**0.511373**
s		0.1	0.4	**0.000005**		**0.000005**			0.2	0.4	**0.000007**		**0.000007**			0.19	1.19	**0.000003**		**0.000003**			0.7	5.7	**0.000003**		**0.000003**
2s (reprod)		0.1	0.9	**0.000010**		**0.000010**			0.4	0.8	**0.000013**		**0.000013**			0.37	2.38	**0.000006**		**0.000006**			1.4	11.4	**0.000005**		**0.000005**

Note
(1) RM - Reference materials
(2) (m) ratio measured
(3) * bias corrected
(4) (2s) - measurement repeatability (in run)
(5) s - standard deviation
(6) 2s - measurement reproducibility

Table S1.5. - 143Nd/144Nd USGS (AGV-1, G-2, BCR-1, BHVO-1and GSP-1) from LAGIR and literature data means.

RM	reference	year	n	mean	2s	[2s]
AGV-1	This work	2023	51	0.512799	0.000010	0.000001
	Weis *et al*	2006	10	0.512791	0.000013	0.000005
	Koornneef *et al.*	2015	4	0.512759	0.000075	0.000060
	Köksal *et al.*	2017	2	0.512784	0.000006	0.000027
G-2	This work	2023	3	0.512227	0.000006	0.000008
	McCoy-West	2020	16	0.512226	0.000007	0.000002
	Weis *et al* .	2006	9	0.512228	0.000006	0.000002
	Köksal *et al* .	2017	2	0.512224	0.000006	0.000027
BCR-1	This work	2023	8	0.512644	0.000014	0.000006
	Weis *et al.*	2006	13	0.512638	0.000006	0.000003
	Hegner *et al.*	1995	12	0.512629	0.000004	0.000001
	Kamenov *et al.*	2008	3	0.512645	0.000011	0.000014
	He *et al.*	2008	3	0.512604	0.000007	0.000009
	Lapen *et al* .	2009	7	0.512647	0.000013	0.000006
	van Kranendonk *et al.*	2009	3	0.512633	0.000006	0.000007
	Li *et al.*	2009	3	0.512604	0.000007	0.000009
	Magna *et al* .	2010	5	0.512621	0.000020	0.000012
	Puchtel *et al* .	2013	3	0.512645	0.000002	0.000002
	Ali *et al.*	2014	2	0.512624	0.000003	0.000009
	Price *et al* .	2014	7	0.512634	0.000018	0.000008
	Schmitz *et al.*	2004	12	0.512643	0.000009	0.000003
GSP-1	This work	2023	3	0.511373	0.000005	0.000006
	Raczek *et al.*	2003	1	0.511373	0.000018	

Note. Measurement reproducibility (2s) and standard deviation of the mean [2s]. Both with 95 % CI.

Table S1.6 - USGS Reference Materials (RMs) in LAGIR

RM	#LAGIR	87Sr/86Sr (m)	(2s)	87Sr/86Sr (m)*	RM	#LAGIR	87Sr/86Sr (m)	(2s)	87Sr/86Sr (m)*	RM	#LAGIR	87Sr/86Sr (m)	(2s)	87Sr/86Sr (m)*	RM	#LAGIR	87Sr/86Sr (m)	(2s)	87Sr/86Sr (m)*	RM	#LAGIR**	87Sr/86Sr (m)	(2s)	87Sr/86Sr (m)*
AGV-1	1	0.703965	0.000005	0.703977	**BCR-1**	10	0.705013	0.000003	0.705024	**G-2**	14	0.709749	0.000002	0.709768	**GSP-1**	15	0.768928	0.000003	0.768941	BHVO-1	2	0.703458	0.000002	0.703470
AGV-1	9	0.703971	0.000006	0.703982	**BCR-1**	170	0.704998	0.000004	0.705010	**G-2**	400	0.709742	0.000004	0.709760	**GSP-1**	15B	0.768924	0.000002	0.768937	BHVO-1	3	0.703456	0.000003	0.703468
AGV-1	21	0.703972	0.000007	0.703984	**BCR-1**	968	0.704997	0.000002	0.705009	**G-2**	1965	0.709736	0.000002	0.709755	**GSP-1**	15C	0.768920	0.000005	0.768933	BHVO-1	4	0.703449	0.000006	0.703461
AGV-1	108	0.703978	0.000005	0.703990	**BCR-1**	1254	0.705015	0.000022	0.705027	**G-2**	2028	0.709734	0.000007	0.709752	**GSP-1**	614	0.768840	0.000007	0.768853	BHVO-1	7	0.703450	0.000006	0.703462
AGV-1	116	0.703965	0.000002	0.703977	**BCR-1**	1266	0.704999	0.000010	0.705011						**GSP-1**	617	0.768879	0.000009	0.768892	BHVO-1	10	0.703467	0.000006	0.703479
AGV-1	169	0.703965	0.000001	0.703977	**BCR-1**	436	0.705016	0.000007	0.705028						**GSP-1**	1961	0.768798	0.000009	0.768811	BHVO-1	11	0.703472	0.000008	0.703483
AGV-1	222	0.703974	0.000003	0.703986	**BCR-1**	437	0.704997	0.000006	0.705009											BHVO-1	15	0.703469	0.000007	0.703480
AGV-1	339	0.703970	0.000004	0.703982	**BCR-1**	1964	0.704999	0.000009	0.705011											BHVO-1	16	0.703474	0.000008	0.703486
AGV-1	410	0.703968	0.000003	0.703980																BHVO-1	18	0.703471	0.000006	0.703483
AGV-1	411	0.703979	0.000008	0.703991																				
AGV-1	413	0.703973	0.000004	0.703985																				
AGV-1	515	0.703966	0.000003	0.703978																				
AGV-1	520	0.703959	0.000004	0.703970																				
AGV-1	545	0.703967	0.000009	0.703979																				
AGV-1	584	0.703971	0.000009	0.703982																				
AGV-1	609	0.703959	0.000006	0.703971																				
AGV-1	850	0.703955	0.000003	0.703967																				
AGV-1	915	0.703956	0.000006	0.703968																				
AGV-1	940	0.703965	0.000009	0.703976																				
AGV-1	941	0.703956	0.000007	0.703968																				
AGV-1	942	0.703959	0.000006	0.703971																				
AGV-1	984	0.703961	0.000009	0.703973																				
AGV-1	1002	0.703962	0.000009	0.703973																				
AGV-1	1023	0.703959	0.000008	0.703971																				
AGV-1	1030	0.703960	0.000003	0.703972																				
AGV-1	1104	0.703962	0.000015	0.703974																				
AGV-1	1128	0.703956	0.000007	0.703968																				
AGV-1	1136	0.703974	0.000012	0.703986																				
AGV-1	1210	0.703973	0.000003	0.703985																				
AGV-1	1235	0.703973	0.000011	0.703985																				
AGV-1	1243	0.703972	0.000008	0.703984																				
AGV-1	1171	0.703966	0.000006	0.703978																				
AGV-1	1282	0.703961	0.000005	0.703973																				
AGV-1	1295	0.703977	0.000007	0.703989																				
AGV-1	1317	0.703961	0.000027	0.703973																				
AGV-1	1331	0.703961	0.000008	0.703973																				
AGV-1	1344	0.703961	0.000005	0.703973																				
AGV-1	1358	0.703970	0.000007	0.703982																				
AGV-1	1360	0.703961	0.000009	0.703973																				
AGV-1	1371	0.703970	0.000010	0.703982																				
AGV-1	1387	0.703958	0.000006	0.703970																				
AGV-1	1424	0.703968	0.000006	0.703980																				
AGV-1	1448	0.703966	0.000006	0.703978																				
AGV-1	1482	0.703959	0.000003	0.703970																				
AGV-1	1524	0.703973	0.000006	0.703985																				
AGV-1	1526	0.703958	0.000011	0.703970																				
AGV-1	1527	0.703962	0.000003	0.703974																				
AGV-1	1529	0.703979	0.000007	0.703991																				
AGV-1	1526	0.703958	0.000011	0.703970																				
AGV-1	1527	0.703962	0.000003	0.703974																				
AGV-1	1529	0.703979	0.000007	0.703991																				
AGV-1	1548	0.703979	0.000006	0.703991																				
AGV-1	1558	0.703962	0.000005	0.703974																				
AGV-1	2027	0.703978	0.000006	0.703990																				
AGV-1	2029	0.703981	0.000009	0.703993																				
Mean		**0.703966**		**0.703978**			**0.705004**		**0.705016**			**0.709740**		**0.709759**			**0.768882**		**0.768895**			**0.703463**		**0.703475**
s		**0.000007**		**0.000007**			**0.000009**		**0.000009**			**0.000007**		**0.000007**			**0.000053**		**0.000053**			**0.000010**		**0.000010**
2s (reprod)		**0.000015**		**0.000015**			**0.000017**		**0.000017**			**0.000014**		**0.000014**			**0.000106**		**0.000106**			**0.000019**		**0.000019**

Note
(1) RM - Reference materials
(2) (m) ratio measured
(3) * bias corrected
(4) (2s) - measurement repeatability (in run)
(5) s - standard deviation
(6) 2s - measurement reproducibility
(7) ** new digestions exclusived for Sr

Table S1.7. 87Sr/86Sr USGS (AGV-1, G-2, BCR-1, BHVO-1and GSP-1) from LAGIR and literature data means values.

RM	reference	year	n	mean	2s	[2s]
AGV-1	This work	2023	51	0.703978	0.000015	0.000002
	Weis *et al.*	2006	10	0.703989	0.000017	0.000006
	Koornneef *et al.*	2015	4	0.704009	0.000010	0.000008
	Yobregat *et al.*	2017	5	0.703986	0.000013	0.000008
	Koksal *et al.*	2017	2	0.703993	0.000012	0.000054
G-2	This work	2023	5	0.709759	0.000012	0.000007
	Weis *et al.*	2006	7	0.709770	0.000014	0.000006
	Robinson *et al.*	2015	3	0.709741	0.000012	0.000015
	Yobregat *et al.*	2017	6	0.709765	0.000014	0.000007
	Koksal *et al.*	2017	2	0.709775	0.000020	0.000090
BCR-1	This work	2023	8	0.705016	0.000017	0.000007
	Weis *et al.*	2006	8	0.705018	0.000013	0.000005
	Beard *et al.*	1995	9	0.705000	0.000030	0.000012
	Altherr *et al.*	2000	2	0.704972	0.000020	0.000090
	Liu *et al.*	2007	7	0.705036	0.000040	0.000018
	Price *et al.*	2012	6	0.705000	0.000040	0.000021
	Doroshkevich *et al.*	2012	6	0.705036	0.000022	0.000012
	Terentiev *et al.*	2016	6	0.705036	0.000022	0.000012
	Martynov *et al.*	2017	6	0.705037	0.000022	0.000012
BHVO-1	This work	2023	9	0.703475	0.000019	0.000007
	Weis *et al.*	2006	8	0.703474	0.000017	0.000007
	Charlier *et al.*	2006	21	0.703490	0.000028	0.000006
	Charlier *et al.*	2006	5	0.703480	0.000094	0.000058
	Price *et al.*	2012	13	0.703480	0.000040	0.000012
	Crummy *et al.*	2014	12	0.703492	0.000066	0.000021
	Yobregat *et al.*	2017	7	0.703475	0.000009	0.000004
GSP-1	This work	2023	6	0.768895	0.000106	0.000093
	Raczek *et al.*	2003	5	0.767310	0.002737	0.001699

Note. Measurement reproducibility (2s) and standard deviation of the mean [2s]. Both with 95 % CI.

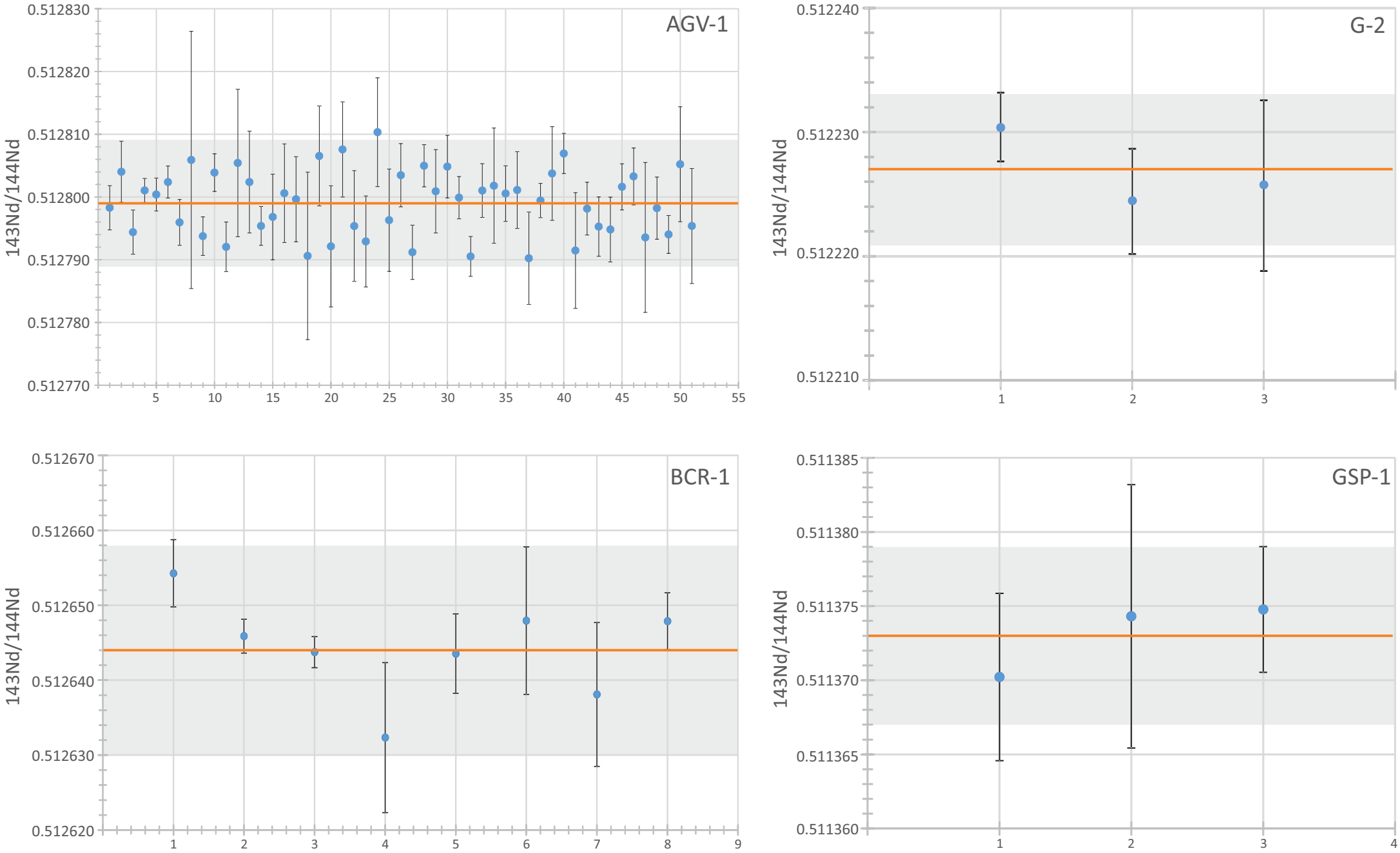

Figure S2.1. Measurement results obtained in LAGIR for 143Nd/144Nd USGS (AGV-1, BCR-1, G-2 and GSP-1), with mean values (orange line), range bars (2s) measurement repeatability (in run) and the grey bands is measurement reproducibility (2s). Both with CI 95 %. The abscissa axis indicates the number of samples (n).

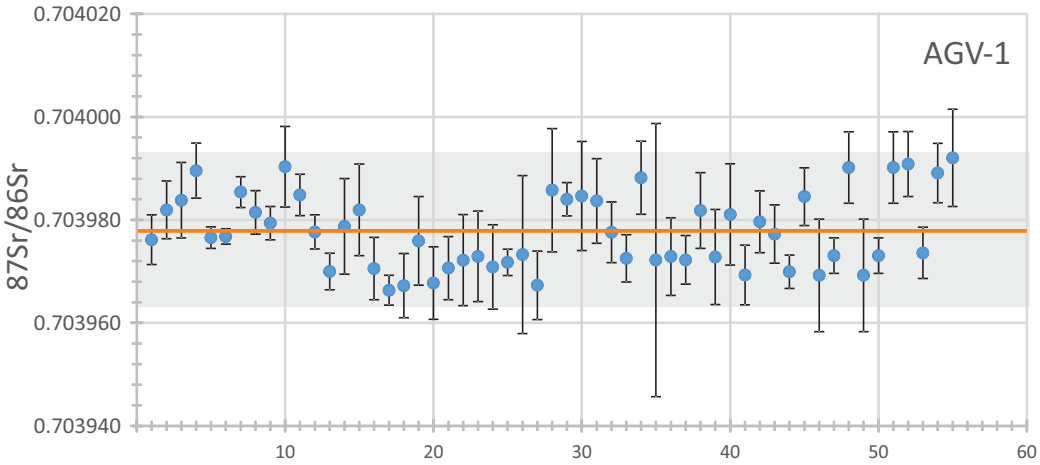

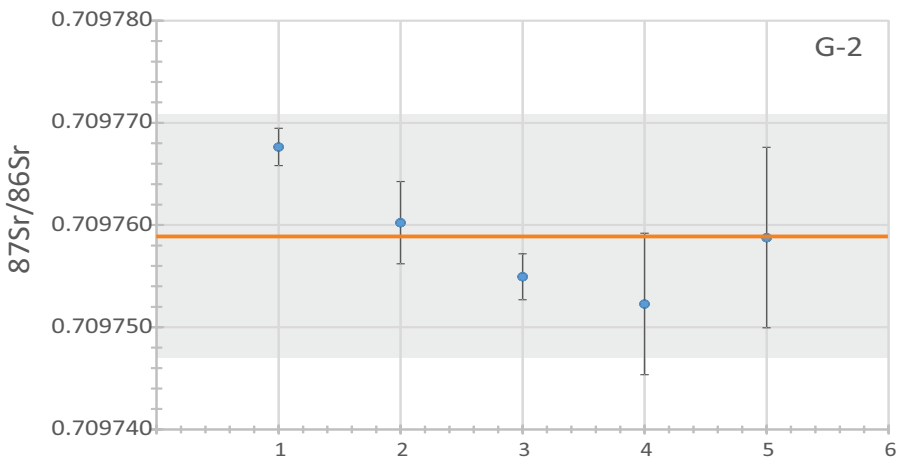

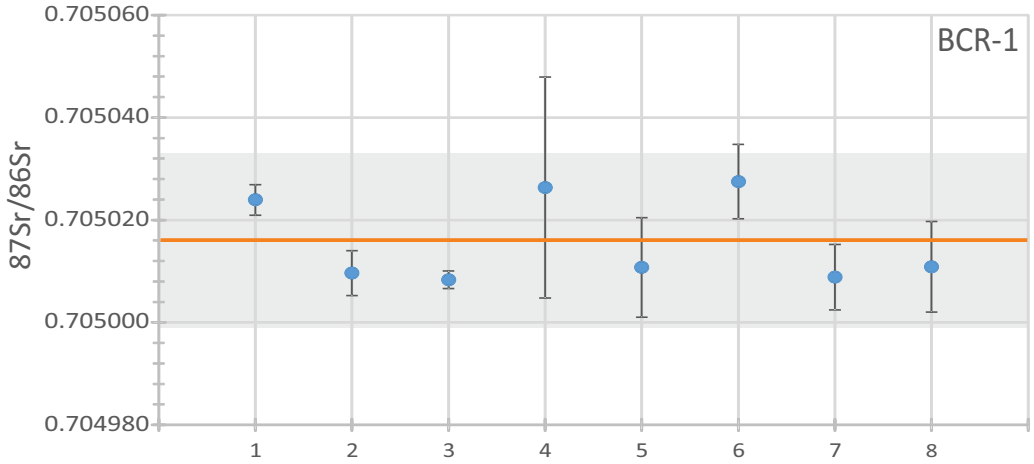

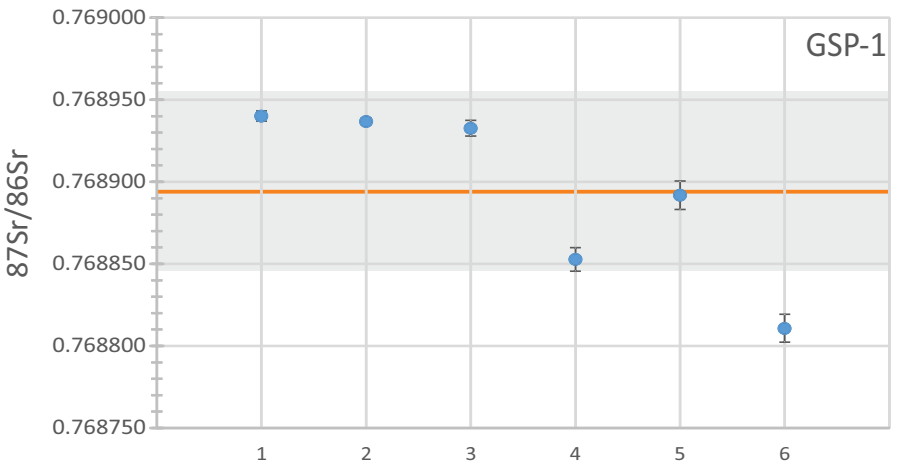

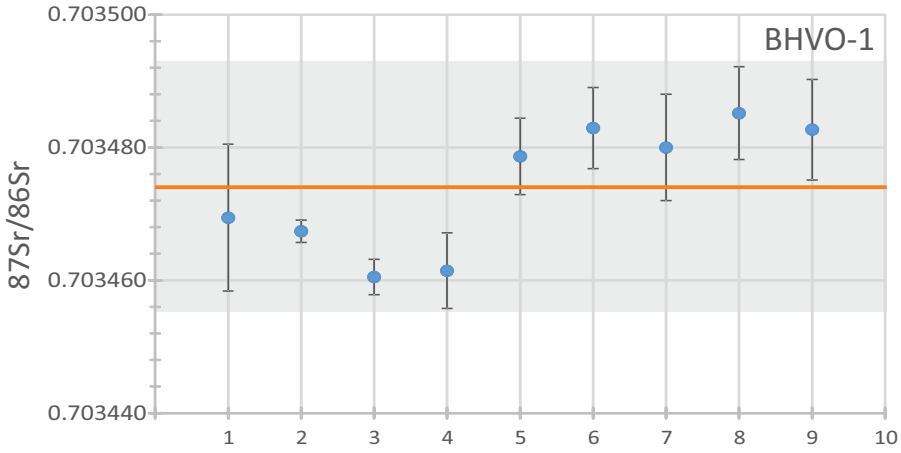

Figure S2.2 87Sr/86Sr USGS (AGV-1, G-2, BCR-1, GSP-1and BHVO-1) in LAGIR: means values (orange line), vertical bars are the measurement repeatability in run (2s); grey bands are the measurement reproducibility (2s) with a confidence interval of 95 %. The abscissa axis indicates the number of samples (n).

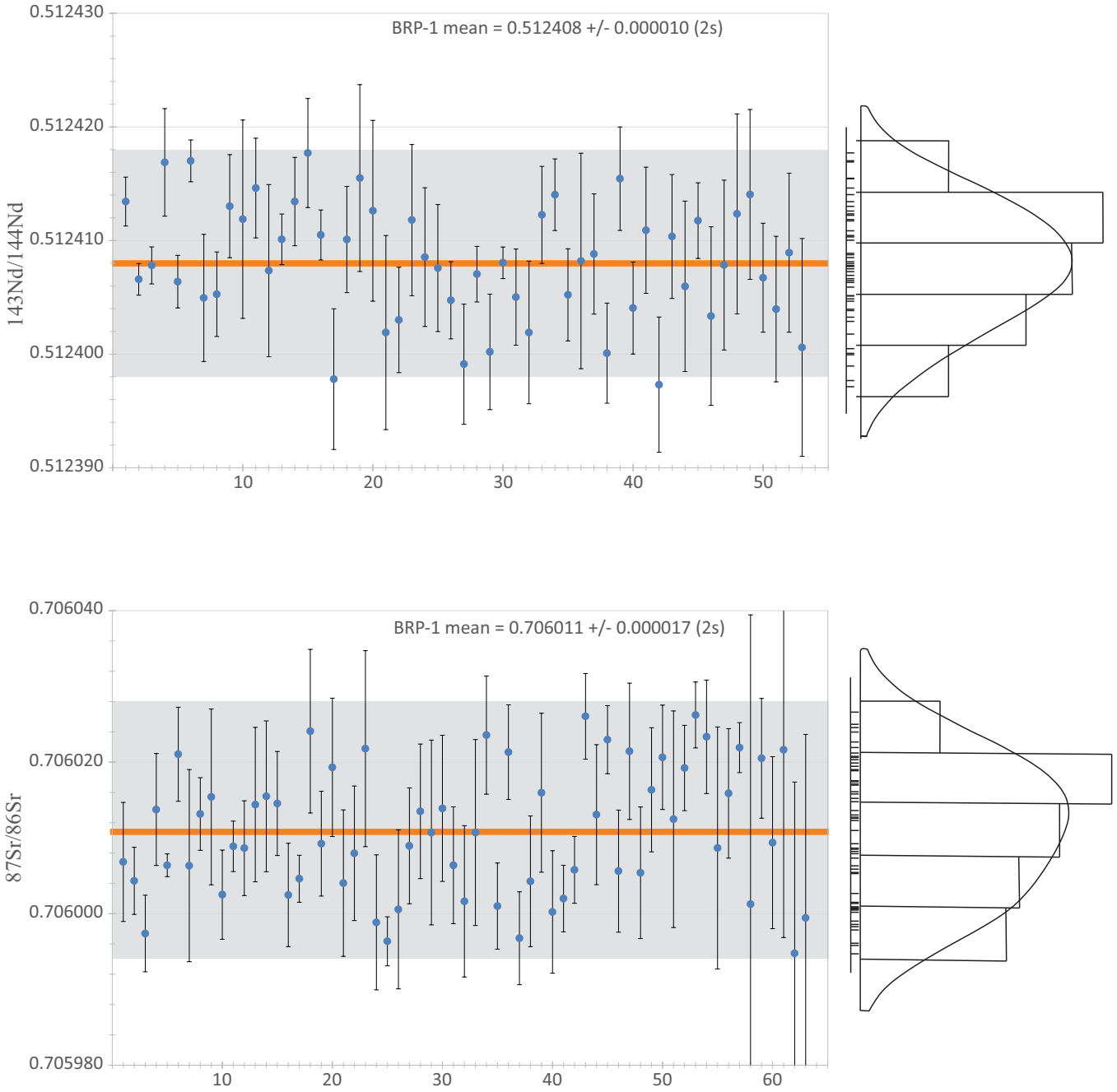

Figure S2.3 - Individual values and mean for Nd. Blue symbols are measured ratio normalised to JNdi-1. The vertical bars on each blue symbol represent the measurement repeatability in run(2s) associated with of the individual sample analysis. Orange line is the normalised mean and light grey band corresponded to measurement reproducibility (2s) at the 95 % CI. Individual values and mean for Sr. Blue symbols are measurement ratios normalised to NIST SRM 987. The vertical bars of each blue symbol represent the measurement repeatability (2s) associated with the individual sample analysis. Orange line is the normalised mean and light grey band corresponds to measurement reproducibility (2s) at 95 % CI. To the right of each graph – KDEs with histograms and a set of vertical lines that mark the individual measurements.

Table S3.1 - BRP-1 data in LAGIR

LAGIR BRP-1 data

#LAGIR	weight date	recipient	sample mass (g)	spike mass (g)	Sm (ug g-1)	Nd (ug g-1)	Nd/Sm	143Nd/144Nd (m)	143Nd/144Nd* (m)	(2s)	cycles	87Sr/86Sr (m)	87Sr/86Sr* (m)	(2s)	cycles	Sr filament
232	2009-06-18	B-3	0.0535	0.0516	11.0	51.9	4.7	0.512398	0.512413	0.000002	160/160	0.705995	0.706007	0.000008	100/100	Re
233	2009-06-18	B-7	0.0575	0.0486	11.0	51.9	4.7	0.512392	0.512407	0.000001	160/160	0.705993	0.706005	0.000004	100/100	Re
234	2009-06-18	B-9	0.0531	0.0528	11.0	51.6	4.7	0.512393	0.512408	0.000002	160/160	0.706053	0,706064	0.000009	100/100	Re
235	2009-06-18	B-11	0.0533	0.0479	11.0	51.9	4.7	0.512402	0.512417	0.000005	160/160	0.705986	0.705998	0.000005	100/100	Re
239	2009-11-08	I-2-6	0,1109 (2)	0.0480	11.0	52.0	4.7	0.512391	0.512406	0.000002	160/160					
239B	2009-11-08	I-2-6	0,1109 (2)	0.0480	11.0	52.0	4.7	0.512402	0.512417	0.000002	160/160	0.706002	0.706014	0.000007	100/100	Re
240	2009-11-08	I-2-5	0,0999 (2)	0.0496	11.0	52.0	4.7	0.512390	0.512405	0.000006	160/160	0.705995	0.706007	0.000042	100/100	Re
240B	2009-11-08	I-2-5	0,0999 (2)	0.0496								0.706010	0.706022	0.000006	100/100	Re
241	2009-11-08	I-2-4	0,1163 (2)	0.0527	10.9	51.7	4.7	0.512390	0.512405	0.000004	100/160	0.705995	0.706007	0.000013	100/100	Re
241B	2009-11-08	I-2-4	0,1163 (2)	0.0527	10.9	51.9	4.7	0.512398	0.512413	0.000005	160/160					
242	2009-11-08	I-1-9	0,0981 (2)	0.0554	10.9	51.8	4.7	0.512397	0.512412	0.000009	100/160					
242B	2009-11-08	I-1-9	0,0981 (2)	0.0554	11.0	51.9	4.7	0.512400	0.512415	0.000004	160/160					
333	2010-09-04	B-5	0,1117 (2)	0.0576	10.8	51.1	4.7	0.512392	0.512407	0.000008	160/160	0.706002	0.706014	0.000005	100/100	Re
334	2010-09-04	B-6	0,1159 (2)	0.0522	10.9	51.7	4.7	0.512395	0.512410	0.000002	160/160	0.706004	0.706016	0.000012	100/100	Re
335A	2010-09-04	B-9	0,1623 (4)					0.512398	0.512413	0.000004	160/160					
335C	2010-09-04	B-9	0,1623 (4)					0.512403	0.512418	0.000005	90/160					
336	2010-09-04	B-11	0,1617 (4)					0.512395	0.512410	0.000002	160/160	0.705991	0.706003	0.000006	100/100	Re
326	2010-05-03	B-7	0.0504	0.0983								0.705997	0.706009	0.000003	100/100	Re
367	2010-07-20	B-9	0,2556 (10)					0.512364	0,512379	0.000007	160/160	0.706035	0,706047	0.000004	100/100	Re
370A	2010-12-08	B-12	0,1594 (8)					0.512383	0.512398	0.000006	160/160					
370B	2010-12-08	B-12	0,1594 (8)					0.512395	0.512410	0.000005	160/160					
416	2011-01-07	I-2-9	0.0264									0.705997	0.706009	0.000006	100/100	Re
417	2011-01-07	I-4-9	0.0336									0.706003	0.706015	0.000010	100/100	Re
418	2011-01-07	I-5-2	0.0231									0.706004	0.706016	0.000010	100/100	Re
419	2011-01-07	I-6-4	0.0511									0.706003	0.706015	0.000007	100/100	Re
421	2011-01-07	I-7-7	0.0476									0.705991	0.706003	0.000007	100/100	Re
438	2011-08-19	B-4	0.0545					0.512400	0.512415	0.000008	160/160					
439	2011-08-19	B-6	0.0335					0.512398	0.512413	0.000008	160/160					
440	2011-08-19	B-7	0.0272					0.512387	0.512402	0.000009	160/160					
441	2011-08-19	B-8	0.021									0.705993	0.706005	0.000003	100/100	Re
454	2011-09-30	B-1	0.0296									0.706013	0.706025	0.000011	100/100	Re
455	2011-09-30	B-3	0.0203									0.705998	0.706010	0.000007	100/100	Re
458	2011-09-30	B-7	0.0235									0.706008	0.706020	0.000009	100/100	Re
469	2011-04-11	B-3	0.0279									0.705993	0.706005	0.000010	100/100	Re
470	2011-04-11	B-4	0.0376									0.705997	0.706008	0.000009	100/100	Re
472	2011-04-11	B-7	0.0215					0.512374	0,512389	0.000004	160/160	0.706010	0.706022	0.000013	100/100	Re
473	2011-04-11	B-8	0.0228									0.705987	0.705999	0.000009	100/100	Re
498A	2012-02-23	B-7	0.1942 (8)					0.512388	0.512403	0.000005	160/160	0.705985	0.705997	0.000003	100/100	Re
498B	2012-02-23	B-7	0.1942 (8)									0.705989	0.706001	0.000011	100/100	Re
498C	2012-02-23	B-7	0.1942 (8)									0.705998	0.706009	0.000008	100/100	Re
498D	2012-02-23	B-7	0.1942 (8)					0.512397	0.512412	0.000007	160/160	0.706002	0.706014	0.000009	100/100	Re
498E	2012-02-23	B-7	0.1942 (8)									0.705999	0.706011	0.000012	100/100	Re
498F	2012-02-23	B-7	0.1942 (8)					0.512394	0.512409	0.000006	160/160	0.706002	0.706014	0.000010	100/100	Re
498G	2012-02-23	B-7	0.1942 (8)					0.512393	0.512408	0.000006	160/160	0.705995	0.706007	0.000008	100/100	Re
498H	2012-02-23	B-7	0.1942 (8)					0.512390	0.512405	0.000003	160/160	0.705990	0.706002	0.000010	100/100	Re
499B	2012-02-23	B-8	0.1798 (8)									0.705999	0.706011	0.000012	100/100	Re
499C	2012-02-23	B-8	0.1798 (8)					0.512384	0.512399	0.000005	160/160					
500A	2012-02-23	B-9	0.2030 (8)					0.512392	0.512407	0.000002	160/160	0.706012	0.706024	0.000008	100/100	Re
500B	2012-02-23	B-9	0.2030 (8)					0.512385	0.512400	0.000005	160/160					
501A	2012-02-23	B-11	0.1686 (8)									0.705990	0.706001	0.000006	100/100	Re
501B	2012-02-23	B-11	0.1686 (8)					0.512393	0.512408	0.000001	160/160					
501C	2012-02-23	B-11	0.1686 (8)									0.706010	0.706022	0.000006	100/100	Re
1584	2017-11-16	I-113B	0.0387									0.705985	0.705997	0.000006	100/100	Re
1585	2017-11-16	I-141	0.0357					0.512390	0.512405	0.000004	160/160	0.705993	0.706005	0.000009	100/100	Re
1587	2017-11-16	I-146	0.0236					0.512387	0.512402	0.000006	160/160	0.706005	0.706016	0.000010	100/100	Re
1608	2018-01-29	I-149	0.0472	0.0734	11.1	52.3	4.7	0.512397	0.512412	0.000004	160/160					
1609	2018-01-29	I-150	0.0494	0.0856								0.705989	0.706001	0.000008	100/100	Re
1621	2018-02-20	I-153	0.0260	0.0423								0.705991	0.706002	0.000004	100/100	Re
1648	2018-03-09	B-5	0.0227	0.0306	11.1	52.1	4.7	0.512399	0.512414	0.000003	160/160	0.706038	0,706050	0.000005	100/100	Re
1678	2018-11-06	I-105	0.0258	0.0331								0.705994	0.706006	0.000004	100/100	Re
1709	2018-06-14	I-98	0.0259	0.0459	11.2	52.5	4.7	0.512390	0.512405	0.000004	160/160	0.706015	0.706027	0.000006	100/100	Re
1715	2018-06-14	I-102B	0.0266	0.0464	11.0	51.4	4.7	0.512426	0,512441	0.000004	160/160	0.706002	0.706014	0.000009	100/100	Re
1782	2018-10-16	I-2-10	0.0252	0.0217								0.706012	0.706023	0.000004	100/100	Re
1812	2018-10-29	I-91	0.0534	0.0476	11.1	52.0	4.7	0.512393	0.512408	0.000009	160/160	0.705994	0.706006	0.000008	100/100	Re
1847	2018-11-30	I-112	0.0274	0.0263	11.1	52.0	4.70	0.512394	0.512409	0.000005	160/160					
1848	2018-11-30	I-114	0.0252	0.0252								0.706010	0.706022	0.000009	100/100	Re
1849	2018-11-30	I-115B	0.0263	0.0264								0.706045	0,706057	0.000001	100/100	Re
1850	2018-11-30	I-116	0.0283	0.0265	11.1	52.1	4.7	0.512385	0.512400	0.000004	160/160					
1852	2018-11-30	I-131	0.0346	0.0334	11.0	51.8	4.7	0.512416	0,512431	0.000006	160/160	0.706057	0,706069	0.000005	100/100	Re
1857	2019-01-15	I-1-6	0.0296	0.0316	11.1	52.0	4.7	0.512400	0.512415	0.000005	160/160					
1881B	2019-04-03	I-150	0.0593	0.0565								0.705994	0.706006	0.000009	100/100	Re
1919	2019-05-20	I-161	0.0222	0.0281								0.706005	0.706017	0.000008	100/100	Re
1967	2019-06-07	I-99	0.0293	0.0484	11.0	51.7	4.7	0.512389	0.512404	0.000004	160/160	0.706009	0.706021	0.000007	100/100	Re
2001	2019-06-27	I-105	0.0342	0.0596	11.0	51.6	4.7	0.512396	0.512411	0.000006	160/160	0.706001	0.706013	0.000014	100/100	Re
2020	2019-06-27	I-163	0.0281	0.0378	11.1	52.0	4.7	0.512382	0.512397	0.000006	160/160	0.706008	0.706020	0.000006	100/100	Re
2036	2019-07-18	I-102	0.0259	0.0362	11.2	52.7	4.7	0.512395	0.512410	0.000005	160/160					
2053	2019-08-09	I-176	0.0258	0.0485	11.0	51.5	4.7	0.512391	0.512406	0.000007	160/160					
2067	2019-08-08	I-149	0.0258	0.0389	11.0	51.6	4.7	0.512397	0.512412	0.000003	160/160	0.706015	0.706027	0.000004	100/100	Re
2101	2019-09-17	I-158	0.0278	0.0483	11.1	52.2	4.7	0.512388	0.512403	0.000008	160/160	0.706012	0.706024	0.000007	100/100	Re
2122	2019-11-25	I-116	0.0247	0.0495	11.0	51.5	4.7	0.512393	0.512408	0.000007	160/160					
2123	2019-11-25	I-146	0.0276	0.0583	11.1	52.0	4.7	0.512397	0.512412	0.000009	160/160					
2133	2020-01-22	I-135	0.0379	0.0692								0.705997	0.706009	0.000016	100/100	Ta
2149	2020-02-11	I-107	0.0549	0.0934								0.706004	0.706016	0.000009	30/100	Ta
2164	2021-04-21	I-103	0.0316	0.0499								0.706010	0.706022	0.000003	100/100	Re
2198	2021-06-11	I-105	0.0469	0.0453	11.0	51.8	4.7	0.512399	0.512414	0.000007	160/160	0.705990	0.706002	0.000038	100/100	Ta
2212	2021-06-24	I-101B	0.0266	0.0235	11.0	51.4	4.7	0.512392	0.512407	0.000005	160/160	0.706009	0.706021	0.000008	100/100	Ta
2236	2021-07-09	I-107	0.0252	0.0377	10.9	51.4	4.7	0.512389	0.512404	0.000006	160/160	0.705998	0.706010	0.000011	100/100	Ta
2255	2021-08-09	I-153	0.0371	0.0344								0.706010	0.706022	0.000025	100/100	Ta
2265	2021-08-13	I-180	0.0278	0.0242	11.1	52.0	4.7	0.512394	0.512409	0.000007	160/160	0.705983	0.705995	0.000023	100/100	Ta
2176	2021-07-05	I-116	0.0300	0.0485	11.1	52.2	4.7	0.512386	0.512401	0.000010	160/160	0.705988	0.706000	0.000024	100/100	Ta
Mean					11.0	51.9			0.512408				0.706011			
2s (repro.)					0.2	0.6			0.000010				0.000017			
[2s]					0.0	0.1			0.000001				0.000002			

Note

(1) The number in parentheses corresponds to the amount of aliquots split in shared digestion

(2) (m) ratio measured

(3) All Nd analyzes were performed on Re filament

(4) 2s - measurement repeatability (in run)

(5) * bias corrected

(6) yellow values - outliers excluded by Grubbs test

Table S3.2 - Digestion types Nd - BRP-1 data in LAGIR

Single			batch			bomb			PFA vials			Natural			ID		
#LAGIR	143Nd/144Nd	(2s)	#LAGIR	143Nd/144Nd	(2s)	#LAGIR	143Nd/144Nd	(2s)	#LAGIR	143Nd/144Nd	(2s)	#LAGIR	143Nd/144Nd	(2s)	#LAGIR	143Nd/144Nd	(2s)
232	0.512413	0.000002	239	0.512406	0.000002	232	0.512413	0.000002	239	0.512406	0.000002	335A	0.512413	0.000004	232	0.512413	0.000002
233	0.512407	0.000001	239B	0.512417	0.000002	233	0.512407	0.000001	239B	0.512417	0.000002	335C	0.512418	0.000005	233	0.512407	0.000001
234	0.512408	0.000002	240	0.512405	0.000006	234	0.512408	0.000002	240	0.512405	0.000006	336	0.512410	0.000002	234	0.512408	0.000002
235	0.512417	0.000005	241	0.512405	0.000004	235	0.512417	0.000005	241	0.512405	0.000004	370A	0.512398	0.000006	235	0.512417	0.000005
333	0.512407	0.000008	241B	0.512413	0.000005	333	0.512407	0.000008	241B	0.512413	0.000005	370B	0.512410	0.000005	239	0.512406	0.000002
334	0.512410	0.000002	242	0.512412	0.000009	334	0.512410	0.000002	242	0.512412	0.000009	438	0.512415	0.000008	239B	0.512417	0.000002
438	0.512415	0.000008	242B	0.512415	0.000004	335A	0.512413	0.000004	242B	0.512415	0.000004	439	0.512413	0.000008	240	0.512405	0.000006
439	0.512413	0.000008	335A	0.512413	0.000004	335C	0.512418	0.000005	1585	0.512405	0.000004	440	0.512402	0.000009	241	0.512405	0.000004
440	0.512402	0.000009	335C	0.512418	0.000005	336	0.512410	0.000002	1587	0.512402	0.000006	498A	0.512403	0.000005	241B	0.512413	0.000005
1585	0.512405	0.000004	336	0.512410	0.000002	370A	0.512398	0.000006	1608	0.512412	0.000004	498D	0.512412	0.000007	242	0.512412	0.000009
1587	0.512402	0.000006	370A	0.512398	0.000006	370B	0.512410	0.000005	1709	0.512405	0.000004	498F	0.512409	0.000006	242B	0.512415	0.000004
1608	0.512412	0.000004	370B	0.512410	0.000005	438	0.512415	0.000008	1812	0.512408	0.000009	498G	0.512408	0.000006	333	0.512407	0.000008
1648	0.512414	0.000003	498A	0.512403	0.000005	439	0.512413	0.000008	1847	0.512409	0.000005	498H	0.512405	0.000003	334	0.512410	0.000002
1709	0.512405	0.000004	498D	0.512412	0.000007	440	0.512402	0.000009	1850	0.512400	0.000004	499C	0.512399	0.000005	1608	0.512412	0.000004
1812	0.512408	0.000009	498F	0.512409	0.000006	498A	0.512403	0.000005	1857	0.512415	0.000005	500A	0.512407	0.000002	1648	0.512414	0.000003
1847	0.512409	0.000005	498G	0.512408	0.000006	498D	0.512412	0.000007	1967	0.512404	0.000004	500B	0.512400	0.000005	1709	0.512405	0.000004
1850	0.512400	0.000004	498H	0.512405	0.000003	498F	0.512409	0.000006	2001	0.512411	0.000006	501B	0.512408	0.000001	1812	0.512408	0.000009
1857	0.512415	0.000005	499C	0.512399	0.000005	498G	0.512408	0.000006	2020	0.512397	0.000006	1585	0.512405	0.000004	1847	0.512409	0.000005
1967	0.512404	0.000004	500A	0.512407	0.000002	498H	0.512405	0.000003	2036	0.512410	0.000005	1587	0.512402	0.000006	1850	0.512400	0.000004
2001	0.512411	0.000006	500B	0.512400	0.000005	499C	0.512399	0.000005	2053	0.512406	0.000007				1857	0.512415	0.000005
2020	0.512397	0.000006	501B	0.512408	0.000001	500A	0.512407	0.000002	2067	0.512412	0.000003				1967	0.512404	0.000004
2036	0.512410	0.000005				500B	0.512400	0.000005	2101	0.512403	0.000008				2001	0.512411	0.000006
2053	0.512406	0.000007				501B	0.512408	0.000001	2122	0.512408	0.000007				2020	0.512397	0.000006
2067	0.512412	0.000003				1648	0.512414	0.000003	2123	0.512412	0.000009				2036	0.512410	0.000005
2101	0.512403	0.000008							2198	0.512414	0.000007				2053	0.512406	0.000007
2122	0.512408	0.000007							2212	0.512407	0.000005				2067	0.512412	0.000003
2123	0.512412	0.000009							2236	0.512404	0.000006				2101	0.512403	0.000008
2198	0.512414	0.000007							2265	0.512409	0.000007				2122	0.512408	0.000007
2212	0.512407	0.000005							2176	0.512401	0.000010				2123	0.512412	0.000009
2236	0.512404	0.000006													2198	0.512414	0.000007
2265	0.512409	0.000007													2212	0.512407	0.000005
2176	0.512401	0.000010													2236	0.512404	0.000006
															2265	0.512409	0.000007
															2176	0.512401	0.000010
Mean	0.512408			0.512408			0.512409			0.512408			0.512407			0.512409	
2s	0.000010			0.000011			0.000011			0.000010			0.000011			0.000010	
[2s]	0.000002			0.000002			0.000002			0.000002			0.000003			0.000002	

Note

(2s) measurement repetibility (in run)

2s measurement reproducibility

[2s] standard deviation of the mean

Table S3.3 - Digestion types Sr - BRP-1 data in LAGIR

Single			batch			bomb			PFA vials			Natural			ID		
#LAGIR	87Sr/86Sr	(2s)	#LAGIR	87Sr/86Sr	(2s)	#LAGIR	87Sr/86Sr	(2s)	#LAGIR	87Sr/86Sr	(2s)	#LAGIR	87Sr/86Sr	(2s)	#LAGIR	87Sr/86Sr	(2s)
232	0.706007	0.000008	239B	0.706014	0.000007	232	0.706007	0.000008	239B	0.706014	0.000007	336	0.705991	0.706003	232	0.706007	0.000008
233	0.706005	0.000004	240	0.706007	0.000042	233	0.706005	0.000004	240	0.706007	0.000042	416	0.706009	0.000006	233	0.706005	0.000004
235	0.705998	0.000005	240B	0.706022	0.000006	235	0.705998	0.000005	240B	0.706022	0.000006	417	0.706015	0.000010	235	0.705998	0.000005
333	0.706014	0.000005	241	0.706007	0.000013	333	0.706014	0.000005	241	0.706007	0.000013	418	0.706016	0.000010	239B	0.706014	0.000007
334	0.706016	0.000012	336	0.706003	0.000006	334	0.706016	0.000012	416	0.706009	0.000006	419	0.706015	0.000007	240	0.706007	0.000042
326	0.706009	0.000003	498A	0.705997	0.000003	336	0.706003	0.000006	417	0.706015	0.000010	421	0.706003	0.000007	240B	0.706022	0.000006
416	0.706009	0.000006	498B	0.706001	0.000011	326	0.706009	0.000003	418	0.706016	0.000010	441	0.706005	0.000003	241	0.706007	0.000013
417	0.706015	0.000010	498C	0.706009	0.000008	441	0.706005	0.000003	419	0.706015	0.000007	454	0.706025	0.000011	333	0.706014	0.000005
418	0.706016	0.000010	498D	0.706014	0.000009	454	0.706025	0.000011	421	0.706003	0.000007	455	0.706010	0.000007	334	0.706016	0.000012
419	0.706015	0.000007	498E	0.706011	0.000012	455	0.706010	0.000007	1584	0.705997	0.000006	458	0.706020	0.000009	326	0.706009	0.000003
421	0.706003	0.000007	498F	0.706014	0.000010	458	0.706020	0.000009	1585	0.706005	0.000009	469	0.706005	0.000010	1608	0.706001	0.000008
441	0.706005	0.000003	498G	0.706007	0.000008	469	0.706005	0.000010	1587	0.706016	0.000010	470	0.706008	0.000009	1609	0.706002	0.000004
454	0.706025	0.000011	498H	0.706002	0.000010	470	0.706008	0.000009	1609	0.706001	0.000008	472	0.706022	0.000013	1648	0.706006	0.000004
455	0.706010	0.000007	499B	0.706011	0.000012	472	0.706022	0.000013	1621	0.706002	0.000004	473	0.705999	0.000009	1678	0.706027	0.000006
458	0.706020	0.000009	500A	0.706024	0.000008	473	0.705999	0.000009	1678	0.706006	0.000004	498A	0.705997	0.000003	1709	0.706014	0.000009
469	0.706005	0.000010	501A	0.706001	0.000006	498A	0.705997	0.000003	1709	0.706027	0.000006	498B	0.706001	0.000011	1715	0.706023	0.000004
470	0.706008	0.000009	501C	0.706022	0.000006	498B	0.706001	0.000011	1715	0.706014	0.000009	498C	0.706009	0.000008	1782	0.706006	0.000008
472	0.706022	0.000013				498C	0.706009	0.000008	1782	0.706023	0.000004	498D	0.706014	0.000009	1847	0.706022	0.000009
473	0.705999	0.000009				498D	0.706014	0.000009	1812	0.706006	0.000008	498E	0.706011	0.000012	1857	0.706006	0.000009
1584	0.705997	0.000006				498E	0.706011	0.000012	1848	0.706022	0.000009	498F	0.706014	0.000010	1881B	0.706017	0.000008
1585	0.706005	0.000009				498F	0.706014	0.000010	1881B	0.706006	0.000009	498G	0.706007	0.000008	1919	0.706021	0.000007
1587	0.706016	0.000010				498G	0.706007	0.000008	1919	0.706017	0.000008	498H	0.706002	0.000010	1967	0.706013	0.000014
1609	0.706001	0.000008				498H	0.706002	0.000010	1967	0.706021	0.000007	499B	0.706011	0.000012	2001	0.706020	0.000006
1621	0.706002	0.000004				499B	0.706011	0.000012	2001	0.706013	0.000014	500A	0.706024	0.000008	2053	0.706027	0.000004
1678	0.706006	0.000004				500A	0.706024	0.000008	2020	0.706020	0.000006	501A	0.706001	0.000006	2067	0.706024	0.000007
1709	0.706027	0.000006				501A	0.706001	0.000006	2067	0.706027	0.000004	501C	0.706022	0.000006	2123	0.706009	0.000016
1715	0.706014	0.000009				501C	0.706022	0.000006	2101	0.706024	0.000007	1584	0.705997	0.000006	2133	0.706016	0.000009
1782	0.706023	0.000004							2133	0.706009	0.000016	1585	0.706005	0.000009	2149	0.706022	0.000003
1812	0.706006	0.000008							2149	0.706016	0.000009	1587	0.706016	0.000010	2164	0.706002	0.000038
1848	0.706022	0.000009							2164	0.706022	0.000003				2198	0.706021	0.000008
1881B	0.706006	0.000009							2198	0.706002	0.000038				2212	0.706010	0.000011
1919	0.706017	0.000008							2212	0.706021	0.000008				2236	0.706022	0.000025
1967	0.706021	0.000007							2236	0.706010	0.000011				2255	0.705995	0.000023
2001	0.706013	0.000014							2255	0.706022	0.000025				2265	0.706000	0.000024
2020	0.706020	0.000006							2265	0.705995	0.000023						
2067	0.706027	0.000004							2176	0.706000	0.000024						
2101	0.706024	0.000007															
2133	0.706009	0.000016															
2149	0.706016	0.000009															
2164	0.706022	0.000003															
2198	0.706002	0.000038															
2212	0.706021	0.000008															
2236	0.706010	0.000011															
2255	0.706022	0.000025															
2265	0.705995	0.000023															
2176	0.706000	0.000024															
Mean	0.706012			0.706010			0.706010			0.706013			0.706010			0.706012	
2s	0.000018			0.000016			0.000016			0.000018			0.000017			0.000018	
[2s]	0.000003			0.000004			0.000003			0.000003			0.000003			0.000003	

Note
(2s) measurement repetibility (in run)
2s measurement reproducibility
[2s] standard deviation of the mean

Table S3.4 - Normalised ratios of BRP-1 in LAGIR.

#LAGIR	weight date	Sm (ug g-1)	Nd (ug g-1)	$^{143}Nd/^{144}Nd_{(g)}$	(2s)	$^{87}Sr/^{86}Sr_{(h)}$	(2s)
232 (a,c,f)	2009-06-18	11.0	51.9	0.512413	0.000002	0.706007	0.000008
233 (a,c,f)	2009-06-18	11.0	51.9	0.512407	0.000001	0.706005	0.000004
234 (a,c,f)	2009-06-18	11.0	51.6	0.512408	0.000002	0.706064*	0.000009
235 (a,c,f)	2009-06-18	11.0	51.9	0.512417	0.000005	0.705998	0.000005
239 (b,d,f)	2009-11-08	11.0	52.0	0.512406	0.000002		
239B (b,d,f)	2009-11-08	11.0	52.0	0.512417	0.000002	0.706014	0.000007
240 (b,d,f)	2009-11-08	11.0	52.0	0.512405	0.000006	0.706007	0.000004
240B (b,d,f)	2009-11-08					0.706022	0.000006
241 (b,d,f)	2009-11-08	10.9	51.7	0.512405	0.000004	0.706007	0.000013
241B (b,d,f)	2009-11-08	10.9	51.9	0.512413	0.000005		
242 (b,d,f)	2009-11-08	10.9	51.8	0.512412	0.000009		
242B (b,d,f)	2009-11-08	11.0	51.9	0.512415	0.000004		
333 (b,c,f)	2010-09-04	10.8	51.1	0.512407	0.000008	0.706014	0.000005
334 (b,c,f)	2010-09-04	10.9	51.7	0.512410	0.000002	0.706016	0.000012
335A (b,c,e)	2010-09-04			0.512413	0.000004		
335C (b,c,e)	2010-09-04			0.512418	0.000005		
336 (b,c,e)	2010-09-04			0.512410	0.000002	0.706003	0.000006
326 (a,c,f)	2010-05-03					0.706009	0.000003
367(b,c,e)	2010-07-20			0.512379*	0.000007	0.706047*	0.000004
370A (b,c,e)	2010-12-08			0.512398	0.000006		
370B (b,c,e)	2010-12-08			0.512410	0.000005		
416 (a,d,e)	2011-01-07					0.706009	0.000006
417 (a,d,e)	2011-01-07					0.706015	0.000010
418 (a,d,e)	2011-01-07					0.706016	0.000010
419 (a,d,e)	2011-01-07					0.706015	0.000007
421 (a,d,e)	2011-01-07					0.706003	0.000007
438 (a,c,e)	2011-08-19			0.512415	0.000008		
439 (a,c,e)	2011-08-19			0.512413	0.000008		
440 (a,c,e)	2011-08-19			0.512402	0.000009		
441 (a,c,e)	2011-08-19					0.706005	0.000003
454 (a,c,e)	2011-09-30					0.706025	0.000011
455 (a,c,e)	2011-09-30					0.706010	0.000007
458 (a,c,e)	2011-09-30					0.706020	0.000009
469 (a,c,e)	2011-04-11					0.706005	0.000010
470 (a,c,e)	2011-04-11					0.706008	0.000009
472 (a,c,e)	2011-04-11			0.512389*	0.000013	0.706022	0.000013
473 (a,c,e)	2011-04-11					0.705999	0.000009
498A (b,c,e)	2012-02-23			0.512403	0.000005	0.705997	0.000003
498B (b,c,e)	2012-02-23					0.706001	0.000011
498C (b,c,e)	2012-02-23					0.706009	0.000008
498D (b,c,e)	2012-02-23			0.512412	0.000007	0.706014	0.000009
498E (b,c,e)	2012-02-23					0.706011	0.000012
498F (b,c,e)	2012-02-23			0.512409	0.000006	0.706014	0.000010
498G (b,c,e)	2012-02-23			0.512408	0.000006	0.706007	0.000008
498H (b,c,e)	2012-02-23			0.512405	0.000003	0.706002	0.000010
499B (b,c,e)	2012-02-23					0.706011	0.000012
499C (b,c,e)	2012-02-23			0.512399	0.000005		
500A (b,c,e)	2012-02-23			0.512407	0.000002	0.706024	0.000008
500B (b,c,e)	2012-02-23			0.512400	0.000005		
501A (b,c,e)	2012-02-23					0.706001	0.000006
501B (b,c,e)	2012-02-23			0.512408	0.000001		
501C (b,c,e)	2012-02-23					0.706022	0.000006
1584 (a,d,e)	2017-11-16					0.705997	0.000006
1585 (a,d,e)	2017-11-16			0.512405	0.000004	0.706005	0.000009
1587 (a,d,e)	2017-11-16			0.512402	0.000006	0.706016	0.000010
1608 (a,d,f)	2018-01-29	11.1	52.3	0.512412	0.000004		
1609 (a,d,f)	2018-01-29					0.706001	0.000008
1621 (a,d,f)	2018-02-20					0.706002	0.000004
1648 (a,c,f)	2018-03-09	11.1	52.1	0.512414	0.000003	0.706050*	0.000005
1678 (a,d,f)	2018-11-06					0.706006	0.000004
1689 (a,d,f)	2018-06-14						
1709 (a,d,f)	2018-06-14	11.2	52.5	0.512405	0.000004	0.706027	0.000006
1715 (a,d,f)	2018-10-16	11.0	51.4	0.512441*	0.000009	0.706014	0.000009
1782 (a,d,f)	2018-10-29					0.706023	0.000004
1812 (a,d,f)	2018-11-30	11.1	52.0	0.512408	0.000009	0.706006	0.000008
1847 (a,d,f)	2018-11-30	11.1	52.0	0.512409	0.000005		
1848 (a,d,f)	2018-11-30					0.706022	0.000009
1849 (a,d,e)	2018-11-30					0.706057*	0.000001
1850 (a,d,f)	2018-11-30	11.1	52.1	0.512400	0.000004		
1852 (a,d,f)	2019-01-15	11.1	51.8	0.512431*	0.000006	0.706069*	0.000005
1857 (a,d,f)	2019-04-03	11.1	52.0	0.512415	0.000005		
1881B (a,d,f)	2019-05-20					0.706006	0.000009
1919 (a,d,f)	2019-06-07					0.706017	0.000008
1967 (a,d,f)	2018-06-14	11.0	51.7	0.512404	0.000004	0.706021	0.000007
2001 (a,d,f)	2019-06-27	11.0	51.6	0.512411	0.000006	0.706013	0.000014
2020 (a,d,f)	2019-06-27	11.1	52.0	0.512397	0.000006	0.706020	0.000006
2036 (a,d,f)	2019-07-18	11.2	52.8	0.512410	0.000005		
2053 (a,d,f)	2019-08-09	11.0	51.5	0.512406	0.000007		
2067 (a,d,f)	2019-08-08	11.0	51.6	0.512412	0.000003	0.706027	0.000004
2101 (a,d,f)	2019-09-17	11.1	52.2	0.512403	0.000008	0.706024	0.000007
2122 (a,d,f)	2019-11-25	11.0	51.5	0.512408	0.000007		
2123 (a,d,f)	2019-11-25	11.1	52.0	0.512412	0.000009		
2133 (a,d,f)	2020-01-22					0.706009	0.000016
2149 (a,d,f)	2020-02-11					0.706016	0.000009
2164 (a,d,f)	2021-04-21					0.706022	0.000003
2198 (a,d,f)	2021-06-11	11.0	51.8	0.512414	0.000007	0.706002	0.000038
2212 (a,d,f)	2021-06-24	11.0	51.4	0.512407	0.000005	0.706021	0.000008
2236 (a,d,f)	2021-07-09	11.0	51.4	0.512404	0.000006	0.706010	0.000011
2255 (a,d,f)	2021-08-09					0.706022	0.000025
2265 (a,d,f)	2021-08-13	11.1	52.0	0.512409	0.000007	0.705995	0.000023
2176 (a,d,f)	2021-07-05	11.1	52.2	0.512401	0.000010	0.706000	0.000024

Subscribed items: a – Single digestion; b – batch digestion; c – Bomb digestion; d – PFA vials digestion; e – natural samples; f – ID samples; g – normalised for JNdi-1; h – normalised for SRM 987. (2s) is the repeatability measurement (in run) and (*) excluded by Grubbs test outliers.

Table S3.5 - Individual values and means of repeatability measures - normalised ratios of BRP-1 in LAGIR.

#LAGIR	weight date	data run Nd	n	$^{143}Nd/^{144}Nd_{(g)}$	(2s) repeatability	data run Sr	n	$^{87}Sr/^{86}Sr_{(h)}$	(2s) repeatability
232 (a,c,f)	2009-06-18			0.512413				0.706007	
233 (a,c,f)	2009-06-18			0.512407				0.706005	
234 (a,c,f)	2009-06-18			0.512408					
235 (a,c,f)	2009-06-18			0.512417				0.705998	
mean 1			**4**	**0.512411**	**0.000009**		**3**	**0.706003**	**0.000009**
239 (b,d,f)	2009-11-08			0.512406					
240 (b,d,f)	2009-11-08			0.512405				0.706007	
241 (b,d,f)	2009-11-08			0.512405				0.706007	
242 (b,d,f)	2009-11-08			0.512412					
mean 2			**4**	**0.512407**	**0.000007**		**2**	**0.706007**	**0.000000**
335A (b,c,e)	2010-09-04			0.512413					
335C (b,c,e)	2010-09-04			0.512418					
mean 3			**2**	**0.512416**	**0.000007**				
416 (a,d,e)	2011-01-07							0.706009	
417 (a,d,e)	2011-01-07							0.706015	
418 (a,d,e)	2011-01-07							0.706016	
419 (a,d,e)	2011-01-07							0.706015	
421 (a,d,e)	2011-01-07							0.706003	
mean 4							**5**	**0.706012**	**0.000011**
439 (a,c,e)	2011-08-19			0.512413					
440 (a,c,e)	2011-08-19			0.512402					
mean 5			**2**	**0.512408**	**0.000016**				
454 (a,c,e)	2011-09-30							0.706025	
455 (a,c,e)	2011-09-30							0.706010	
mean 6							**2**	**0.706018**	**0.000021**
469 (a,c,e)	2011-04-11							0.706005	
470 (a,c,e)	2011-04-11							0.706008	
472 (a,c,e)	2011-04-11							0.706022	
473 (a,c,e)	2011-04-11							0.705999	
mean 7							**4**	**0.706009**	**0.000019**
498B (b,c,e)	2012-02-23							0.706001	
498C (b,c,e)	2012-02-23							0.706009	
498D (b,c,e)	2012-02-23							0.706014	
498E (b,c,e)	2012-02-23							0.706011	
mean 8							**4**	**0.706009**	**0.000011**
501A (b,c,e)	2012-02-23							0.706001	
501C (b,c,e)	2012-02-23							0.706022	
mean 9							**2**	**0.706012**	**0.000030**
1584 (a,d,e)	2017-11-16							0.705997	
1585 (a,d,e)	2017-11-16			0.512405				0.706005	
1587 (a,d,e)	2017-11-16			0.512402				0.706016	
mean 10			**2**	**0.512404**	**0.000004**		**3**	**0.706006**	**0.000019**
2001 (a,d,f)	2019-06-27							0.706013	
2020 (a,d,f)	2019-06-27							0.706020	
mean 11							**2**	**0.706017**	**0.000010**
2122 (a,d,f)	2019-11-25			0.512408					
2123 (a,d,f)	2019-11-25			0.512412					
mean 12			**2**	**0.512410**	**0.000006**				

Subscribed items: a – Single digestion; b – batch digestion; c – Bomb digestion; d – PFA vials digestion; e – natural samples; f – ID samples; g – normalised for JNdi-1; h – normalised for SRM 987. (2s) is the repeatability measurement

Table S3.6 - Mean values under repeatability conditions - normalised ratios of BRP-1 in LAGIR.

#LAGIR	n	143Nd/144Nd	repeatibility (2s)	n	87Sr/86Sr	repeatibility (2s)
mean 1	4	0.512411	0.000009	3	0.706003	0.000009
mean 2	4	0.512407	0.000007	2	0.706007	0.000000
mean 3	2	0.512416	0.000007			
mean 4				5	0.706012	0.000011
mean 5	2	0.512408	0.000016			
mean 6				2	0.706018	0.000021
mean 7				4	0.706009	0.000019
mean 8				4	0.706009	0.000011
mean 9				2	0.706012	0.000030
mean 10	2	0.512404	0.000004	3	0.706006	0.000019
mean 11				2	0.706017	0.000010
mean 12	2	0.512410	0.000006			
mean 13	**53**	**0.512408**	**0.000010**	**63**	**0.706011**	**0.000017**

mean value under intermediate precision conditions (2s)

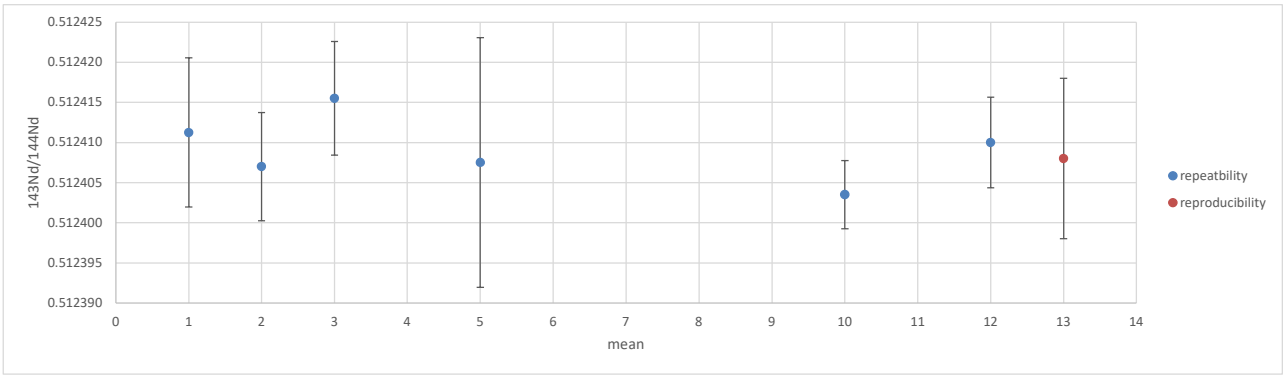

Figure S3.6.1 - Mean values under repeatability conditions 143Nd/144Nd in LAGIR (blue symbol) and mean value under intermediate precision conditions n=53 (red symbol). Range bars represent 2s.

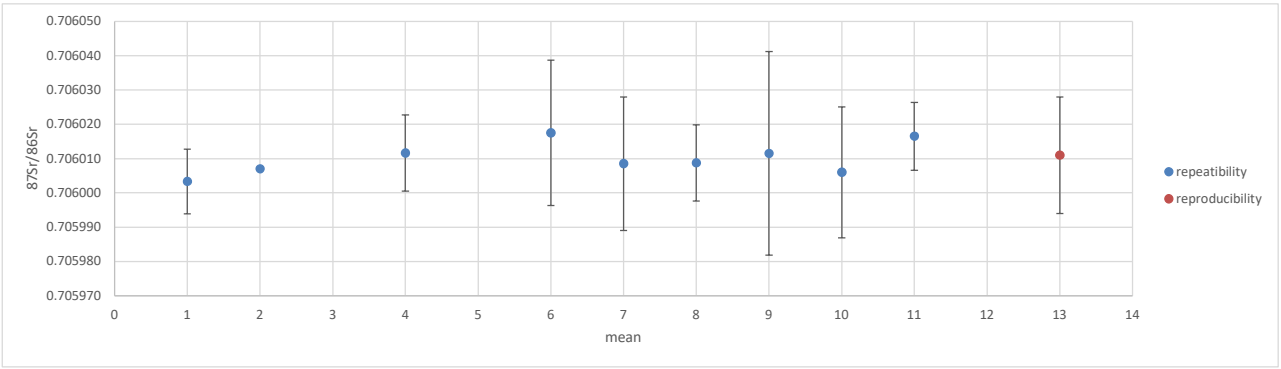

Figure S3.6.2 - Mean values under repeatability conditions 87Sr/86Sr in LAGIR (blue symbol) and mean value under intermediate precision conditions n=63 (red symbol). Range bars represent 2s.

Table S3.7 - Statistics tests BRP-1 - Nd and Sr in LAGIR

	Test	Statistic	df	p
Nd Single X batch	Student's t Independent Samples	-0.040	51	0.969
Nd Bomb X PFA vials	Student's t Independent Samples	0.491	51	0.625
Nd Natural X ID	Student's t Independent Samples	-1.061	51	0.294
Sr Single X batch	Student's t Independent Samples	0.838	61	0.405
Sr Bomb X PFA vials	Student's t Independent Samples	-1.353	61	0.181
Sr Natural X ID	Student's t Independent Samples	-1.339	61	0.186
Nd Single X batch	Shapiro-Wilk Test of Normality	0.982	51	0.585
Nd Bomb X PFA vials	Shapiro-Wilk Test of Normality	0.979	51	0.489
Nd Natural X ID	Shapiro-Wilk Test of Normality	0.988	51	0.870
Sr Single X batch	Shapiro-Wilk Test of Normality	0.966	61	0.074
Sr Bomb X PFA vials	Shapiro-Wilk Test of Normality	0.973	61	0.175
Sr Natural X ID	Shapiro-Wilk Test of Normality	0.973	61	0.188
Nd Single X batch	Homogeneity of Variances Test (Levene's)	0.181	51	0.672
Nd Bomb X PFA vials	Homogeneity of Variances Test (Levene's)	0.071	51	0.791
Nd Natural X ID	Homogeneity of Variances Test (Levene's)	0.688	51	0.411
Sr Single X batch	Homogeneity of Variances Test (Levene's)	1.059	61	0.308
Sr Bomb X PFA vials	Homogeneity of Variances Test (Levene's)	0.933	61	0.338
Sr Natural X ID	Homogeneity of Variances Test (Levene's)	0.221	61	0.640

Note. A low p-value suggests a violation of the assumption of equal variances

df - degrees of freedom

p - p-value the probability

Table S3.8.1 - Mass fractions BRP-1 Sm and Nd in LAGIR

#LAGIR	Sm (ug g-1)	Nd (ug g-1)
232	11.0	51.9
233	11.0	51.9
234	11.0	51.6
235	11.0	51.9
239	11.0	52.0
239B	11.0	52.0
240	11.0	52.0
241	10.9	51.7
241B	10.9	51.9
242	10.9	51.8
242B	11.0	51.9
333	10.8	51.1
334	10.9	51.7
1608	11.1	52.3
1648	11.1	52.1
1709	11.2	52.5
1715	11.0	51.4
1812	11.1	52.0
1847	11.1	52.0
1850	11.1	52.1
1852	11.1	51.8
1857	11.1	52.0
1967	11.0	51.7
2001	11.0	51.6
2020	11.1	52.0
2036	11.2	52.8
2053	11.0	51.5
2067	11.0	51.6
2101	11.1	52.2
2122	11.0	51.5
2123	11.1	52.0
2198	11.0	51.8
2212	11.0	51.4
2236	11.0	51.4
2265	11.1	52.0
2176	11.1	52.2
Mean	**11.0**	**51.9**
Standard deviation (2s)	**0.2**	**0.6**
Std. Dev of the mean [2s]	**0.1**	**0.2**
Cotta and Enzweiler 2008	**11.2**	**51.9**
U	**0.2**	**0.9**

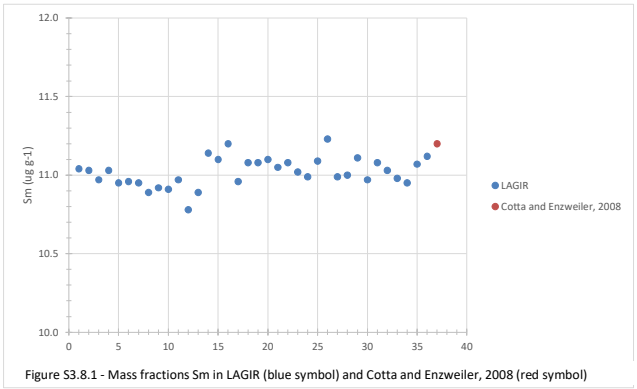

Figure S3.8.1 - Mass fractions Sm in LAGIR (blue symbol) and Cotta and Enzweiler, 2008 (red symbol)

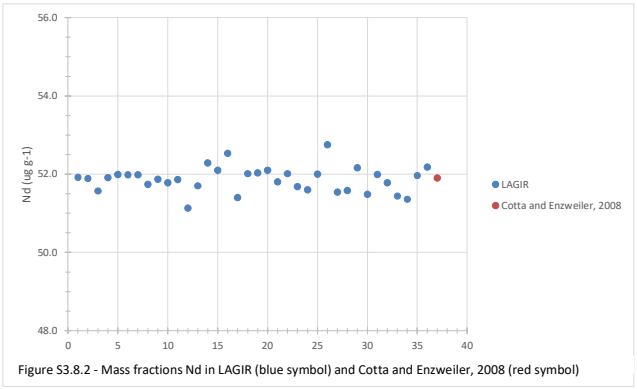

Figure S3.8.2 - Mass fractions Nd in LAGIR (blue symbol) and Cotta and Enzweiler, 2008 (red symbol)

Table S3.8.2 - Descriptive Statistics and Shapiro Wilk test

	Sm (µg g^{-1})	Nd (µg g^{-1})
n	36	36
Mean	11.02	51.86
Standard deviation (2s)	0.18	0.64
Variance	0.01	0.10
Range	0.45	1.62
Minimum	10.78	51.13
Maximum	11.23	52.75
Shapiro-Wilk W	0.98	0.97
Shapiro-Wilk p	0.83	0.53

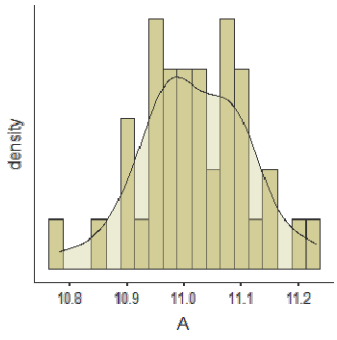

Figure S3.8.3 - Sm Histogram and density

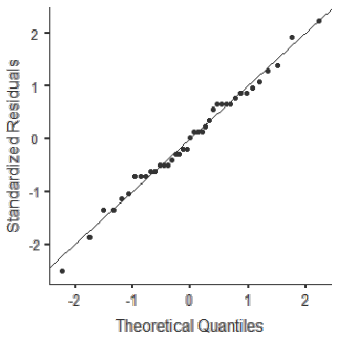

Figure S3.8.4 - Sm Q-Q plot

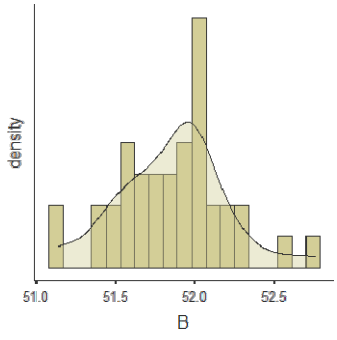

Figure S3.8.5 - Nd Histogram and density

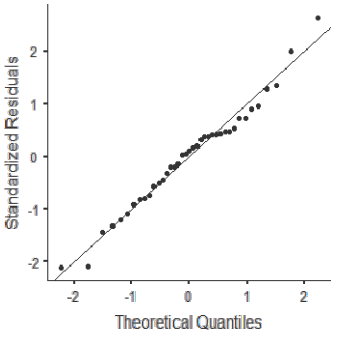

Figure S3.8.6 - Nd Q-Q plot

APÊNDICE B – Material suplementar do 2º artigo

Table S1 - TIMS Sr isotope data from RM EN-1

Sample	mass of Sr (ng)	~87Sr (mV)	$^{87}Sr/^{86}Sr_{(m)}{}^{*}$	(2s)
EN-1 (10907)	1	13	0.709184	0.000042
EN-1 (10368)	1	15	0.709161	0.000040
EN-1 (10289)	2	15	0.709154	0.000034
EN-1 (10288)	2	11	0.709172	0.000027
EN-1 (10905)	3	18	0.709146	0.000033
EN-1 (10287)	3	17	0.709198	0.000025
EN-1 (10366)	10	21	0.709157	0.000029
EN-1 (10906)	10	26	0.709175	0.000020
EN-1 (10284)	10	24	0.709196	0.000028
EN-1 (10367)	15	31	0.709167	0.000015
EN-1 (10331)	15	32	0.709190	0.000010
EN-1 (10904)	20	50	0.709184	0.000015
EN-1 (10286)	20	49	0.709166	0.000018
EN-1 (10369)	30	52	0.709179	0.000019
EN-1 (10972)	30	70	0.709186	0.000016
LAGIR mean (n=15)			**0.709174**	
2s (LAGIR mean)			**0.000032**	
RSD			**0.002**	
GeoReM mean (TIMS)			**0.709172**	
2s (GeoReM)			**0.000027**	

Note

(1) RM - Reference materials

(2) (m) ratio measured

(3) * bias corrected

(4) (2s) - measurement repeatability (in run)

(5) s - standard deviation

(6) 2s - measurement reproducibility

(7) RSD - Relative Standard Deviation

Table S2 - TIMS Sr isotope data from Durango Apatite RM

Sample	mass of Sr (ng)	~87Sr (mV)	$^{87}Sr/^{86}Sr_{(m)}{}^{*}$	(2s)
AP-DG (10384)	0.3	42	0.706326	0.000041
AP-DG (11031)	0.3	21	0.706352	0.000061
AP-DG (11032)	0.3	34	0.706347	0.000063
AP-DG (11073)	0.3	50	0.706340	0.000044
AP-DG (11074)	0.3	35	0.706338	0.000037
AP-DG (11076)	0.3	26	0.706313	0.000070
AP-DG (10411)	3	67	0.706325	0.000027
AP-DG (11060)	3	52	0.706322	0.000018
AP-DG (11030)	3	48	0.706345	0.000030
AP-DG (10412)	3	69	0.706343	0.000024
AP-DG (10416)	10	76	0.706341	0.000027
AP-DG (11072)	10	41	0.706323	0.000018
AP-DG (10410)	20	137	0.706334	0.000023
AP-DG (10414)	20	91	0.706328	0.000010
AP-DG (10413)	30	144	0.706319	0.000021
AP-DG (10415)	30	140	0.706342	0.000018
LAGIR mean (n=16)			**0.706334**	
2s (LAGIR mean)			**0.000023**	
RSD			**0.002**	
Yang et al (2014)			**0.706328**	
2s (Yang et al 2014)			**0.000023**	

Note

(1) RM - Reference material

(2) (m) ratio measured

(3) * bias corrected

(4) (2s) - measurement repeatability (in run)

(5) s - standard deviation

(6) 2s - measurement reproducibility

(7) RSD - Relative Standard Deviation

Table S3 - RM EN-1 data from the GeoReM database

$^{87}Sr/^{86}Sr$	Uncertainty	Uncertainty Type	Method	Institution	Last name	First name	Year
0.709160	0.000020	2SIGMA	TIMS	Ruhr-Universität Bochum	Fichtner	V.	2017
0.709202	0.000006	2SD	TIMS	Polish Geological Institute	Wierzbowski	H.	2017
0.709194	0.000013	2SD	TIMS	University of Wisconsin-Madison	Satkoski	A.M.	2017
0.709197	0.000010	2SIGMA	TIMS	Russian Academy of Sciences	Kuznetsov	A.B.	2017
0.709176	0.000002	2SE	TIMS	U.S. Geological Survey	Neymark	L.A.	2018
0.709171	0.000029	2SE	TIMS	Czech Geological Survey	Erban Kochergina	Y.V.	2022
0.709157	0.000009	2SIGMA	TIMS	Ruhr Universität Bochum	Buhl	D.	2007
0.709160	0.000029	2SIGMA	TIMS	Ruhr Universität Bochum	Buhl	D.	2007
0.709156	0.000009	2SIGMA	TIMS	Ruhr Universität Bochum	Buhl	D.	2007
0.709191	0.000025	2SIGMA	TIMS	Russian Academy of Sciences	Melezhik	V.A.	2008
0.709180	0.000011	2SIGMA	TIMS	University of Texas at Austin	Miller	N.R.	2009
0.709157	0.000004	2SIGMA	TIMS	Ruhr Universität Bochum	Brand	U.	2010
0.709170	0.000010	2SIGMA	TIMS	Russian Academy of Sciences	Kuznetsov	A.B.	2010
0.709171	0.000007	2SIGMA	TIMS	Ruhr-Universität Bochum	Huck	S.	2011
0.709168	0.000005	2SIGMA	TIMS	Ruhr-Universität Bochum	Huck	S.	2011
0.709176	0.000032	2SIGMA	TIMS	University of Queensland	Uysal	I.T.	2011
0.709159	0.000004	2SIGMA	TIMS	Ruhr-Universität Bochum	Brand	U.	2012
0.709159	0.000004	2SIGMA	TIMS	Ruhr-Universität Bochum	Brand	U.	2012
0.709160	0.000027	2SIGMA	TIMS	Ruhr Universität Bochum	Geske	A.	2012
0.709172	0.000010	2SIGMA	TIMS	US Geological Survey	Neymark	L.A.	2013
0.709176	0.000003	2SE	ID-TIMS	US Geological Survey	Neymark	L.A.	2014
0.709176	0.000014	2SD	TIMS	USGS Microbeam Laboratory	Drexler	J.Z.	2014
0.709178	0.000005	2SIGMA	TIMS	Russian Academy of Sciences	Melezhik	V.A.	2015
0.709160	0.000027	2SIGMA	TIMS	Ruhr Universität Bochum	Geske	A.	2015

Note: Download from GeoReM - The Reference Material Database. Date of Query: 07. 2024Nov

Table S4 - LA-ICP-MS analytical data of zircon U-Pb geochronology for samples BG-200 and BG-14B

Sample	SPOT	U(ppm)	Th/U	207Pb(cps)	206Pb(cps)	208Pb(cps)	207Pb/206Pb	2sigma(%)	207Pb/235U	2sigma(%)	206Pb/238U	2sigma(%)	Rho	206Pb/238U	2sigma(s)	207Pb/235U	2sigma(s)	207Pb/206Pb	2sigma(s)	Disc (%)
BG-200	005std.exp	405.2	0.184	26843.9	448740.4	-0.000088	0.060	1.1	0.798177	3.2	0.096041	3.0	0.9	591	17	596	14	613	24	0.7
BG-200	006std.exp	230.1	0.046	14545.4	248873.2	-0.000065	0.059	0.9	0.763359	1.7	0.093838	1.5	0.8	578	8	576	8	567	20	-0.5
BG-200	007std.exp	123.7	0.324	7773.5	134794.0	-0.000074	0.059	1.9	0.763122	2.6	0.094513	1.7	0.7	582	10	576	11	551	42	-1.2
BG-200	008std.exp	736.2	0.200	47566.5	789903.6	-0.000067	0.059	0.6	0.754842	1.3	0.092985	1.2	0.9	573	6	571	6	563	14	-0.5
BG-200	009std.exp	219.6	0.130	16035.3	250308.1	-0.000099	0.060	11.4	0.812312	11.9	0.098560	3.6	0.3	606	21	604	56	595	246	-0.5
BG-200	010std.exp	549.1	0.122	35437.2	599284.6	-0.000095	0.060	0.9	0.777129	1.3	0.094717	1.0	0.7	583	5	584	6	586	20	0.0
BG-200	011std.exp	258.0	0.219	14546.2	254794.2	-0.000105	0.058	1.2	0.679805	2.5	0.085717	2.2	0.9	530	11	527	10	512	26	-0.8
BG-200	012std.exp	386.3	0.168	24319.3	413553.5	-0.000086	0.059	0.7	0.758684	1.1	0.092950	0.9	0.8	573	5	573	5	574	15	0.0
BG-200	013std.exp	492.9	0.130	31405.4	530825.2	-0.000039	0.060	0.6	0.767311	1.1	0.093515	0.9	0.8	576	5	578	5	586	12	0.2
BG-200	014std.exp	28.8	0.433	2494.0	32411.0	-0.000055	0.059	13.3	0.789078	13.7	0.096248	3.0	0.2	592	17	591	63	584	289	-0.4
BG-200	015std.exp	303.7	0.119	19032.1	323075.4	-0.000027	0.059	0.7	0.755982	1.1	0.092407	0.9	0.8	570	5	572	5	579	16	0.2
BG-200	016std.exp	402.4	0.129	27097.1	452635.7	-0.000128	0.060	0.9	0.811344	1.4	0.097705	1.1	0.8	601	6	603	7	612	20	0.3
BG-200	017std.exp	286.0	0.266	19368.5	326389.8	-0.000110	0.060	0.8	0.816742	1.4	0.099147	1.2	0.8	609	7	606	7	594	17	-0.6
BG-200	018std.exp	453.8	0.249	28390.8	482369.1	-0.000122	0.059	1.1	0.754018	1.4	0.092361	1.0	0.7	569	5	571	6	575	23	0.1
BG-200	019std.exp	226.5	0.249	14130.9	242709.0	-0.000110	0.059	1.0	0.755259	1.4	0.093132	1.0	0.7	574	6	571	6	560	22	-0.6
BG-200	025std.exp	297.5	0.148	24496.1	387986.1	-0.000079	0.064	1.2	0.994232	2.9	0.113432	2.6	0.9	693	17	701	15	727	25	1.1
BG-200	026std.exp	421.2	0.076	26678.9	454134.7	-0.000127	0.059	0.8	0.764881	1.7	0.093813	1.5	0.9	578	8	577	7	572	18	-0.3
BG-200	027std.exp	641.3	0.136	42656.9	686692.8	-0.000087	0.059	1.1	0.754133	1.6	0.092909	1.1	0.7	573	6	571	7	562	25	-0.5
BG-200	028std.exp	230.8	0.305	15798.5	258109.8	-0.000107	0.060	1.7	0.797752	2.0	0.097174	1.1	0.5	598	6	596	9	587	37	-0.5
BG-200	029std.exp	668.0	0.148	43829.2	727681.3	-0.000079	0.061	0.8	0.791903	1.1	0.094820	0.7	0.7	584	4	592	5	624	16	1.3
BG-200	030std.exp	218.3	0.151	14969.4	249000.9	-0.000065	0.060	1.9	0.819829	2.8	0.099304	2.0	0.7	610	11	608	13	599	42	-0.5
BG-200	031std.exp	226.7	0.261	15150.8	257522.8	-0.000130	0.059	1.0	0.808873	2.0	0.098936	1.8	0.9	608	10	602	9	578	21	-1.1
BG-200	032std.exp	274.2	0.161	17467.8	296462.0	-0.000075	0.059	0.9	0.770379	1.5	0.094156	1.2	0.8	580	6	580	7	580	20	-0.1
BG-200	033std.exp	480.5	0.196	36059.2	467708.3	-0.000070	0.078	3.5	0.906882	4.4	0.084780	2.8	0.6	525	14	655	22	1136	69	19.9
BG-200	034std.exp	419.8	0.116	27914.3	466295.8	-0.000099	0.060	0.7	0.803886	1.2	0.096885	1.0	0.8	596	6	599	6	610	16	0.4
BG-14B	035std.exp	2751	0.161	150766.8	2621966.5	-0.000082	0.058	0.8	0.661390	1.0	0.083021	0.6	0.6	514	3	515	4	521	18	1.3
BG-14B	036std.exp	1299	0.166	71501.6	1266313.2	-0.000130	0.057	0.5	0.664893	0.9	0.085000	0.7	0.8	526	4	518	4	482	12	-9.2
BG-14B	037std.exp	2451	0.251	153262.7	2354421.5	-0.000113	0.057	2.6	0.657712	3.2	0.083157	1.9	0.6	514	9	513	13	511	56	-0.7
BG-14B	038std.exp	2054	0.121	103446.2	1806821.0	-0.000100	0.058	0.9	0.608465	1.9	0.076725	1.7	0.9	478	8	482	7	502	18	4.7
BG-14B	039std.exp	2028	0.098	108467.7	1881314.1	-0.000116	0.058	0.8	0.646246	1.1	0.080883	0.7	0.7	502	3	506	4	524	17	4.1
BG-14B	040std.exp	5129	0.351	307319.2	4942736.2	-0.000112	0.057	1.9	0.662853	3.9	0.083677	3.4	0.9	520	17	516	16	501	38	-3.8
BG-14B	045std.exp	2184	0.240	120848.5	2098600.5	-0.000130	0.058	0.9	0.668983	1.3	0.083840	0.9	0.7	520	5	520	5	521	20	0.2
BG-14B	046std.exp	1765	0.236	93686.0	1610116.3	-0.000068	0.058	0.8	0.641951	1.5	0.079607	1.3	0.8	496	6	504	6	537	20	7.7
BG-14B	047std.exp	3091	0.295	169999.7	2194206.0	-0.000096	0.078	2.1	0.665230	2.4	0.061970	1.3	0.5	388	5	518	10	1142	41	66.0
BG-14B	049std.exp	2981	0.110	166162.6	2880571.9	-0.000104	0.058	0.5	0.674504	1.0	0.084403	0.8	0.9	520	4	524	4	540	10	3.8
BG-14B	050std.exp	2392	0.123	122439.1	2130705.5	-0.000086	0.058	0.7	0.619712	1.3	0.077831	1.1	0.9	484	5	490	5	517	13	6.3
BG-14B	051std.exp	9629	0.709	462185.1	6847022.4	-0.000061	0.058	2.1	0.589345	3.5	0.074159	2.7	0.8	460	12	470	13	519	46	11.0
BG-14B	052std.exp	3246	0.301	186303.7	2838212.5	-0.000081	0.066	2.3	0.694853	2.6	0.076469	1.3	0.5	472	6	536	11	817	47	42.0
BG-14B	053std.exp	1447	0.080	73008.9	1279274.8	-0.000128	0.057	1.2	0.611129	1.5	0.077296	0.9	0.6	478	4	484	6	513	26	6.7
BG-14B	054std.exp	1739	0.086	89462.2	1537329.2	-0.000114	0.058	1.3	0.623101	1.6	0.077266	1.0	0.6	478	5	492	6	555	28	14.0
BG-14B	055std.exp	3005	0.147	164992.1	2884832.2	-0.000137	0.057	0.6	0.665269	1.1	0.083930	0.9	0.8	520	5	518	5	508	15	-2.4
BG-14B	056std.exp	5587	0.159	253855.5	4031963.3	-0.000076	0.063	2.7	0.550487	7.0	0.063096	6.4	0.9	394	25	445	25	719	65	45.0
BG-14B	057std.exp	1067	0.056	53601.2	907122.9	-0.000090	0.059	0.6	0.609040	1.1	0.074460	1.0	0.9	460	4	483	4	592	10	22.0
BG-14B	058std.exp	2085	0.115	115390.1	2008599.4	-0.000095	0.058	0.4	0.670968	1.1	0.084284	1.0	0.9	520	5	521	5	527	11	1.4
BG-14B	059std.exp	2002	0.087	111177.0	1870208.4	-0.000092	0.060	0.7	0.673486	1.4	0.081740	1.2	0.9	508	6	523	6	586	13	13.0
BG-14B	060std.exp	1734	0.093	92925.7	1592988.5	-0.000145	0.059	0.8	0.650016	1.2	0.080382	0.9	0.7	496	4	509	5	564	19	12.0
91500 (RM)	003std.exp	68.1	0.183	10444.8	140153.9	-0.000096	0.075	1.1	1.847635	1.5	0.178334	1.1	0.7	1058	10	1063	10	1072	21	
BB9 (RM)	004std.exp	313.5	0.178	19106.5	327714.1	-0.000057	0.059	0.6	0.733818	1.0	0.090652	0.8	0.8	559	4	559	4	556	13	
91500 (RM)	023std.exp	79.8	0.187	12032.6	161961.8	-0.000087	0.075	0.8	1.824936	1.3	0.176527	1.0	0.8	1048	9	1054	8	1068	16	
BB9 (RM)	024std.exp	313.6	0.177	19019.6	325696.4	-0.000117	0.059	0.6	0.732720	1.0	0.090446	0.8	0.8	558	4	558	4	558	14	
91500 (RM)	043std.exp	65.0	0.178	9940.6	133568.5	-0.000084	0.075	0.9	1.861046	1.3	0.179496	1.0	0.8	1064	10	1067	9	1074	17	
BB9(RM)	044std.exp	294.7	0.176	18100.0	310499.3	-0.000137	0.059	0.6	0.744358	1.0	0.091914	0.8	0.8	567	4	565	4	557	12	

Table S5 - Whole rock major and trace elements compositions of granitoid rocks

Sample	SMM-CMM-172	BG-200	BG-14B
SiO2	64.79	69.69	56.26
Al2O3	16.12	14.10	15.64
FeOt	4.88	3.61	8.79
Fe2O3(T)	5.43	4.01	9.77
MnO	0.08	0.06	0.21
MgO	1.51	0.82	3.81
CaO	4.27	2.95	6.64
Na2O	3.10	2.44	3.62
K2O	2.96	4.45	1.85
TiO2	0.91	0.83	0.94
P2O5	0.21	0.25	0.16
LOI	0.6	0.25	0.28
Total	99.97	99.86	99.18
Na2O/K2O	1.05	0.55	1.96
Al2O3mol	0.16	0.14	0.15
FeOmol	0.07	0.05	0.12
MgOmol	0.04	0.02	0.09
CaOmol	0.08	0.05	0.12
Na2Omol	0.05	0.04	0.06
K2Omol	0.03	0.05	0.02
2*ACNK	2.01	1.99	1.56
ACNK	1.00	0.99	0.78
CNK	0.16	0.14	0.20
#mg	0.36	0.29	0.44
FMSB	0.65	0.91	0.61
2*FMSB	1.30	1.82	1.21
#mg*100	35.55	28.84	43.59
Sc	10	6	26
Be	2	1	3
V	93	31	206
Ba	732	1739	261
Sr	287	321	221
Ba/10000	0.0732	0.1739	0.0261
Sr/10000	0.0287	0.0321	0.0221
Y	25	16	23
Zr	283	334	86
Cr	70	< 20	<20
Co	11	15	26
Ni	<20	< 20	<20
Cu	<10	10	10
Zn	110	70	120
Ga	23	20	21
Ge	1	1	1
As	<5	< 5	<5
Rb	128	137	97
Nb	16	17	10
Mo	<2	< 2	<2
Ag	1	1.1	<0.5
In	<0.2	< 0.2	<0.2
Sn	<1	1	7
Sb	<0.5	< 0.5	<0.5
Cs	1.8	2.5	2.3
La	35.6	63.8	12.6
Ce	76.1	129	29.7
Pr	9.1	15.1	3.92
Nd	35.2	57.7	17.5
Sm	8.1	10.1	4.3
Eu	1.5	1.92	1.5
Gd	7.2	6.2	3.8
Tb	1	0.9	0.7
Dy	5.8	4.1	4.6
Ho	1	0.6	0.9
Er	2.6	1.5	2.7
Tm	0.3	0.15	0.39
Yb	1.7	0.8	2.6
Lu	0.3	0.11	0.42
Hf	6.8	8.2	2.3
Ta	0.9	1	1.1
W	37	153	17
Tl	0.5	0.5	0.4
Pb	14	14	14
Bi	<0.4	< 0.4	<0.4
Th	9.7	13.1	3
U	0.9	1.6	2.2

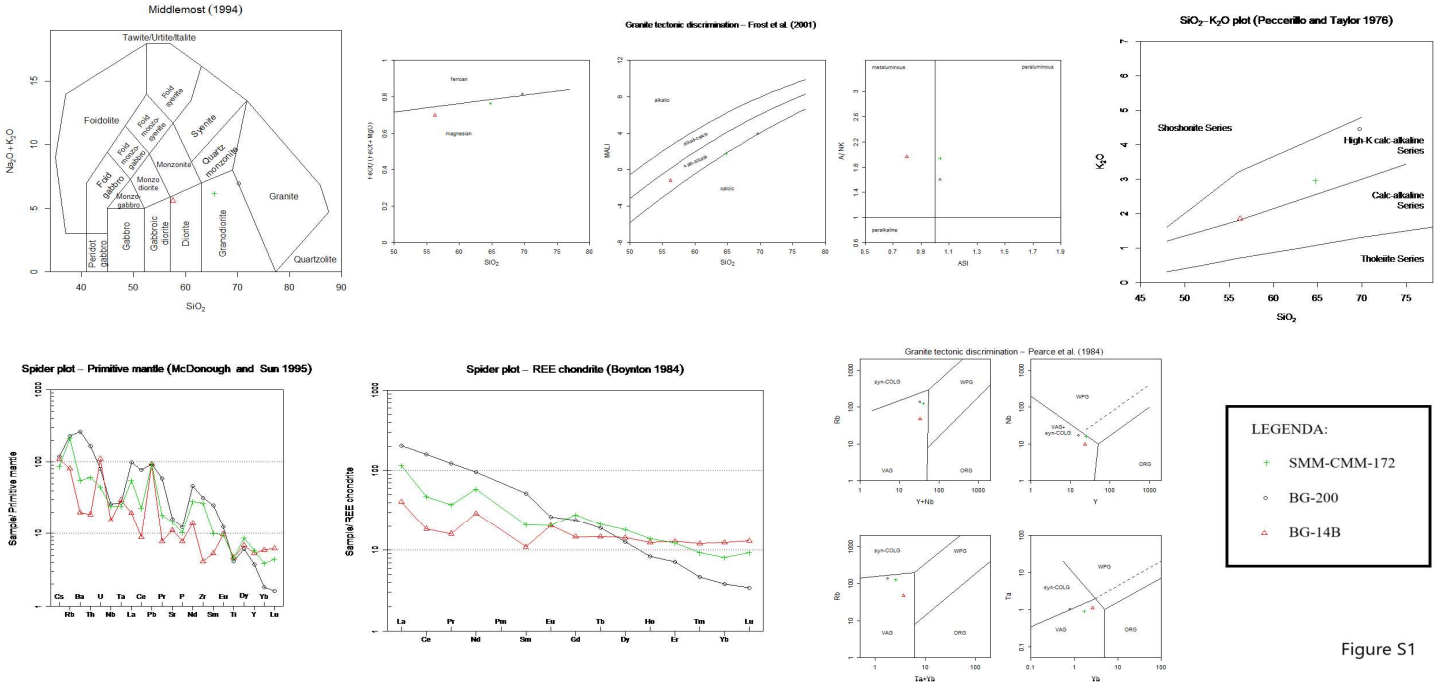

LEGENDA:

- SMM-CMM-172
- BG-200
- BG-14B

Figure S1

Table S6 - TIMS Nd and Sr isotope data from granitoid rocks samples

Sample	Rock type	Rb (ppm)	2s	Sr (ppm)	2s	$^{87}Sr/^{86}Sr_{(m)}{}^{*}$	2s	time (Ma)	2s	$^{87}Sr/^{86}Sr_{(i)}$	u (c)	U (k=2)	$^{143}Nd/^{144}Nd_{(m)}{}^{*}$	2s	$^{143}Nd/^{144}Nd_{(i)}$	ε(Nd) i
SMM-CMM-172 (**)	granodiorite	128	2.6	287	2.9	0.722254	0.000006	629	10	0.710833	0.000314	0.000628	0.511931	0.000007	0.511395	-8.4
BG-200	granite	137	2.7	321	3.2	0.724903	0.000007	602.2	4.9	0.714438	0.000249	0.000498	0.511778	0.000006	0.511362	-9.8
BG-14B	diorite	97	1.9	221	2.2	0.720435	0.000011	518.3	1.9	0.711182	0.000210	0.000420	0.512105	0.000007	0.511603	-7.2

Note

(1) (m) ratio measured

(2) * bias corrected

(3) 2s - measurement repeatability (in run)

(4) s - standard deviation

(5) u(c) - combined standard uncertainty

(6) U - expanded uncertainty

(7) k =2 - coverage factor with a confidence level of approximately 95%

(8) ** Reference: Peixoto et al, (2017)

(9) References: Taylor, John. An Introduction to Error Analysis - The Study of Uncertainties in Physical Measurements, Second Edition. University Science Books and Evaluation of Measurement Data — Guide to the Expression of Uncertainty In Measurement (GUM). September, 2008.

Table S7 - TIMS isotope data of apatite grains from granitoid rocks samples

Sample	number of grains	mass of Sr (ng)	~87Sr (mV)	$^{87}Sr/^{86}Sr_{(m)}{}^{*}$	(2s)
AP-SMM-CMM-172 (173)	1	5	8	0.714130	0.000061
AP-SMM-CMM-172 (174)	1	5	15	0.713970	0.000036
AP-SMM-CMM-172 (175)	1	5	12	0.713948	0.000069
AP-SMM-CMM-172 (202)	1	5	18	0.714399	0.000077
AP-SMM-CMM-172 (289)	1	5	15	0.714306	0.000124
AP-SMM-CMM-172 (290)	1	5	23	0.714373	0.000062
AP-SMM-CMM-172 (291)	1	5	24	0.714039	0.000077
AP-SMM-CMM-172 (311)	5	24	28	0.714598	0.000076
AP-SMM-CMM-172 (312)	8	38	40	0.714444	0.000047
AP-SMM-CMM-172 (313)	8	38	69	0.714423	0.000027
AP-SMM-CMM-172 (314)	10	47	101	0.714318	0.000020
AP-SMM-CMM-172 (316)	10	47	70	0.714555	0.000026
AP-SMM-CMM-172 (349)	8	38	34	0.714727	0.000048
AP-SMM-CMM-172 (347)	5	24	28	0.714425	0.000038
AP-SMM-CMM-172 (348)	5	24	31	0.714372	0.000027
AP-SMM-CMM-172 (401)	8	38	42	0.714131	0.000038
AP-SMM-CMM-172 (403)	10	47	150	0.714166	0.000010
LAGIR mean (n=17)				**0.714313**	
2s				**0.000442**	
AP-BG-200 (106)	1	1	13	0.717079	0.000126
AP-BG-200 (125)	1	1	9	0.716154	0.000200
AP-BG-200 (119)	1	1	11	0.716906	0.000229
AP-BG-200 (127)	1	1	16	0.716135	0.000147
AP-BG-200 (211)	1	1	16	0.716638	0.000106
AP-BG-200 (119)	8	9	44	0.716569	0.000028
AP-BG-200 (122)	7	8	88	0.716657	0.000023
AP-BG-200 (212)	10	12	25	0.715920	0.000064
AP-BG-200 (294)	5	6	18	0.716226	0.000076
AP-BG-200 (295)	10	12	30	0.716599	0.000048
AP-BG-200 (306)	10	12	50	0.716504	0.000033
AP-BG-200 (307)	10	12	20	0.716808	0.000066
AP-BG-200 (308)	10	12	100	0.716767	0.000008
AP-BG-200 (317)	10	12	53	0.716421	0.000059
LAGIR mean (n=14)				**0.716527**	
2s				**0.000653**	
AP-BG-14B (131)	1	0.5	15	0.713011	0.000351
AP-BG-14B (136)	1	0.5	7	0.712979	0.000101
AP-BG-14B (220)	1	0.5	21	0.712775	0.000110
AP-BG-14B (296)	1	0.5	12	0.712656	0.000109
AP-BG-14B (402)	1	0.5	25	0.712887	0.000169
AP-BG-14B (309)	10	4	41	0.713017	0.000054
AP-BG-14B (318)	10	4	50	0.713190	0.000043
AP-BG-14B (344)	8	3	24	0.713028	0.000092
AP-BG-14B (345)	5	2	14	0.713222	0.000081
AP-BG-14B (346)	10	4	35	0.712913	0.000060
AP-BG-14B (402)	10	4	30	0.712756	0.000110
AP-BG-14B (404)	10	4	31	0.712810	0.000058
LAGIR mean (n=12)				**0.712937**	
2s				**0.000344**	

Note

(1) (m) ratio measured

(2) * bias corrected

(3) (2s) - measurement repeatability (in run)

(4) s - standard deviation

(5) 2s - measurement reproducibility